OPTIMIZATION OF ACCELERATOR PARAMETERS USING NORMAL FORM METHODS ON HIGH-ORDER TRANSFER MAPS

By

Pavel Snopok

A DISSERTATION

Submitted to
Michigan State University
in partial fulfillment of the requirements
for the degree of

DOCTOR OF PHILOSOPHY

Department of Physics and Astronomy

2007

ABSTRACT

OPTIMIZATION OF ACCELERATOR PARAMETERS USING NORMAL FORM METHODS ON HIGH-ORDER TRANSFER MAPS

By

Pavel Snopok

Methods of analysis of the dynamics of ensembles of charged particles in collider rings are developed. The following problems are posed and solved using normal form transformations and other methods of perturbative nonlinear dynamics:

- Optimization of the Tevatron dynamics:

  - Skew quadrupole correction of the dynamics of particles in the Tevatron in the presence of the systematic skew quadrupole errors in dipoles;

  - Calculation of the nonlinear tune shift with amplitude based on the results of measurements and the linear lattice information;

- Optimization of the Muon Collider storage ring:

  - Computation and optimization of the dynamic aperture of the Muon Collider 50×50 GeV storage ring using higher order correctors;

  - 750×750 GeV Muon Collider storage ring lattice design matching the Tevatron footprint.

The normal form coordinates have a very important advantage over the particle optical coordinates: if the transformation can be carried out successfully (general restrictions for that are not much stronger than the typical restrictions imposed on the behavior of the particles in the accelerator) then the motion in the new coordinates has a very clean representation allowing to extract more information about the dynamics of particles, and they are very convenient for the purposes of visualization.

All the problem formulations include the derivation of the objective functions, which are later used in the optimization process using various optimization algorithms. Algorithms used to solve the problems are specific to collider rings, and applicable to similar problems arising on other machines of the same type.

The details of the long-term behavior of the systems are studied to ensure the their stability for the desired number of turns. The algorithm of the normal form transformation is of great value for such problems as it gives much extra information about the disturbing factors. In addition to the fact that the dynamics of particles is represented in a way that is easy to understand, such important characteristics as the strengths of the resonances and the tune shifts with amplitude and various parameters of the system are calculated.

Each major section is supplied with the results of applying various numerical optimization methods to the problems stated. The emphasis is made on the efficiency comparison of various approaches and methods. The main simulation tool is the arbitrary order code COSY INFINITY written by M. Berz, K. Makino, et al. at Michigan State University. Also, the code MAD is utilized to design the 750×750 GeV Muon Collider storage ring baseline lattice.

The OptiM to COSY lattice converter is written specifically for the need of the studies included into the dissertation, and tested on the Tevatron accelerator lattice.

Dedicated to my beloved Olga

ACKNOWLEDGMENTS

The acknowledgments page is really the opportunity to slow down for a moment, to look back and observe the whole aeon of the graduate program studies, to recall the names of the persons who helped me a great deal in reaching my goal in the form of this dissertation piece. Without these people and their help the task of the Ph.D. program would be next to impossible to accomplish.

For sure, the last four year were not the easiest for me, but definitely the most interesting in the sense of new impressions, acquaintances, professional growth and gaining invaluable experience. I am thankful to all the people who worked hard on giving me the opportunity to pursue the graduate program at Michigan State University: Dr. Martin Berz, my scientific adviser at MSU; Dr. Carol Johnstone, my adviser at Fermi National Accelerator Laboratory; Dr. Dmitry Ovsyannikov and Dr. Alexander Ovsyannikov, my scientific advisers at St.Petersburg State University, both in undergraduate and graduate level programs; Dr. Viktor Yarba from Fermi National Accelerator Laboratory.

I personally think it is very useful to be involved in a joint program, where the participants can study at the university and work on their research at some national laboratory. It gives you broader exposure and more areas to explore in addition to fairly different working environments.

Graduate program at MSU/FNAL gave me a lot: the vision of the scientific process as it is in the international scientific community; the opportunity to do my research at Fermilab, one of the biggest accelerator physics centers in the world; the multinational multicultural team work experience.

Besides that, I gained priceless experience of applying my knowledge and expertise in Mathematics to the field of Beam Physics, to solving the theoretical and applied

problems connected to the optimization of the parameters of the accelerating structures.

I hope during the course of my graduate studies I acquired the necessary experience to conduct independent research, scientific studies; to teach both undergraduate and graduate level courses. This dissertation work should serve as a proof of my competence. I also hope that the results derived in the dissertation will be interesting to someone else, and not only me, and serve as a source of inspiration on how to improve the methods of accelerator optimization proposed in the work.

I'm thankful to my fellow students from the Beam Theory group, who were always willing to give a helping hand no matter what the situation was: Dr. Shashikant Manikonda, Johannes Grote, Alex Wittig, Youn-Kyung Kim; and even more so to my brother in arms Alexey Poklonskiy, with whom I went through the graduate studies side by side.

Dr. Kyoko Makino (MSU), Dr. David Neuffer (Fermilab), Dr. Kevin Paul (Muons, Inc.), Dr. Michael Syphers (Fermilab) I thank for interesting discussions, good advice and willingness to help at all stages of my research.

I cannot express how much I'm obliged for everything that happened in my life and scientific career to my parents — Vyacheslav Snopok and Anna Snopok. I am so sorry my father will not see me a Ph.D., but I'm sure he would be proud of me.

Endless thanks for love, constant support and boundless patience to my beloved one — Olga Safronova. I dedicate this work to her.

Unfortunately, I cannot go on mentioning people I'm thankful to, otherwise this acknowledgment section will grow to the size of the dissertation itself. So, many thanks to everyone taking part in my scientific and private life, I hope these people will easily recognize themselves; a profound bow and my sincere gratitude.

TABLE OF CONTENTS

LIST OF TABLES

LIST OF FIGURES

1. INTRODUCTION

The problems of calculation and optimization of the dynamics of charged particles in accelerators are studied by the field of physics called accelerator physics, or more generally, beam physics. Beam physics deals with charged particle beams as well as other beams in various electrophysical devices such as electron microscopes, lasers, x-ray devices, and computer tomography devices, and also in the most general sense — with sets of nearby trajectories in a large phase space.

Despite the fact that the article by Courant and Snyder [21], where the details of the linear dynamics of particles in the accelerating structures are discussed, was published less than half a century ago, the theory of control and optimization of the dynamics of particles in the accelerators nowadays has firm grounds as well as a large number of classical studies and research methods.

However, this is not surprising, taking into account the pace of the growth of the requirements and the constraints applied to the designed devices in the sense of the final energy of the particles, the components manufacturing precision and the strength of the steering and accelerating electromagnetic fields. For example, the accelerator whose name will be seen again and again in this dissertation work — the Tevatron — supplies a center of mass energy of 2 TeV at collision; particles typically stay in the accelerating channel for 10^9–10^{10} turns, while the beam has the size of the order of millimeters, which results in at least 10^{13} of difference in scale. This fact, in turn,

results in the necessity of precise orbit calculations as well as accurate estimates of the particle stability and engineering and alignment error limits.

Mathematical models accompany any accelerating structure during its whole life span, starting from the instant when the accelerator is merely an idea, and to the last particle acceleration cycle, or even after that, as in the case of the Tevatron accelerator and one of the possible options for the Muon Collider storage ring discussed later in this work. At this point, the question of the destiny of the Tevatron project is unclear. Currently it is scheduled for the decommission by the end of 2009. However, the question is what could replace the accelerator which was at the edge of scientific and engineering achievements for many years. There is a tunnel of 6.28 km in circumference, and it could house a next generation accelerator, thus effectively cutting down its cost. There are studies conducted toward this direction [49,50].

In this dissertation the lattice for a small Muon Collider storage ring with a center of mass energy at collision of 100 GeV is discussed. Due to the small final energy of the particles, the circumference of the ring measures 345 meters. At the same time, a similar ring with a collision energy of about 1.5–2 TeV could be designed to match the footprint of the Tevatron tunnel with minor changes. Until now there was no explicit interest in this project, but recently this situation has changed dramatically. Various Muon Collider lattices are studied at Fermi National Accelerator Laboratory (FNAL or Fermilab) and a number of other laboratories around the world. These studies include models that fit exactly or approximately the geometry of the Tevatron tunnel to make use of its infrastructure. One variant of the lattice for such a storage ring was proposed by the author and Dr. Carol Johnstone at the Muon Collaboration Workshop at UCLA in January 2007 [49] and this proposal is included in the dissertation work.

To support the lattice design process with adequate physical and mathematical models and methods, a number of software packages are under constant development by various research groups around the world [3, 14, 18, 32]. In general these software packages can be divided into two large categories, depending on the problems solved. Some of the programs allow for the dynamics calculation of the individual particles of the beam, and as such, they require solving of the systems of differential or integro-differential equations for each different set of beam parameters. This approach is justified if one needs to have as much information as possible about individual particles of the beam or for taking into account the interaction of the particles in the beam (space charge of the beam). On the other hand, one obvious disadvantage of such an approach would be the need to recalculate the whole trajectory of each individual particle, which results in an incredible volume of calculations in the case of a circular accelerator, for which particles stay in the beam tube for millions of turns.

Another group of programs allows to calculate the overall effect of the accelerator optics on the particles, e.g. in the form of the transfer map connecting the initial and final coordinates of the particles, and then track an arbitrary distribution of particles by applying the resulting transfer map to the coordinates of the particles in the distribution. This gives a natural way to treat repetitive systems by merely applying the transfer map over and over again for virtually infinite number of times to study the behavior of the particles for a large number of turns, without spending much computational effort in recalculating the dynamics of individual particles. COSY INFINITY (COSY) [13, 36], developed at Michigan State University by Dr. Martin Berz, Dr. Kyoko Makino and others, falls into this category of programs. COSY is one of the main analysis tools used for the studies presented in this work.

Nowadays it is hard to find a software package that falls exactly into one of the

categories described above. As a rule, programs combine the advantages of various general approaches to beam dynamics calculation and optimization.

To make sure the calculations in the presented studies are correct, most of the results have been cross-checked with other popular codes for beam dynamics optimization, such as MAD [3] and OptiM [32] for aspects these codes can handle.

One of the most important criteria for the development of beam dynamics codes is the running speed: how efficient the computation algorithms are, how fast one can obtain the results and how much information should be sacrificed for speed considerations, or how long it takes to obtain the results with the desired precision, or even rigorous results if runtime is not a critical factor.

To increase the efficiency, COSY employs high-performance differential algebra methods and Taylor model methods for rigorous computations [10–12, 34].

In addition to that, COSY supports the transformation from particle optical coordinates to a special set of coordinates called the normal form coordinates, which could be obtained using a complicated order-by-order nonlinear transformation. The normal form coordinates have a very important advantage over the particle optical coordinates: if the transformation can be carried out successfully (general restrictions for that are not much stronger than the typical restrictions imposed on the behavior of the particles in the accelerator) then the motion in the new coordinates has a very clean representation allowing to extract more information about the dynamics of particles, and very convenient for the purposes of visualization. The algorithm of the normal form transformation [12] is set forth in details in Chapter 3, and in the subsequent chapters it is used multiple times to assist in solving various problems.

Logically the dissertation is divided into chapters and sections according to the applied problems and subproblems stated and solved, as follows.

- Optimization of the Tevatron dynamics:

  – Skew quadrupole correction of the dynamics of particles in the Tevatron in the presence of the systematic skew quadrupole errors in dipoles;

  – Calculation of the nonlinear tune shift with amplitude based on the results of measurements and the linear lattice information;

- Optimization of the Muon Collider storage ring:

  – Computation and optimization of the dynamic aperture of the Muon Collider 50×50 GeV storage ring using higher order correctors;

  – A 750×750 GeV Muon Collider storage ring lattice design matching the Tevatron footprint.

All the problem formulations include the derivation of the objective functions, which are later used in the optimization process using various optimization algorithms. Algorithms used to solve the problems are specific to collider rings, and applicable to similar problems arising on other machines of the same type.

In linear accelerators, particles go down the accelerator channel only once, so the most important aspect is to have as much information as possible about the steering and accelerating fields and their fluctuations, about the particle interaction in the beam and about the deviations of various parameters of the system. In other words, one needs as much information about the linear and nonlinear components of the dynamics, and it needs to be as precise as possible.

To a large extent the above statement is true for circular accelerators too, but there is a significant difference: the particles in the beam pass the same elements of the structure multiple times. So the most important task for this case is to study the

details of the long-term behavior of the system and ensure its stability for the desired number of turns [15]. This includes factors that could disturb the long-term stability. The algorithm of the normal form transformation is of great value for such problems as it gives a lot of extra information about the disturbing factors. In addition to the fact that the dynamics of particles is represented in a way that is easy to understand, such important characteristics as the strengths of the resonances and the tune shifts with amplitude and various parameters of the system are calculated.

In Chapter 4, details of the optimization of the Tevatron accelerator parameters are discussed. The Tevatron is a large and complicated accelerator complex with lots of features complicating the process of establishing a mathematical model appropriately reflecting the state of the machine. Nonetheless, one can pick out various independent families of the elements of the machine's optics, and use as a figure of merit certain characteristics controlled by each family or a group of families. In the Tevatron at injection, the problem of the skew quadrupole error arises due to the displacement (the so-called cold lift) of the superconducting coils in the main bending dipole magnets, resulting in a skew quadrupole component increase in the magnetic field. Two families of skew quadrupole correctors are used in the Tevatron to minimize the cross-coupling between the horizontal and vertical planes. The problem of finding optimized values for the correctors is stated and solved and the sum of the absolute values of the transfer map terms responsible for the coupling between the two planes is used as an objective function.

The skew quadrupole correction problem was studied by different scientists at Fermilab and the corresponding results can be found in [26,52,53]. At the same time, the problem has never been stated before as that of minimization of the functions (4.1.7) or (4.1.11) and (4.1.13). Also, the differential algebra approach has never been em-

ployed to attempt solving the problem. Certain correction schemes were proposed by the author in collaboration with Dr. Carol Johnstone and Dr. Michael Syphers, and the best scheme was chosen and implemented during the planned Tevatron shutdown in August 2004 with minimal modifications due to additional manpower available to fix more than 50% of the errors in dipoles, which was not the part of the initial problem statement [48]. Two main correction schemes together with the corresponding numerical analysis and visual results are presented in Section 4.1 of Chapter 4.

The calculation of the nonlinear tune shift with amplitude based on the results of measurements and the linear lattice information is discussed in Section 4.2 of Chapter 4. Finding the nonlinear tune shift depending on the position of the particle in the beam might not be an easy task, because the nonlinear component of the dynamics is not known to the desired precision or because there are reasons to doubt the correspondence between the model and the real machine.

At the same time, there is still a way to find the tune shift, if there is a set of specific measurements and some extra information which is usually available, namely that about the geometry of the beam (its size and particle distribution) and the linear optics effect on the particles (in the form of the one-turn linear transfer matrix).

The method to solve this problem uses the potential of the normal form transformation with its advantages to the full extent. In particular, it is known that in the case that there are no resonances in the system, the dynamics in the normal form coordinates is described by a rotation with the amplitude dependent frequency. Besides, as the tune of the particle can be viewed as the limit of the total phase advance divided by the number of turns when the number of turns goes to infinity, the average tune for a large number of turns is the same in both sets of coordinates, as the contribution of the normal form transformation and the inverse normal form

transformation becomes negligible.

Two different flavors of objective functions are introduced in Section 4.2.1, both requiring the tracking of the beam center of mass $r(N)$ for a thousand turns. Expressions for $r(N)$ for various shapes of the beam and distributions of particles in the beam are obtained in Sections 4.2.3 though 4.2.5.

To confirm that the proposed model for the nonlinear tune shift calculation is valid, it is compared to both the numerical results for the nonlinear model of the Tevatron and the independent approximate formula for the tune shift by Meller et al. [40]. Both comparisons lead to similar results: the proposed model shows a discrepancy of less than 2%, which can be considered a very good result taking into account that only the information on the one-turn linear transfer map and the geometry of the beam has been used.

Chapter 5 addresses two problems connected to the Muon Collider storage ring designs. The studies of the dynamics in muon colliders date back to 1960's, when Tikhonin, Budker [17,54] and later Neuffer [42] proposed ideas of accelerating μ^+ and μ^- particles. Muon accelerators form a distinctive class of accelerating structures different from both proton and electron accelerators. The advantage that muons (and electrons) have over protons is that they are truly elementary in the sense of the Standard Model. Thus, when muons collide, they do not divide up the energy load as does a particle that is made up of quarks. Muon–antimuon collisions are therefore clean and the effective collision energy is about 10 times higher than that of the proton beams with the same energy. Muons also have an advantage over electrons. Since muons (and protons) are more massive than electrons, they produce less synchrotron radiation, when in a circular path. There are also drawbacks in using muons: they are unstable and decay rather quickly ($\tau = 2.2\ \mu$sec). This imposes a restriction on

the length of the structure and the intensity of the acceleration. For example, in the case of the 50×50 GeV storage ring, the number of turns for which particles stay in the channel is not more than 1000, since otherwise the loss of luminosity due to the decay is too significant. On the other hand, due to the relativistic effects of increase of lifetime with velocity, this number stays approximately constant independent of the final energy of muons, so for the 750×750 GeV storage ring the number of turns is again of the order of 1000.

The problem of increasing the volume of the part of the phase space that stays stable (not lost) after 1000 turns, and as a result, the number of particles being stored and brought to a collision, represented by the luminosity, is stated and solved in Section 5.1 of Chapter 5.

Basic principles and building blocks of the Muon Collider storage ring are discussed in [5,7,27,28,43,55,56]. After the linear lattice and the chromaticity correction section lattice have been designed to minimize chromatic and geometric aberrations, higher order aberrations must be optimized in order to enhance the system performance. The interaction region is the primary target region for this problem. In general, the more nonlinearities progress to the interaction point, the smaller the dynamic aperture and the momentum acceptance are, which means smaller beam sizes, and hence, lower luminosity. Various methods for solving the problem of this kind for the 50×50 GeV storage ring are discussed. The baseline lattice is described in [28, 55]. Using the existing model and deliberately adding certain high order multipole components to the superconducting final focus magnets to compensate for the nonlinearities of the lattice, one can achieve larger dynamic apertures, and hence better stability and higher luminosity.

The main problem with the task of improving the dynamic aperture of the ac-

celerator channel is a large number of nonlinearities to control, while the number of correctors is limited, and in general one wants to keep this number as small as possible. One very effective approach for achieving the goal is to use the dynamic aperture itself as a figure of merit and try to maximize it using optimization methods. The corresponding objective function is derived in Section 5.1.4, and it is given by Eq. (5.1.3). Other approaches, such as the minimization of the most important aberrations of higher orders or the minimization of the resonance strengths, show less pronounced results. For each of the proposed approaches, the objective functions are introduced in the form of Eqs. (5.1.1) and (5.1.2), correspondingly. The normal form transformation plays an important role in two of the three approaches' implementations, namely, the resonance strength minimization and the dynamic aperture maximization. This transformation allows for the calculation of the values on the right hand side of the equations and for representing the results of different approaches in a uniform way (in one common coordinate system).

The second part of Chapter 5 addresses the issues with a totally different machine, yet intimately connected to the 50×50 GeV Muon Collider storage ring lattice. It is the problem of the design and optimization of the 750×750 GeV storage ring that matches the footprint of the Tevatron accelerator. This lattice has all the same building blocks as its 50×50 GeV counterpart, and thus shares most of the advantages of its clear and highly optimized design.

Each major section is supplied with the results of numerical experiments of applying various optimization methods to the problems stated. The emphasis is made on the efficiency comparison of various approaches and methods.

Various optimization methods, such as the Nelder–Mead simplex method [41], modified Newton method (Levenberg–Marquardt method [33,37]), and the simulated

annealing method [31] are used in the computations.

2. EQUATIONS OF MOTION, FIELDS AND POTENTIALS

2.1 Equations of Motion of the Particles in Accelerators

2.1.1 Curvilinear Coordinates

Consider the motion of the particles in the electromagnetic field [8]:

$$\frac{d\vec{p}}{dt} = q\left(\vec{E} + \vec{v} \times \vec{B}\right). \qquad (2.1.1)$$

Usually when studying the dynamics of particles, the time t plays the role of the independent variable, and the positions $\vec{x}$ and velocities $\vec{v}$ or momenta $\vec{p}$ serve as phase space coordinates. In beam physics it is more convenient to use a system coordinates relative to some reference particle. Besides, instead of the independent variable t the arc length s along the reference orbit is used. In the new coordinates, called *particle optical coordinates*, each point is determined by the state vector

$$\vec{z} = \begin{pmatrix} x \\ y \\ l = k(t - t_0) \\ a = p_x/p_0 \\ b = p_y/p_0 \\ \delta = (E - E_0)/E_0 \end{pmatrix}, \qquad (2.1.2)$$

where x, y are the horizontal and vertical positions of the current particle with respect to the reference particle, l is a space-like variable characterizing the deviation of the current particle from the reference particle in the time of flight $(t - t_0)$ multiplied by a constant k of the dimension of the velocity, a and b are the horizontal and vertical reduced momenta, δ is a relative difference between the total energy of the current particle (E) and reference particle (E_0), and p_0 is the momentum of the reference particle at the beginning.

By this definition of $\vec{z}$, the reference particle corresponds to $\vec{z} = 0$, hence the vector $\vec{z}$ does indeed describe relative motion.

2.1.2 Equations of Motion in Curvilinear Coordinates

Consider the case when the reference orbit is allowed to bend in only one plane. Define the momentary curvature of the reference orbit $h(s)$ as a function of the arc length s. If the curvature is nonzero, the radius of curvature is then given by $R(s) = 1/h(s)$. Consider the bend angle that the reference orbit experiences as we move from position s_0 to position s:

$$\alpha = \int_{\alpha_0}^{\alpha} d\alpha = \int_{s_0}^{s} \frac{ds}{R(s)} = \int_{s_0}^{s} h(s)ds. \tag{2.1.3}$$

The equations of the dynamics in the Cartesian coordinates have the form (2.1.1), or in the integral form

$$\begin{aligned}
\vec{p}(s) &= \vec{p}(s_0) + \int_{t(s_0)}^{t(s)} \vec{F}(t)dt \\
&= \vec{p}(s_0) + \int_{s_0}^{s} \vec{F}(\tilde{s})t'd\tilde{s},
\end{aligned} \tag{2.1.4}$$

where $t' = dt/ds$, and $\vec{F}(s)$ depends on $\vec{x}$ and $\vec{p}$.

The orientation of the locally attached particle optical coordinate system changes from s_0 to $\bar{s}$, as it was rotated by the angle α from Eq. (2.1.3). So in the new local

coordinates

$$\vec{p}_l(\bar{s}) = \begin{pmatrix} \cos \int_{s_0}^{\bar{s}} h\,ds & 0 & \sin \int_{s_0}^{\bar{s}} h\,ds \\ 0 & 1 & 0 \\ -\sin \int_{s_0}^{\bar{s}} h\,ds & 0 & \cos \int_{s_0}^{\bar{s}} h\,ds \end{pmatrix} \cdot \left(\vec{p}(s_0) + \int_{s_0}^{\bar{s}} \vec{F}(s) t'\,ds \right). \qquad (2.1.5)$$

Let $\hat{M}(s_0, \bar{s})$ denote the matrix on the right hand side of Eq. (2.1.5). Differentiating with respect to $\bar{s}$ and evaluating at $s_0 = s$, $\bar{s} = s$ allows to conveniently obtain the rate of change of the momentum $\vec{p}_l$:

$$\begin{aligned} \vec{p}_l(s) &= \left[\hat{M}(s,\bar{s})\vec{F}(\bar{s})t' + \hat{M}'(s,\bar{s}) \left(\vec{p}(s) + \int_s^{\bar{s}} \vec{F}(\tilde{s})t'd\tilde{s} \right) \right]_{\bar{s}=s} \\ &= \vec{F}(s)t' + \begin{pmatrix} 0 & 0 & h(s) \\ 0 & 0 & 0 \\ -h(s) & 0 & 0 \end{pmatrix} \vec{p}(s), \end{aligned} \qquad (2.1.6)$$

where the matrix $\hat{M}$ is unity and the integral on the right hand side is zero under the condition $\bar{s} = s$.

Hence, the first resulting term depends on the actual forces, and the factor t' accounts for the fact that there was a change to s as an independent variable. The second term is a pseudo force due to the fact that we are located in a rotating frame. If there was an out-of-plane motion of the reference orbit allowed, the matrix M would depend on two curvatures. Unfortunately, in this case an additional complication arises from the fact that rotations around different axes do not generally commute.

Now consider the particle having a position $x \neq 0$. In this case

$$\frac{dl}{ds} = \frac{x + R}{R} = 1 + hx, \qquad (2.1.7)$$

$$\frac{dx}{ds} = \frac{dx}{dl}\frac{dl}{ds} = \frac{dx}{dl}(1 + hx) = \frac{dx/ds}{dl/ds}(1 + hx) = (1 + hx)\frac{p_x}{p_s}. \qquad (2.1.8)$$

Similarly for y one obtains

$$\frac{dy}{ds} = (1 + hx)\frac{p_y}{p_s}, \qquad (2.1.9)$$

14

and for the time of flight using the above expressions,

$$\frac{dt}{ds} = \frac{1}{v}\sqrt{\left(\frac{dx}{ds}\right)^2 + \left(\frac{dy}{ds}\right)^2 + \left(\frac{dl}{ds}\right)^2}$$

$$= \frac{1}{v}(1+hx)\sqrt{\frac{p_x^2 + p_y^2 + p_s^2}{p_s^2}} = \frac{1}{v}(1+hx)\frac{p}{p_s}, \qquad (2.1.10)$$

where $p = \sqrt{p_x^2 + p_y^2 + p_s^2}$ and $v = \sqrt{v_x^2 + v_y^2 + v_s^2}$ are the magnitude of momentum and velocity of the particle under consideration.

Therefore, the equations of motion in local coordinates with s as the independent variable were obtained. The next step is to change to particle optical coordinates (2.1.2).

To take into account relativistic effects, it is convenient to introduce the relativistic measure

$$\eta = \frac{E - eV(x,y,s)}{mc^2}, \qquad (2.1.11)$$

characterizing the ratio of kinetic energy to rest mass energy. It follows that

$$\gamma = \frac{1}{\sqrt{1 - \frac{v^2}{c^2}}} = 1 + \eta, \qquad (2.1.12)$$

as

$$E = \gamma mc^2, \; E = mc^2 + K, \; K = (\gamma - 1)mc^2, \; \eta = \frac{K}{mc^2} = \frac{(\gamma - 1)mc^2}{mc^2},$$

and

$$\frac{v}{c} = \sqrt{1 - \left(\frac{1}{1+\eta}\right)^2} = \sqrt{\frac{2\eta + \eta^2}{(1+\eta)^2}}, \qquad (2.1.13)$$

$$\frac{p}{mc} = \frac{mv\gamma}{mc} = \frac{v\gamma}{c} = \sqrt{\eta(2+\eta)}. \qquad (2.1.14)$$

Express the rate of change of the particle optical variable l in terms of particle

15

optical quantities:

$$
\begin{aligned}
l' &= \frac{dl}{ds} = k(t' - t_0') = \frac{k}{v}(1 + hx)\frac{p}{p_s} - kt_0' \\
&= (1 + hx)\frac{k}{p_0}\frac{p_0}{p_s}\frac{p}{v} - \frac{k}{v_0} \\
&= (1 + hx)\frac{k}{p_0}\frac{p_0}{p_s}(1 + \eta)m - \frac{k}{v_0} \\
&= \left[(1 + hx)\frac{1 + \eta}{1 + \eta_0}\frac{p_0}{p_s} - 1\right]\frac{k}{v_0},
\end{aligned}
\tag{2.1.15}
$$

where the following relations have been used:

$$
t_0' = \left[\frac{1}{v}(1 + hx)\frac{p_0}{p_s}\right]_0 = \frac{1}{v_0},
$$

$$
\frac{p}{v} = (1 + \eta)m, \quad \frac{p_0}{v_0} = (1 + \eta_0)m_0.
$$

The next step is to obtain p_0/p_s, which is on the right hand side of the equation (2.1.15):

$$
\frac{p_0}{p_s} = \frac{p_0}{\sqrt{p^2 - p_x^2 - p_y^2}} = \left(\frac{p^2}{p_0^2} - a^2 - b^2\right)^{-\frac{1}{2}} = \left(\frac{\eta(2 + \eta)m^2}{\eta_0(2 + \eta_0)m_0^2} - a^2 - b^2\right)^{-\frac{1}{2}},
\tag{2.1.16}
$$

where the expression for the momentum (2.1.14) is used.

Because it is always true that $\vec{v} \parallel \vec{p}$, it follows that $\vec{v}/v = \vec{p}/p$. This fact is useful for the derivation of the equations for the reduced momenta:

$$
\begin{aligned}
\frac{d}{ds}&\left(\frac{p_x}{p_0}, \frac{p_y}{p_0}, \frac{p_s}{p_0}\right) = \\
&= \frac{1}{p_0}\vec{F}(s)t' + \begin{pmatrix} 0 & 0 & h(s) \\ 0 & 0 & 0 \\ -h(s) & 0 & 0 \end{pmatrix}\frac{\vec{p}}{p_0} = \\
&= ze\vec{E}\frac{t'}{p_0} + ze\frac{\vec{v}}{v} \times \vec{B}(1 + hx)\frac{p}{p_s}\frac{1}{p_0} + h\left(\frac{p_s}{p_0}, 0, -\frac{p_x}{p_0}\right) = \\
&= \frac{\vec{E}}{\chi_{e0}}\left(1 + \frac{l'v_0}{k}\right) + \frac{\vec{p}}{p_0} \times \frac{\vec{B}}{\chi_{m0}}(1 + hx)\frac{p_0}{p_s} + h\left(\frac{p_s}{p_0}, 0, -\frac{p_x}{p_0}\right),
\end{aligned}
\tag{2.1.17}
$$

16

where the following notation has been introduced:

$$\chi_{m0} = \frac{p_0}{ze}, \ \chi_{e0} = \frac{p_0 v_0}{ze}.$$

The first term is transformed according to the following relation:

$$l' = k(t' - t_0'), \ t' = t_0' + \frac{l'}{k} = \frac{1}{v_0}\left(1 + \frac{l' v_0}{k}\right),$$

and in the second term the quantity p is reduced, while the numerator and the denominator have an extra factor of p_0.

The expression $\left(1 + \frac{l' v_0}{k}\right)$ can be transformed using Eq. (2.1.15), so ultimately

$$
\begin{aligned}
\frac{d}{ds}&\left(\frac{p_x}{p_0}, \frac{p_y}{p_0}, \frac{p_s}{p_0}\right) = \\
= \ & \frac{\vec{E}}{\chi_{e0}}(1 + hx)\frac{1 + \eta}{1 + \eta_0}\frac{p_0}{p_s} + \\
+ \ & \left(bB_s - \frac{p_s}{p_0}B_y, \ \frac{p_s}{p_0}B_x - aB_s, \ aB_y - bB_x\right)(1 + hx)\frac{1}{\chi_{m0}}\frac{p_0}{p_s} + \\
+ \ & h\left(\frac{p_s}{p_0}, 0, -\frac{p_x}{p_0}\right).
\end{aligned}
\tag{2.1.18}
$$

The equation for the full energy deviation has a very simple form $\delta' = 0$, as long as there is a conservation of energy. In RF cavities the equation has a more complicated structure, but that is not the issue for the storage rings, where the energy of the particles is constant.

Hence, the equations of motion in particle optical coordinates are

$$
\begin{aligned}
x' &= a(1 + hx)\frac{p_0}{p_s}, & (2.1.19) \\
y' &= b(1 + hx)\frac{p_0}{p_s}, & (2.1.20) \\
l' &= \left[(1 + hx)\frac{1 + \eta}{1 + \eta_0}\frac{p_0}{p_s} - 1\right]\frac{k}{v_0}, & (2.1.21) \\
a' &= (1 + hx)\left[\frac{1 + \eta}{1 + \eta_0}\frac{p_0}{p_s}\frac{E_x}{\chi_{e0}} + b\frac{B_s}{\chi_{m0}}\frac{p_0}{p_s} - \frac{B_y}{\chi_{m0}}\right] + h\frac{p_s}{p_0}, & (2.1.22) \\
b' &= (1 + hx)\left[\frac{1 + \eta}{1 + \eta_0}\frac{p_0}{p_s}\frac{E_y}{\chi_{e0}} - a\frac{B_s}{\chi_{m0}}\frac{p_0}{p_s} + \frac{B_x}{\chi_{m0}}\right], & (2.1.23) \\
\delta' &= 0, & (2.1.24)
\end{aligned}
$$

17

where η is determined by Eq. (2.1.11), and $\frac{p_0}{p_s}$ — by Eq. (2.1.16).

2.2   Fields and Potentials

A large part of the problems of electrodynamics is described by the set of laws expressed by the system of Maxwell's equations. In the international system of units (SI), these equations have the following form:

$$\begin{cases} \vec{\nabla} \cdot \vec{D} = \rho \text{ (Coulomb's law)}, \\ \vec{\nabla} \cdot \vec{B} = 0 \text{ (absence of magnetic monopoles)}, \\ \vec{\nabla} \times \vec{E} + \dfrac{\partial \vec{B}}{\partial t} = \vec{0} \text{ (Faraday's law)}, \\ \vec{\nabla} \times \vec{H} - \dfrac{\partial \vec{D}}{\partial t} = \vec{J} \text{ (Ampere's law)}, \end{cases} \tag{2.2.1}$$

where $\vec{D}$ is the vector of the electric flux density, ρ is the charge density, $\vec{B}$ is the magnetic flux density, $\vec{E}$ is the vector of the electric field, $\vec{H}$ is the vector of the magnetic field, and $\vec{J}$ is the electric current density.

The system of equations (2.2.1) is not closed, three more equations need to be established: the so-called constitutive relations connecting $\vec{D}$ with $\vec{E}$ and $\vec{H}$ with $\vec{B}$, and one more relation connecting $\vec{J}$ with $\vec{E}$. The first two of them have the following general form:

$$\begin{aligned} \vec{D} &= \varepsilon_0 \vec{E} + \vec{P}, \\ \vec{B} &= \mu_0 \vec{H} + \vec{M}, \end{aligned} \tag{2.2.2}$$

where $\vec{P}, \vec{M}$ are the vectors of electric and magnetic polarization of the medium; ε_0, μ_0 are the electric permittivity constant (dielectric constant of vacuum) and the magnetic permeability constant of vacuum, respectively.

In the case of a homogeneous and isotropic medium, the equations (2.2.2) are simplified, and besides, there is often one more relation, namely, Ohm's law for the

18

linear medium:

$$\vec{D} = \varepsilon\vec{E},$$

$$\vec{B} = \mu\vec{H}, \tag{2.2.3}$$

$$\vec{J} = \sigma\vec{E}.$$

Here $\vec{P}, \vec{M}$ are proportional to the field applied, and hence, their influence can be included in the form of new constants. Therefore, ε, μ characterize the medium and are referred to as the relative electric permittivity (dielectric constant) and the relative magnetic permeability, respectively. The constant σ characterizes the electric conductivity of the matter.

In many cases, it is of interest to study Maxwell's equations in the absence of matter at the point of interest. In this case

$$\rho = 0; \quad \vec{J} = \vec{0}. \tag{2.2.4}$$

Thus, Maxwell's equations take the simplified form:

$$\begin{cases} \vec{\nabla} \cdot \vec{D} = 0, \\ \vec{\nabla} \cdot \vec{B} = 0, \\ \vec{\nabla} \times \vec{E} = -\dfrac{\partial \vec{B}}{\partial t}, \\ \vec{\nabla} \times \vec{H} = \dfrac{\partial \vec{D}}{\partial t}, \end{cases} \tag{2.2.5}$$

and in the stationary case

$$\begin{cases} \vec{\nabla} \cdot \vec{E} = 0, \\ \vec{\nabla} \cdot \vec{B} = 0, \\ \vec{\nabla} \times \vec{E} = 0, \\ \vec{\nabla} \times \vec{B} = 0. \end{cases} \tag{2.2.6}$$

2.2.1 Fields and Potentials of the Magnetic Multipole (Stationary Case)

As a rule, the guiding magnets of the accelerating structure create a field which changes slowly with time or does not change at all, and the beam of particles being controlled by the magnets is inside a vacuum beam pipe. Therefore, one can use Eqs. (2.2.6). There is one limitation however, in that this model does not take into account the interaction of the particles. Nonetheless, in most cases this is not a significant limitation, and if necessary, the particle interaction and beam-beam effects can be considered separately.

In most cases only the magnetic component of the electromagnetic field is used for focusing purposes, as the particles are running in the beam tube with the velocity compared to that of light, and for this ultra-relativistic case a moderate magnetic field of 1 T corresponds to a huge electric field of $3 \cdot 10^8$ V/m, which is very hard to create and control.

In various sources the multipole expansion for the transversal guide field described below is treated differently [12, 57]: expansion of the magnetic field $\vec{B}$, expansion of the magnetic vector potential $\vec{A}$, expansion of the scalar potential V, using cylindrical or Cartesian coordinates. The most appropriate approach is chosen for the specific problem, but the physical meaning is always the same.

Consider the transversal dynamics of the particle. Denote $z = x + iy$, where x is the horizontal displacement of the particle from the magnet axis, y is the vertical displacement (the "verticality" and "horizontality" are relative to the plane of the orbit of the reference particle). Assuming that the edge field contribution is negligibly

small, the second equation of (2.2.6) yields:

$$\text{div}\vec{B} = \vec{\nabla} \cdot B = 0 \quad \Rightarrow \quad B = \vec{\nabla} \times \vec{A} = \text{rot}\vec{A}, \tag{2.2.7}$$

where $\vec{A}$ is the vector potential of the magnetic field. As the magnetic field is transversal, the vector potential has only one component A_s in the direction of the motion of the particles. The fourth equation of the system (2.2.6) yields that

$$\text{rot}\vec{B} = \vec{0} \quad \Rightarrow \quad \vec{B} = -\vec{\nabla}V, \tag{2.2.8}$$

where V is the scalar potential of the stationary transversal magnetic field.

Combining Eqs. (2.2.7) and (2.2.8), one obtains

$$B_x = -\frac{\partial V}{\partial x} = \frac{\partial A_s}{\partial y} \quad \text{and} \quad B_y = -\frac{\partial V}{\partial y} = -\frac{\partial A_s}{\partial x}. \tag{2.2.9}$$

Define a complex potential as a function of $z = x + iy$ in the following way:

$$\tilde{A}(z) = A_s(x,y) + iV(x,y) = A_s(z) + iV(z). \tag{2.2.10}$$

Then Eqs. (2.2.9) are the Cauchy-Riemann conditions for $\tilde{A}(z)$. Therefore, the complex potential is an analytic function and can be expanded in a power series

$$\tilde{A}(z) = \sum_{n=0}^{+\infty} \kappa_n z^n; \qquad \kappa_n = \lambda_n + i\mu_n; \tag{2.2.11}$$

where λ_n, μ_n are real constants.

The expansion (2.2.11) converges inside a circle $|z| < r_c$, where r_c is the minimal distance between the origin of the expansion and the iron yoke or the superconducting coil or any other field source causing the non-homogeneity to appear on the right hand side of Eq. (2.2.8). As a result, Eq. (2.2.9) does not hold anymore.
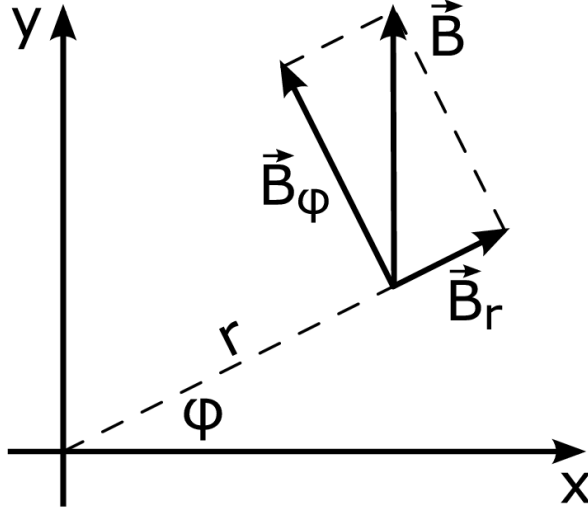
Fig. 2.1. Axes orientation for the cylindrical coordinates

2.2.2 Multipole Expansion in Cylindrical Coordinates

In many cases it is convenient to express the field in cylindrical coordinates (r, φ, s), such that

$$
\begin{cases} x = r \cos \varphi \\ y = r \sin \varphi \end{cases}. \tag{2.2.12}
$$

In this case $z^n = r^n e^{in\varphi} = r^n(\cos n\varphi + i \sin n\varphi)$. Eqs. (2.2.10), (2.2.11) yield that

$$
\begin{aligned}
V(r, \varphi) &= \sum_{n=0}^{+\infty} (\mu_n \cos n\varphi + \lambda_n \sin n\varphi) r^n, \tag{2.2.13} \\
A_s(r, \varphi) &= \sum_{n=0}^{+\infty} (\lambda_n \cos n\varphi - \mu_n \sin n\varphi) r^n.
\end{aligned}
$$

Using Eqs. (2.2.8) and (2.2.13), one can get the expansion of the magnetic field in cylindrical coordinates (see Fig. 2.1).

$$
\begin{aligned}
B_\varphi &= -\frac{1}{r}\frac{\partial V}{\partial \varphi} = -\sum_{n=1}^{+\infty} n(\lambda_n \cos n\varphi - \mu_n \sin n\varphi) r^{n-1}, \\
B_r &= -\frac{\partial V}{\partial r} = -\sum_{n=1}^{+\infty} n(\mu_n \cos n\varphi + \lambda_n \sin n\varphi) r^{n-1}.
\end{aligned} \tag{2.2.14}
$$

22

Let us introduce the following notation: r_0 is the reference radius for the multipole expansion, usually chosen to be equal to the maximum deviation of the particles in the beam from the reference orbit; B_{main} is the main field component of the magnet under consideration; b_n is the so-called "normal" multipole coefficient, and a_n is a "skew" multipole coefficient, defined as follows:

$$b_n = -\frac{n\lambda_n}{B_{main}} r_0^{n-1} \quad \text{and} \quad a_n = \frac{n\mu_n}{B_{main}} r_0^{n-1}. \tag{2.2.15}$$

The meaning of the notation becomes clear from Eq. (2.2.20) below. Using this notation,

$$B_\varphi(r,\varphi) = B_{main} \sum_{n=1}^{+\infty} (b_n \cos n\varphi + a_n \sin n\varphi) \left(\frac{r}{r_0}\right)^{n-1}, \tag{2.2.16}$$

$$B_r(r,\varphi) = B_{main} \sum_{n=1}^{+\infty} (-a_n \cos n\varphi + b_n \sin n\varphi) \left(\frac{r}{r_0}\right)^{n-1}, \tag{2.2.17}$$

$$V(r,\varphi) = -B_{main} r_0 \sum_{n=1}^{+\infty} (-\frac{a_n}{n} \cos n\varphi + \frac{b_n}{n} \sin n\varphi) \left(\frac{r}{r_0}\right)^{n}, \tag{2.2.18}$$

$$A_s(r,\varphi) = -B_{main} r_0 \sum_{n=1}^{+\infty} (\frac{b_n}{n} \cos n\varphi + \frac{a_n}{n} \sin n\varphi) \left(\frac{r}{r_0}\right)^{n}, \tag{2.2.19}$$

where each value of n corresponds to the $2n$-pole component of the field. For an ideal $2n$-pole magnet, $b_n = 1$, while all other coefficients vanish.

Consider

$$B_\varphi + iB_r = B_{main} \sum_{n=1}^{+\infty} \left(\frac{r}{r_0}\right)^{n-1} (b_n(\cos n\varphi + i\sin n\varphi) - ia_n(\cos n\varphi + i\sin n\varphi)),$$

$$B_\varphi + iB_r = B_{main} \sum_{n=1}^{+\infty} \left(\frac{r}{r_0}\right)^{n-1} (b_n - ia_n)e^{in\varphi}.$$

This representation allows to find the strength of the $2n$-pole component:

$$(|\vec{B}|)_n = \left(\sqrt{B_r^2 + B_\varphi^2}\right)_n = B_{main} \left(\frac{r}{r_0}\right)^{n-1} \sqrt{b_n^2 + a_n^2}. \tag{2.2.20}$$

Eq. (2.2.20) yields that the magnitude of the $2n$-pole component does not depend on the azimuthal angle and scales with the $(n-1)$-th power of r; a_n and b_n are the relative field contribution of the nth multipole component to the main field at the reference radius $r = r_0$. This is the reason for the normalization given by Eq. (2.2.15).

Applications of the cylindrical coordinate representation include:

- Superconducting magnets design, where it is convenient to find the arrangement of the current coils;

- Multipole component measurement with a coil rotating in the field, where the induced voltage is proportional to $\sqrt{b_n^2 + a_n^2}$, while its phase is related to a_n/b_n;

- Problems where it is easy to see which multipole components are forbidden, if specific symmetry properties of the field are assumed.

2.2.3   Multipole Expansion in Cartesian Coordinates

In Cartesian coordinates the expansion (2.2.11) assumes the form

$$\tilde{A}(z) = \sum_{n=0}^{+\infty} \kappa_n z^n = \sum_{n=0}^{+\infty} (\lambda_n + i\mu_n)(x + iy)^n. \qquad (2.2.21)$$

Separation of real and imaginary parts of Eq. (2.2.21), yields the following using

the notation introduced in Eq. (2.2.15):

$$
\begin{aligned}
A_s(x,y) \;=\;& \operatorname{Re}\sum_{n=0}^{+\infty}\kappa_n z^n = -B_{main}\Big\{b_1 x + a_1 y + \frac{b_2}{2r_0}(x^2 - y^2) + \frac{a_2}{r_0}xy + \\
&+ \frac{b_3}{3r_0^2}(x^3 - 3xy^2) + \frac{a_3}{3r_0^2}(3x^2 y - y^3) + \\
&+ \frac{b_4}{4r_0^3}(x^4 - 6x^2 y^2 + y^4) + \frac{a_4}{r_0^3}(x^3 y - xy^3) + \dots\Big\},
\end{aligned}
\tag{2.2.22}
$$

$$
\begin{aligned}
V(x,y) \;=\;& \operatorname{Im}\sum_{n=0}^{+\infty}\kappa_n z^n = B_{main}\Big\{a_1 x - b_1 y + \frac{a_2}{2r_0}(x^2 - y^2) - \frac{b_2}{r_0}xy + \\
&+ \frac{a_3}{3r_0^2}(x^3 - 3xy^2) - \frac{b_3}{3r_0^2}(3x^2 y - y^3) + \\
&+ \frac{a_4}{4r_0^3}(x^4 - 6x^2 y^2 + y^4) - \frac{b_4}{r_0^3}(x^3 y - xy^3) + \dots\Big\}.
\end{aligned}
\tag{2.2.23}
$$

Similar to the case of cylindrical coordinates, the components of the magnetic field can be obtained by virtue of Eq. (2.2.8):

$$
\begin{aligned}
B_x(x,y) \;=\;& -\frac{\partial V}{\partial x} = B_{main}\Big\{-a_1 + \frac{b_2}{r_0}y - \frac{a_2}{r_0}x - \frac{a_3}{r_0^2}(x^2 - y^2) + \frac{b_3}{r_0^2}2xy - \\
&+ \frac{a_4}{r_0^3}(x^3 - 3xy^2) + \frac{b_4}{r_0^3}(3x^2 y - y^3) + \dots\Big\},
\end{aligned}
\tag{2.2.24}
$$

$$
\begin{aligned}
B_y(x,y) \;=\;& -\frac{\partial V}{\partial y} = B_{main}\Big\{b_1 + \frac{a_2}{r_0}y - \frac{b_2}{r_0}x + \frac{a_3}{r_0^2}2xy + \frac{b_3}{r_0^2}(x^2 - y^2) + \\
&+ \frac{a_4}{r_0^3}(3x^2 y - y^3) + \frac{b_4}{r_0^3}(x^3 - 3xy^2) + \dots\Big\}.
\end{aligned}
\tag{2.2.25}
$$

Applications of the Cartesian coordinate representation:

- If the dynamics of particles is described in Cartesian coordinates, it is easy to identify the contribution of each individual multipole to the equation of motion. For example, if all the "skew" coefficients a_n vanish, a flat beam ($y \equiv 0$) remains flat, which means there is no coupling of the horizontal motion into the vertical motion;

- Each term in the representation (2.2.23) describes the shape of the magnet pole, creating the field, as this contour is an equipotential surface.

Note that in the case of the electrostatic focusing elements, the derivation of the formulas for fields and potentials will follow the above scheme due to the equivalence of the first equation to the second and also that of the third equation to the fourth equation of the system (2.2.6). On the other hand, as it was mentioned in the beginning of the section, in most cases using the magnetic fields for the focusing purposes is much more convenient.

Now, as the representations for the scalar magnetic potential V and the components of the magnetic field $\vec{B}$ have been found in both cylindrical and Cartesian coordinates, one can return to the equations of motion of the particles (2.1.19–2.1.24), and claim that all the quantities on the right hand side are known as functions of fields and potentials: $\eta = \eta(V)$, $\vec{B} = (B_x, B_y, B_s)$, $\vec{E} = (E_x, E_y, E_s)$.

3. NORMAL FORM ALGORITHMS

Normal form algorithms are used throughout this dissertation work, and the problems considered in Chapters 4 and 5 make use of the algorithm either in the main optimization step, or for better representation and visualization of the results obtained. The main ideas of the nonlinear normal form transformation algorithm are presented in [9, 12]. The idea of this chapter is to introduce the notation used in the subsequent chapters and place more emphasis on the steps of the algorithm which are not in the book and might not be obvious. All the systems considered in the dissertation are symplectic, so the emphasis is made on the normal form transformation algorithm for the systems satisfying the symplecticity condition.

3.1   Nonlinear Normal Form Transformation

The idea of the transformation is to find such a nonlinear change of variables that the motion in the new variables, up to a certain order, is circular with an amplitude-dependent frequency.

Consider the nonlinear transfer map [8, 12, 47] of a particle optical system

$$\vec{z}_f = \mathcal{M}(\vec{z}_i, \vec{\delta}), \tag{3.1.1}$$

where $\vec{z}$ is the vector of $2v$ phase space coordinates, $\vec{\delta}$ is the vector of parameters of the system, $\vec{z}_i$ is the initial state of the system, and $\vec{z}_f$ is its final state. Thus, $\mathcal{M}$ is

the function connecting the initial and final states of the system for some interval of time.

The transformation to the normal form coordinates consists of a sequence of non-linear coordinate transformations of the form

$$\mathcal{N} = \mathcal{A} \circ \mathcal{M} \circ \mathcal{A}^{-1}, \tag{3.1.2}$$

where $\circ$ denotes a composition of transfer maps.

Assume that the transformation matrix satisfies the following relation:

$$\mathcal{M}(\vec{0}, \vec{\delta}) = (\vec{0}, \vec{\delta}). \tag{3.1.3}$$

If this does not hold, one can find the fixed point and transform the map to this fixed point, and therefore the new transfer map satisfies Eq. (3.1.3). To be able to do this it should be assumed that none of the eigenvalues of the linear part of the map is 1, which is always the case for stable multi-turn systems. Also, if the map has certain parameters (the vector $\vec{\delta}$ is not empty), $\mathcal{M} - \mathcal{I}_H$ must be invertible, where $\mathcal{I}_H$ is the block matrix with a square unity submatrix $2v \times 2v$ in the upper-left corner and all the other elements are zeros.

The first step of the transformation to the normal form coordinates is the diagonalization of the linear part of the map. This can only be done with the assumption that all the $2v$ eigenvalues are different. For most of the circular accelerators this does not represent a limitation.

All the eigenvalues can be written as complex conjugate pairs $r_j e^{\pm i\mu_j}$, as in [12], where for the stable symplectic systems $r_j = 1$ and μ_j is real $\forall j = \overline{1, v}$. In the basis of the complex conjugate vectors $\vec{v}_j^{\pm}$ corresponding to the complex conjugate

eigenvalues the linear part of the transfer map has the following form:

$$
\mathcal{R} = \begin{pmatrix} r_1 e^{i\mu_1} & 0 & \cdots & 0 & 0 \\ 0 & r_1 e^{-i\mu_1} & \cdots & 0 & 0 \\ \vdots & \vdots & \ddots & \vdots & \vdots \\ 0 & 0 & \cdots & r_v e^{i\mu_v} & 0 \\ 0 & 0 & \cdots & 0 & r_v e^{-i\mu_v} \end{pmatrix}.
\tag{3.1.4}
$$

After the diagonal form of the linear transfer map is found, one proceeds to a sequence of order-by-order transformations, each of which affects only one particular order of nonlinearities. The aim of the transformation is to simplify the nonlinear part of the transfer map as much as possible, ideally removing all the nonlinear elements up to a certain order.

At the mth step one divides the transfer map into the linear part $\mathcal{R}$ and the part $\mathcal{S}_m$, containing all the nonlinearities. If the previous step was successful, the map $\mathcal{S}_m$ contains only the terms of order m and higher.

The desired transformation has the form

$$
\mathcal{A}_m = \mathcal{I} + \mathcal{T}_m,
\tag{3.1.5}
$$

where $\mathcal{T}_m$ vanishes to order $m - 1$. As the linear part of $\mathcal{A}_m$ is invertible, the map $\mathcal{A}_m$ itself is invertible [12], and the inverse to order m is

$$
\mathcal{A}_m^{-1} =_m \mathcal{I} - \mathcal{T}_m.
\tag{3.1.6}
$$

After the transformation, one has up to order m

$$
\begin{aligned}
\mathcal{A}_m \circ \mathcal{M} \circ \mathcal{A}_m^{-1} &=_m \\
&=_m (\mathcal{I} + \mathcal{T}_m) \circ (\mathcal{R} + \mathcal{S}_m) \circ (\mathcal{I} - \mathcal{T}_m) =_m \\
&=_m (\mathcal{I} + \mathcal{T}_m) \circ (\mathcal{R} - \mathcal{R} \circ \mathcal{T}_m + \mathcal{S}_m) =_m \\
&=_m \mathcal{R} - \mathcal{R} \circ \mathcal{T}_m + \mathcal{S}_m + \mathcal{T}_m \circ \mathcal{R} =_m \\
&=_m \mathcal{R} + \mathcal{S}_m + (\mathcal{T}_m \circ \mathcal{R} - \mathcal{R} \circ \mathcal{T}_m).
\end{aligned}
\tag{3.1.7}
$$

29

The goal is to simplify the terms of order m of $\mathcal{M}$, or in other words, it is necessary to find $\mathcal{T}_m$ such that $\mathcal{S}_m = -\mathcal{C}_m$, where $\mathcal{C}_m = (\mathcal{T}_m \circ \mathcal{R} - \mathcal{R} \circ \mathcal{T}_m)$. If the range of $\mathcal{C}_m$ is the full space, $\mathcal{S}_m$ can be removed entirely. However, there are circumstances limiting the range of $\mathcal{C}_m$.

Consider the representation of the unknown $\mathcal{T}_m$ in the form of the Taylor polynomial of degree m in the eigenvector basis. Hereafter, the pairs $s_j^{\pm} \ \forall j = \overline{1, v}$ denote the coordinates in this basis.

$$\begin{cases} \mathcal{T}_{mj}^{+} = \sum (\mathcal{T}_{mj}^{+}|\vec{k}^{+}, \vec{k}^{-}) \cdot (s_1^{+})^{k_1^{+}} (s_1^{-})^{k_1^{-}} \ldots (s_v^{+})^{k_v^{+}} (s_v^{+})^{k_v^{+}} \\ \mathcal{T}_{mj}^{-} = \sum (\mathcal{T}_{mj}^{-}|\vec{k}^{+}, \vec{k}^{-}) \cdot (s_1^{+})^{k_1^{+}} (s_1^{-})^{k_1^{-}} \ldots (s_v^{+})^{k_v^{+}} (s_v^{+})^{k_v^{+}} \end{cases}, \tag{3.1.8}$$

where $(\mathcal{T}_{mj}^{+}|\vec{k}^{+}, \vec{k}^{-})$ are the coefficients of the corresponding orders in the expansion, $\vec{k}^{+} = (k_1^{+}, \ldots, k_v^{+})$, and $\vec{k}^{-} = (k_1^{-}, \ldots, k_v^{-})$.

Derive the equation expressing the coefficient $\mathcal{T}_m$ in terms of the known components of $\mathcal{S}_m$. It is true that $\mathcal{C}_m = (\mathcal{T}_m \circ \mathcal{R} - \mathcal{R} \circ \mathcal{T}_m)$, and also the form of $\mathcal{R}$ is given by Eq. (3.1.4). Besides that, the goal is to achieve $\mathcal{C}_{mj} = -\mathcal{S}_{mj}$. Hence,

$$\begin{aligned} -(\mathcal{S}_{mj}^{\pm}|\vec{k}^{+}, \vec{k}^{-}) &= (\mathcal{C}_{mj}^{\pm}|\vec{k}^{+}, \vec{k}^{-}) = \\ &= \left(\{\mathcal{T}_m \circ \mathcal{R} - \mathcal{R} \circ \mathcal{T}_m\}_{mj}^{\pm}|\vec{k}^{+}, \vec{k}^{-}\right) = \\ &= \left(\prod_{l=1}^{2v} \lambda_l - \lambda_j\right) \cdot (\mathcal{T}_{mj}^{\pm}|\vec{k}^{+}, \vec{k}^{-}) = \\ &= \left(\left(\prod_{l=1}^{v} r_l^{k_l^{+} + k_l^{-}}\right) \cdot e^{i\vec{\mu}(\vec{k}^{+} - \vec{k}^{-})} - r_j \cdot e^{\pm i\mu_j}\right) \cdot (\mathcal{T}_{mj}^{\pm}|\vec{k}^{+}, \vec{k}^{-}), \end{aligned} \tag{3.1.9}$$

where $\lambda_{2j-1} = r_j e^{+i\mu_j}$, $\lambda_{2j} = r_j e^{-i\mu_j}$, and $j = \overline{1, v}$ are the eigenvalues of the linear part of $\mathcal{M}$, or ultimately,

$$(\mathcal{T}_{mj}^{\pm}|\vec{k}^{+}, \vec{k}^{-}) = \frac{-(\mathcal{S}_{mj}^{\pm}|\vec{k}^{+}, \vec{k}^{-})}{\left(\left(\prod_{l=1}^{v} r_l^{k_l^{+} + k_l^{-}}\right) \cdot e^{i\vec{\mu}(\vec{k}^{+} - \vec{k}^{-})} - r_j \cdot e^{\pm i\mu_j}\right)}. \tag{3.1.10}$$

The algorithm efficiency, therefore, depends on the conditions for which the denominator in the equation (3.1.10) is zero. In this case it is not possible to eliminate all the elements of $\mathcal{S}_m$. The next section addresses such conditions for the specific case of r_j and μ_j.

3.2 Stable Symplectic Case, Nonlinear Tune Shift with Amplitude

In the case of the stable symplectic system, all the r_j's are equal to 1, all the μ_j's are purely real, and the condition for (3.1.10) to become zero can be written as

$$\vec{\mu} \cdot (\vec{k}^+ - \vec{k}^-) = \pm \mu_j \quad \text{mod } 2\pi, \tag{3.2.1}$$

where the sign on the right hand side corresponds to the member of the pair $\vec{v}_j^{\pm}$.

Assume the equation $\vec{\mu} \cdot \vec{n} = 0 \mod 2\pi$ does not have any nontrivial solutions. In this case, the only way Eq. (3.2.1) can hold is

$$k_l^+ = k_l^- \ \forall \, l \neq j, \ k_j^+ = k_j^- \pm 1. \tag{3.2.2}$$

Proposition 3.2.1: *In the basis comprised of the complex conjugate vectors, $\overline{\mathcal{T}_{mj}^+} = \mathcal{T}_{mj}^-$ as the polynomials of $s_1^+, s_1^-, \ldots, s_v^+, s_v^-$. The same holds true for the pairs $\mathcal{S}_{mj}^+, \mathcal{S}_{mj}^-$.*

Proof. First of all, prove that $\mathcal{S}_{mj}^{\pm}$ are the complex conjugate functions of $s_1^+, s_1^-, \ldots, s_v^+, s_v^-$. As after the diagonalization all the variables are split into independent pairs, it is sufficient to show that the proposition holds true for one such pair.

$$\mathcal{A}^{-1} = \left(\vec{v}_1^+, \vec{v}_1^-, \cdots, \vec{v}_v^+, \vec{v}_v^- \right); \qquad \mathcal{A} = \left(\vec{v}_1^+, \vec{v}_1^-, \cdots, \vec{v}_v^+, \vec{v}_v^- \right)^{-1}. \tag{3.2.3}$$

According to Eq. (3.2.3), in the case of one pair of variables

$$\mathcal{A}^{-1} = \left(\vec{v}^+, \vec{v}^-\right), \qquad \mathcal{A} = \left(\vec{v}^+, \vec{v}^-\right)^{-1}, \tag{3.2.4}$$

where the indices of $\vec{v}^+$ and $\vec{v}^-$ are left out. As $\overline{\vec{v}^+} = \vec{v}^-$,

$$\mathcal{A}^{-1} = \begin{pmatrix} a + ib & a - ib \\ c + id & c - id \end{pmatrix} = \left(\vec{v}^+, \overline{\vec{v}^+}\right); \tag{3.2.5}$$

$$\mathcal{A} = \frac{i}{2(ad - bc)} \begin{pmatrix} c - id & -a + ib \\ -c - id & a + ib \end{pmatrix}. \tag{3.2.6}$$

$$\mathcal{A} \circ \mathcal{M} \circ \mathcal{A}^{-1} = \mathcal{R} + \mathcal{A} \circ \mathcal{N} \circ \mathcal{A}^{-1}, \tag{3.2.7}$$

where $\mathcal{N}$ contains all the nonlinear components of the map $\mathcal{M}$. Consider

$$\mathcal{N} \circ \mathcal{A}^{-1} \begin{pmatrix} s^+ \\ s^- \end{pmatrix} = \begin{pmatrix} \mathcal{N}_1((a + ib)s^+ + (a - ib)s^-; (c + id)s^+ + (c - id)s^-) \\ \mathcal{N}_2((a + ib)s^+ + (a - ib)s^-; (c + id)s^+ + (c - id)s^-) \end{pmatrix}. \tag{3.2.8}$$

$$(a + ib)s^+ + (a - ib)s^- = a(s^+ + s^-) + ib(s^+ - s^-),$$
$$(c + id)s^+ + (c - id)s^- = c(s^+ + s^-) + id(s^+ - s^-). \tag{3.2.9}$$

Before the coordinate transformation, all the coordinates of the vectors under consideration were real. The matrix $\mathcal{A}^{-1}$ gives the transformation back to the old coordinates. Hence the left hand side of Eq. (3.2.9) is purely real, which means $s^+ + s^-$ is purely real, while $s^+ - s^-$ is purely imaginary.

As $\mathcal{N}_1$ and $\mathcal{N}_2$ are the polynomials with real coefficients (Taylor polynomials of the original map $\mathcal{M}$, of which all the elements are real), and hence the values of these polynomials after s^+ and s^- are substituted, will be real:

$$\mathcal{N}_1((a + ib)s^+ + (a - ib)s^-; (c + id)s^+ + (c - id)s^-) =$$
$$\mathcal{N}_1(a(s^+ + s^-) + ib(s^+ - s^-); c(s^+ + s^-) + id(s^+ - s^-)) = \eta_1 \in \mathbb{R},$$
$$\mathcal{N}_2((a + ib)s^+ + (a - ib)s^-; (c + id)s^+ + (c - id)s^-) =$$
$$\mathcal{N}_2(a(s^+ + s^-) + ib(s^+ - s^-); c(s^+ + s^-) + id(s^+ - s^-)) = \eta_2 \in \mathbb{R}. \tag{3.2.10}$$

Denote

$$\frac{1}{2(ad - bc)} = \kappa, \tag{3.2.11}$$

then the ultimate form of the transformation to the new coordinates is

$$\mathcal{A} \circ \mathcal{N} \circ \mathcal{A}^{-1} \begin{pmatrix} s^+ \\ s^- \end{pmatrix} = \kappa \begin{pmatrix} i(c - id) & -i(a - ib) \\ -i(c + id) & i(a + ib) \end{pmatrix} \begin{pmatrix} \eta_1 \\ \eta_2 \end{pmatrix} =$$

$$= \kappa \begin{pmatrix} (d + ic)\eta_1 - (b + ia)\eta_2 \\ (d - ic)\eta_1 - (b - ia)\eta_2 \end{pmatrix} =$$

$$= \kappa \begin{pmatrix} (d\eta_1 - b\eta_2) + i(c\eta_1 - a\eta_2) \\ (d\eta_1 - b\eta_2) - i(c\eta_1 - a\eta_2) \end{pmatrix}. \tag{3.2.12}$$

All the expressions in the parentheses are real, and hence $\mathcal{S}_{mj}^{\pm}$ are a pair of complex conjugate polynomials of s^+, s^-.

To show that $\overline{\mathcal{T}_{mj}^+} = \mathcal{T}_{mj}^-$, it suffices to consider the denominators of (3.1.10) and assure that they are complex conjugate as well.

In the symplectic case all $r_j = 1$, and hence the expression for the denominator reduces to

$$e^{i\vec{\mu}} \cdot (\vec{k}^+ - \vec{k}^-) - e^{\pm i\mu_j}. \tag{3.2.13}$$

By virtue of

$$\begin{cases} k_l^+ = k_l^- \ \forall l \neq j \\ k_j^+ = k_j^- \pm 1 \end{cases}, \tag{3.2.14}$$

one can obtain

$$\vec{k}^+ - \vec{k}^- = (0, \ldots, 0, \pm 1, 0, \ldots, 0),$$

with ± 1 at the position j. Hence,

$$e^{i\vec{\mu} \cdot (\vec{k}^+ - \vec{k}^-)} = e^{\pm i\mu_j}.$$

It is necessary to show that

$$\overline{e^{\pm i\mu_j} - e^{+i\mu_j}} = e^{\mp i\mu_j} - e^{-i\mu_j}. \tag{3.2.15}$$

33

Depending on the sign, there are two cases:

⊕:

$$\overline{e^{+i\mu_j} - e^{+i\mu_j}} = \overline{0} = 0 = e^{-i\mu_j} - e^{-i\mu_j};$$

⊖:

$$\overline{e^{-i\mu_j} - e^{+i\mu_j}} = e^{+i\mu_j} - e^{-i\mu_j}.$$

In both cases Eq. (3.2.15) holds, which completes the proof of the proposition. ∎

According to the proposition above, in the symplectic stable case the elements of the transfer map in the new coordinates $s_1^+, s_1^-, \ldots, s_v^+, s_v^-$ corresponding to the pairs of the complex conjugate eigenvectors $\vec{v}_1^\pm \ldots \vec{v}_v^\pm$ have the form

$$\begin{cases} \mathcal{M}_j^+ = s_j^+ \cdot f_j(s_1^+ s_1^-, \ldots, s_v^+ s_v^-) \\ \mathcal{M}_j^- = s_j^- \cdot \overline{f_j}(s_1^+ s_1^-, \ldots, s_v^+ s_v^-) \end{cases}. \tag{3.2.16}$$

The fact that s_j^+ in the first line and s_j^- in the second line can be taken outside the parentheses, and that f depends only on the products of the form $s_j^+ s_j^-$, follows from the condition (3.2.2):

s_j^+:

$$k_j^+ = k_j^- + 1;\ (s_j^+)^{k_j^+} (s_j^-)^{k_j^-} = (s_j^+)^{k_j^-} s_j^+ (s_j^-)^{k_j^-} = s_j^+ (s_j^+ s_j^-)^{k_j^-};$$

s_j^-:

$$k_j^+ = k_j^- - 1;\ (s_j^+)^{k_j^+} (s_j^-)^{k_j^-} = (s_j^+)^{k_j^+} (s_j^-)^{k_j^+} s_j^- = s_j^- (s_j^+ s_j^-)^{k_j^+}.$$

The conjugation in the second line of Eq. (3.2.16) follows from Proposition 3.2.1 and the fact that $\overline{s_j^+} = s_j^-$ as the coordinates in the complex conjugate vector basis. Indeed, if the basis vectors are complex conjugate, the rows of the matrix $\mathcal{A}$ will be complex conjugate as well, and hence s_j^+ and s_j^- are complex conjugate. Thus, from Eq. (3.2.12) the result in Eq. (3.2.16) follows for arbitrary $\eta_1, \eta_2 \in \mathbb{R}$.

34

It is not convenient to work with the pairs $s_j^{\pm}$ for the purpose of obtaining the ultimate equation for $\mathcal{M}_j^{\pm}$, therefore the resulting map is expressed in terms of the pairs $t_j^{\pm}$, such that

$$\begin{cases} t_j^+ = (s_j^+ + s_j^-)/2 \\ t_j^- = (s_j^+ - s_j^-)/2i \end{cases}.$$

(3.2.17)

Then

$$\begin{cases} s_j^+ = t_j^+ + it_j^- \\ s_j^- = t_j^+ - it_j^- \end{cases},$$

(3.2.18)

$$s_j^+ \cdot s_j^- = (t_j^+)^2 + (t_j^-)^2,$$

$$\mathcal{A} = \frac{1}{2}\begin{pmatrix} 1 & 1 \\ -i & i \end{pmatrix}; \quad \mathcal{A}^{-1} = \begin{pmatrix} 1 & i \\ 1 & -i \end{pmatrix}.$$

(3.2.19)

For the complex conjugate $s_j^{\pm}$ the values of $t_j^{\pm}$ are purely real, besides,

$$\mathcal{M}_j^{\pm} = \begin{pmatrix} s_j^+ \cdot f_j(s_1^+ s_1^-, \ldots, s_v^+ s_v^-) \\ s_j^- \cdot \overline{f_j}(s_1^+ s_1^-, \ldots, s_v^+ s_v^-) \end{pmatrix} =$$

$$= \frac{1}{2}\begin{pmatrix} 1 & 1 \\ -i & i \end{pmatrix} \cdot$$

$$\begin{pmatrix} (t_j^+ + it_j^-)f_j((t_1^+)^2 + (t_1^-)^2, \ldots, (t_v^+)^2 + (t_v^-)^2) \\ (t_j^+ - it_j^-)\overline{f_j}((t_1^+)^2 + (t_1^-)^2, \ldots, (t_v^+)^2 + (t_v^-)^2) \end{pmatrix} =$$

$$= \frac{1}{2}\begin{pmatrix} 1 & 1 \\ -i & i \end{pmatrix} a_j \begin{pmatrix} (t_j^+ + it_j^-)(\cos(\varphi_j) + i\sin(\varphi_j)) \\ (t_j^+ - it_j^-)(\cos(\varphi_j) - i\sin(\varphi_j)) \end{pmatrix} =$$

$$= a_j \begin{pmatrix} \cos(\varphi_j) & -\sin(\varphi_j) \\ \sin(\varphi_j) & \cos(\varphi_j) \end{pmatrix}\begin{pmatrix} t_j^+ \\ t_j^- \end{pmatrix},$$

(3.2.20)

where $f_j = a_j \cdot e^{i\varphi_j((t_1^+)^2 + (t_1^-)^2, \ldots, (t_v^+)^2 + (t_v^-)^2)}$ and $a_j = \text{const}$, as a symplectic motion is considered, and $\varphi_j = \varphi_j((t_1^+)^2 + (t_1^-)^2, \ldots, (t_v^+)^2 + (t_v^-)^2)$ depends on the rotationally invariant quantity.

Therefore, in the new coordinates the dynamics of particles is described by a rotation, the frequency of which depends only on the amplitudes $(t_j^+)^2 + (t_j^-)^2$ and

possibly the system parameters. The functions φ_j for $j = \overline{1, v}$ give the tunes of the nonlinear motion. Indeed, for any repetitive system the tune of the particle is the total polar angle advance divided by the number of turns in the limit of turn number going to infinity if this limit exists. Consider an arbitrary particle of the beam. The first change of the phase is due to the transformation to the new coordinates, and after that each turn produces an equal polar angle φ_j which depends on the amplitude and parameters of the particle. To obtain the final angle, it is necessary to perform a transformation back to the original coordinates.

As the number of turns increases, the contribution of the initial and final polar angles due to the transformation becomes increasingly insignificant, and in the limit the tune results in only φ_j. Hence, the limit exists and it can be computed analytically as a by-product of the normal form transformation. This fact is a key point to understanding the algorithm of the nonlinear tune shift calculation using the measurement results, discussed in Section 4.2.

3.3 Motivation for the Differential Algebra Approach

Consider one of the simplest possible nonlinear transfer maps, the sextupole kick (thin lens approximation) superimposed on an idealized linear dynamics in a one-dimensional phase space (x, x'), where x is the position of the particle, and x' is its velocity [16, 58]:

$$\begin{pmatrix} x_1 \\ x_1' \end{pmatrix} = \begin{pmatrix} \cos(2\pi\mu)x_0 + \sin(2\pi\mu)x_0' \\ -\sin(2\pi\mu)x_0 + \cos(2\pi\mu)x_0' + k_s\left[\cos(2\pi\mu)x_0 + \sin(2\pi\mu)x_0'\right]^2 \end{pmatrix},$$

(3.3.1)

where k_s is the parameter, characterizing the sextupole strength.

Introduce the following change of variables:

$$\begin{cases} \tilde{x} =_2 x + A_{11}x^2 + A_{12}xx' + A_{22}(x')^2 \\ \tilde{x}' =_2 x' + B_{11}x^2 + B_{12}xx' + B_{22}(x')^2 \end{cases}, \tag{3.3.2}$$

where the coefficients $A_{11}, A_{12}, A_{22}, B_{11}, B_{12}, B_{22}$ are to be defined in such a way that all the second order aberrations vanish. This is equivalent to the first step of the nonlinear normal form transformation (3.1.5), described in Section 3.1. The "$=_2$" means that the partial derivatives of orders up to 2 of the right hand side and the left hand side match at the origin.

As up to the second order it is true that

$$\tilde{x}^2 =_2 x^2$$
$$\tilde{x}\tilde{x}' =_2 xx' \tag{3.3.3}$$
$$(\tilde{x}')^2 =_2 (x')^2$$

(all the other terms are of higher orders, and hence, omitted), it follows that

$$\begin{cases} x =_2 \tilde{x} - A_{11}\tilde{x}^2 - A_{12}\tilde{x}\tilde{x}' - A_{22}(\tilde{x}')^2 \\ x' =_2 \tilde{x}' - B_{11}\tilde{x}^2 - B_{12}\tilde{x}x' - B_{22}(\tilde{x}')^2 \end{cases}. \tag{3.3.4}$$

Substituting these expressions into Eq. (3.3.1) yields in the new coordinates:

$$\begin{aligned} &\begin{pmatrix} \tilde{x}_1 - A_{11}\tilde{x}_1^2 - A_{12}\tilde{x}_1\tilde{x}_1' - A_{22}(\tilde{x}_1')^2 \\ \tilde{x}_1' - B_{11}\tilde{x}_1^2 - B_{12}\tilde{x}_1\tilde{x}_1' - B_{22}(\tilde{x}_1')^2 \end{pmatrix} =_2 \\ &=_2 \begin{pmatrix} \cos(2\pi\mu)(\tilde{x}_0 - A_{11}\tilde{x}_0^2 - A_{12}\tilde{x}_0\tilde{x}_0' - A_{22}(\tilde{x}_0')^2) \\ -\sin(2\pi\mu)(\tilde{x}_0 - A_{11}\tilde{x}_0^2 - A_{12}\tilde{x}_0\tilde{x}_0' - A_{22}(\tilde{x}_0')^2) \end{pmatrix} + \\ &+ \begin{pmatrix} +\sin(2\pi\mu)(\tilde{x}_0' - B_{11}\tilde{x}_0^2 - B_{12}\tilde{x}_0\tilde{x}_0' - B_{22}(\tilde{x}_0')^2) \\ +\cos(2\pi\mu)(\tilde{x}_0' - B_{11}\tilde{x}_0^2 - B_{12}\tilde{x}_0\tilde{x}_0' - B_{22}(\tilde{x}_0')^2) \end{pmatrix} + \\ &+ \begin{pmatrix} 0 \\ k_s\left[\cos(2\pi\mu)\tilde{x}_0 + \sin(2\pi\mu)\tilde{x}_0'\right]^2 \end{pmatrix}, \end{aligned} \tag{3.3.5}$$

or, carrying all the second order terms to the right hand side and utilizing Eqs. (3.3.3):

$$
\begin{pmatrix} \tilde{x}_1 \\ \tilde{x}_1' \end{pmatrix} =2 \begin{pmatrix} \cos(2\pi\mu) \\ -\sin(2\pi\mu) \end{pmatrix} \left(\tilde{x}_0 - A_{11}\tilde{x}_0^2 - A_{12}\tilde{x}_0\tilde{x}_0' - A_{22}(\tilde{x}_0')^2 \right) +
$$

$$
+ \begin{pmatrix} \sin(2\pi\mu) \\ \cos(2\pi\mu) \end{pmatrix} \left(\tilde{x}_0' - B_{11}\tilde{x}_0^2 - B_{12}\tilde{x}_0\tilde{x}_0' - B_{22}(\tilde{x}_0')^2 \right) +
$$

$$
+ \begin{pmatrix} 0 \\ k_s \left[\cos(2\pi\mu)\tilde{x}_0 + \sin(2\pi\mu)\tilde{x}_0' \right]^2 \end{pmatrix} +
$$

$$
+ \begin{pmatrix} A_{11} \\ B_{11} \end{pmatrix} \left(\cos^2(2\pi\mu)\tilde{x}_0^2 + \sin(4\pi\mu)\tilde{x}_0\tilde{x}_0' + \sin^2(2\pi\mu)(\tilde{x}_0')^2 \right) +
$$

$$
+ \begin{pmatrix} A_{12} \\ B_{12} \end{pmatrix} \left(-\frac{1}{2}\sin(4\pi\mu)\tilde{x}_0^2 + \cos(4\pi\mu)\tilde{x}_0\tilde{x}_0' + \frac{1}{2}\sin(4\pi\mu)(\tilde{x}_0')^2 \right) +
$$

$$
+ \begin{pmatrix} A_{22} \\ B_{22} \end{pmatrix} \left(\sin^2(2\pi\mu)\tilde{x}_0^2 - \sin(4\pi\mu)\tilde{x}_0\tilde{x}_0' + \cos^2(2\pi\mu)(\tilde{x}_0')^2 \right).
$$

$$(3.3.6)$$

Gathering like terms in Eq. (3.3.6) yields a system of six equations allowing to find all the second order coefficients of the transformation:

$$
A_{11}\cos^2(2\pi\mu) - \frac{1}{2}A_{12}\sin(4\pi\mu) + A_{22}\sin^2(2\pi\mu) -
$$
$$
- A_{11}\cos(2\pi\mu) - B_{11}\sin(2\pi\mu) = 0
$$

$$(3.3.7)$$

$$
A_{11}\sin(4\pi\mu) + A_{12}\cos(4\pi\mu) - A_{22}\sin(4\pi\mu) -
$$
$$
- A_{12}\cos(2\pi\mu) - B_{12}\sin(2\pi\mu) = 0
$$

$$(3.3.8)$$

$$
A_{11}\sin^2(2\pi\mu) + \frac{1}{2}A_{12}\sin(4\pi\mu) + A_{22}\cos^2(2\pi\mu) -
$$
$$
- A_{22}\cos(2\pi\mu) - B_{22}\sin(2\pi\mu) = 0
$$

$$(3.3.9)$$

$$
B_{11}\cos^2(2\pi\mu) - \frac{1}{2}B_{12}\sin(4\pi\mu) + B_{22}\sin^2(2\pi\mu) +
$$
$$
+ A_{11}\sin(2\pi\mu) - B_{11}\cos(2\pi\mu) = -k_s\cos^2(2\pi\mu)
$$

$$(3.3.10)$$

$$
B_{11}\sin(4\pi\mu) + B_{12}\cos(4\pi\mu) - B_{22}\sin(4\pi\mu) +
$$
$$
+ A_{12}\sin(2\pi\mu) - B_{12}\cos(2\pi\mu) = -k_s\sin(4\pi\mu)
$$

$$(3.3.11)$$

38

$$B_{11}\sin^2(2\pi\mu) + \frac{1}{2}B_{12}\sin(4\pi\mu) + B_{22}\cos^2(2\pi\mu)+$$

$$+ A_{22}\sin(2\pi\mu) - B_{22}\cos(2\pi\mu) = -k_s\sin^2(2\pi\mu) \tag{3.3.12}$$

The sum of Eqs. (3.3.7) and (3.3.9) gives:

$$A_{11} + A_{22} - \cos(2\pi\mu)(A_{11} + A_{22}) - \sin(2\pi\mu)(B_{11} + B_{22}) = 0. \tag{3.3.13}$$

The sum of Eqs. (3.3.10) and (3.3.12) gives:

$$B_{11} + B_{22} - \cos(2\pi\mu)(B_{11} + B_{22}) + \sin(2\pi\mu)(A_{11} + A_{22}) = -k_s. \tag{3.3.14}$$

Eqs. (3.3.13) and (3.3.14) together yield the following:

$$\begin{pmatrix} 1 - \cos(2\pi\mu) & -\sin(2\pi\mu) \\ \sin(2\pi\mu) & 1 - \cos(2\pi\mu) \end{pmatrix} \begin{pmatrix} A_{11} + A_{22} \\ B_{11} + B_{22} \end{pmatrix} = \begin{pmatrix} 0 \\ -k_s \end{pmatrix}, \tag{3.3.15}$$

hence,

$$\begin{pmatrix} A_{11} + A_{22} \\ B_{11} + B_{22} \end{pmatrix} = \frac{1}{2(1 - \cos(2\pi\mu))} \begin{pmatrix} 1 - \cos(2\pi\mu) & \sin(2\pi\mu) \\ -\sin(2\pi\mu) & 1 - \cos(2\pi\mu) \end{pmatrix} \begin{pmatrix} 0 \\ -k_s \end{pmatrix} =$$

$$= \frac{1}{2(1 - \cos(2\pi\mu))} \begin{pmatrix} -k_s\sin(2\pi\mu) \\ -k_s(1 - \cos(2\pi\mu)) \end{pmatrix} = \begin{pmatrix} -\frac{1}{2}k_s\cot(\pi\mu) \\ -\frac{1}{2}k_s \end{pmatrix}. \tag{3.3.16}$$

The difference between Eqs. (3.3.7) and (3.3.9) gives:

$$\cos(4\pi\mu)(A_{11} - A_{22}) - A_{12}\sin(4\pi\mu)-$$

$$- (A_{11} - A_{22})\cos(2\pi\mu) - (B_{11} - B_{22})\sin(2\pi\mu) = 0. \tag{3.3.17}$$

The difference between Eqs. (3.3.10) and (3.3.12) gives:

$$\cos(4\pi\mu)(B_{11} - B_{22}) - B_{12}\sin(4\pi\mu)-$$

$$- (B_{11} - B_{22})\cos(2\pi\mu) + (A_{11} - A_{22})\sin(2\pi\mu) = -k_s\cos(4\pi\mu). \tag{3.3.18}$$

Eqs. (3.3.8), (3.3.11), (3.3.17), and (3.3.18) together can be represented in the matrix form:

$$\begin{cases} \begin{pmatrix} B_{11} - B_{22} \\ B_{12} \end{pmatrix} = \frac{1}{\sin(2\pi\mu)} \cdot M \cdot \begin{pmatrix} A_{11} - A_{22} \\ A_{12} \end{pmatrix} \\ M \cdot \begin{pmatrix} B_{11} - B_{22} \\ B_{12} \end{pmatrix} + \sin(2\pi\mu) \begin{pmatrix} A_{11} - A_{22} \\ A_{12} \end{pmatrix} = -k_s \begin{pmatrix} \cos(4\pi\mu) \\ \sin(4\pi\mu) \end{pmatrix} \end{cases}, \tag{3.3.19}$$

where

$$M = \begin{pmatrix} \cos(4\pi\mu) - \cos(2\pi\mu) & -\sin(4\pi\mu) \\ \sin(4\pi\mu) & \cos(4\pi\mu) - \cos(2\pi\mu) \end{pmatrix}.$$

Eq. (3.3.19) yields

$$\left(M^2 + \sin^2(2\pi\mu) \cdot I \right) \begin{pmatrix} A_{11} - A_{22} \\ A_{12} \end{pmatrix} = -k_s \sin(2\pi\mu) \begin{pmatrix} \cos(4\pi\mu) \\ \sin(4\pi\mu) \end{pmatrix}, \qquad (3.3.20)$$

where I is the 2×2 unity matrix. Thus,

$$R \cdot \begin{pmatrix} A_{11} - A_{22} \\ A_{12} \end{pmatrix} = -k_s \sin(2\pi\mu) \begin{pmatrix} \cos(4\pi\mu) \\ \sin(4\pi\mu) \end{pmatrix}, \qquad (3.3.21)$$

where

$$R = \begin{pmatrix} 1 + \cos(8\pi\mu) - \cos(6\pi\mu) - \cos(2\pi\mu) & -\sin(8\pi\mu) + \sin(6\pi\mu) + \sin(2\pi\mu) \\ \sin(8\pi\mu) - \sin(6\pi\mu) - \sin(2\pi\mu) & 1 + \cos(8\pi\mu) - \cos(6\pi\mu) - \cos(2\pi\mu) \end{pmatrix}.$$

$$\det(R) = (1 + \cos(8\pi\mu) - \cos(6\pi\mu) - \cos(2\pi\mu))^2 +$$

$$(\sin(8\pi\mu) - \sin(6\pi\mu) - \sin(2\pi\mu))^2 = 16 \sin^2(\pi\mu) \sin^2(3\pi\mu).$$

Hence, one can invert the matrix R, effectively solving the system (3.3.21):

$$\begin{pmatrix} A_{11} - A_{22} \\ A_{12} \end{pmatrix} = -\frac{k_s \sin(2\pi\mu)}{16 \sin^2(\pi\mu) \sin^2(3\pi\mu)} \cdot R^{-1} \cdot \begin{pmatrix} \cos(4\pi\mu) \\ \sin(4\pi\mu) \end{pmatrix} =$$

$$- \frac{k_s \cos(\pi\mu)}{8 \sin(\pi\mu) \sin^2(3\pi\mu)} \begin{pmatrix} 2(\cos(4\pi\mu) - \cos(2\pi\mu)) \\ 0 \end{pmatrix} = \begin{pmatrix} \frac{k_s \cos(\pi\mu)}{2 \sin(3\pi\mu)} \\ 0 \end{pmatrix}. \qquad (3.3.22)$$

$$\begin{pmatrix} B_{11} - B_{22} \\ B_{12} \end{pmatrix} = -\frac{k_s \cos(\pi\mu)}{2 \sin(2\pi\mu) \sin^2(3\pi\mu)} \begin{pmatrix} \cos(4\pi\mu) - \cos(2\pi\mu) \\ \sin(4\pi\mu) \end{pmatrix} =$$

$$\begin{pmatrix} -\frac{1}{2} k_s \\ \frac{1}{2} k_s \left(\cot(3\pi\mu) + \frac{\cos(\pi\mu)}{\sin(3\pi\mu)} \right) \end{pmatrix} = \begin{pmatrix} \frac{1}{2} k_s \\ \frac{k_s \cos(\pi\mu) \cos(2\pi\mu)}{\sin(3\pi\mu)} \end{pmatrix}. \qquad (3.3.23)$$

Ultimately,

$$
\begin{cases}
A_{11} = -\dfrac{k_s \cos(\pi\mu)\cos(2\pi\mu)}{2\sin(3\pi\mu)} \\[2.5ex]
A_{12} = 0 \\[2.5ex]
A_{22} = -\dfrac{k_s \cos^3(\pi\mu)}{\sin(3\pi\mu)} \\[2.5ex]
B_{11} = -\dfrac{k_s}{2} \\[2.5ex]
B_{12} = \dfrac{k_s \cos(\pi\mu)\cos(2\pi\mu)}{\sin(3\pi\mu)} \\[2.5ex]
B_{22} = 0
\end{cases}
. \tag{3.3.24}
$$

As one can see, solving the system (3.3.7) requires a lot of heavy algebraic and trigonometric transformations. The most important part is that these transformations cannot be generalized, and hence, the methods to solve the system will vary depending on the transfer map under consideration.

If $\sin(3\pi\mu)$ goes to zero, the coefficients A_{11}, A_{22}, B_{12} grow to infinity, and the normal form algorithm fails. That is why it was assumed in Section 3.2 that the equation $\vec{\mu} \cdot \vec{n} = 0 \mod 2\pi$ does not have any nontrivial solutions.

To verify that Eq. (3.3.24) is indeed the solution, substitute the resulting values

of the coefficients back into Eqs. (3.3.7)–(3.3.12):

$$A_{11}\cos^2(2\pi\mu) - \frac{1}{2}A_{12}\sin(4\pi\mu) + A_{22}\sin^2(2\pi\mu) - A_{11}\cos(2\pi\mu) - B_{11}\sin(2\pi\mu) =$$

$$-\frac{k_s\cos(\pi\mu)\cos(2\pi\mu)}{2\sin(3\pi\mu)}\cos^2(2\pi\mu) - \frac{k_s\cos^3(\pi\mu)}{\sin(3\pi\mu)}\sin^2(2\pi\mu) +$$

$$+\frac{k_s\cos(\pi\mu)\cos(2\pi\mu)}{2\sin(3\pi\mu)}\cos(2\pi\mu) + \frac{k_s}{2}\sin(2\pi\mu) =$$

$$= -\frac{k_s\cos(\pi\mu)}{2\sin(3\pi\mu)}\left[\cos^3(2\pi\mu) + 2\cos^2(\pi\mu)\sin^2(2\pi\mu) - \cos^2(2\pi\mu)\right] + \frac{k_s\sin(2\pi\mu)}{2} =$$

$$= -\frac{k_s\cos(\pi\mu)}{2\sin(3\pi\mu)}\left[\cos^3(2\pi\mu) + \cos(2\pi\mu)\sin^2(2\pi\mu) + \sin^2(2\pi\mu) - \cos^2(2\pi\mu)\right] + \frac{k_s\sin(2\pi\mu)}{2} =$$

$$= -\frac{k_s\cos(\pi\mu)}{2\sin(3\pi\mu)}\left[\cos(2\pi\mu) - \cos(4\pi\mu)\right] + \frac{k_s\sin(2\pi\mu)}{2} =$$

$$= -\frac{k_s\cos(\pi\mu)}{2\sin(3\pi\mu)}2\sin(3\pi\mu)\sin(\pi\mu) + \frac{k_s\sin(2\pi\mu)}{2} = 0.$$

$$(3.3.25)$$

The other five equations of the system (3.3.7) can be verified using a similar technique.

It is already clear after one step that the manual computation of the normal form transformation is not straightforward, and it does not imply any algorithm which can be efficiently implemented and suitable for a large class of transfer maps.

On the other hand, the normal form algorithm in the differential algebra framework is perfectly clear and very efficient to any order desired. It is implemented in COSY INFINITY and used throughout the subsequent chapters to assist solving various problems of the optimization of accelerator parameters.

3.4   Normal Form Transformation Result

To see the effect of the normal form transformation, let us consider a particular transfer map and its representation after the normal form transformation.

The transfer map is a function, connecting the initial and final states of some

deterministic dynamical system:

$$\dot{\vec{z}} = \vec{F}(\vec{z}), \qquad (3.4.1)$$

$$\vec{z}_f = \mathcal{M}(\vec{z}_i, \vec{\delta}), \qquad (3.4.2)$$

where F is continuous in $\vec{z}$ and continuous almost everywhere in the independent variable t, the time, or s, the arc length, z_i and z_f are the initial and final states of the system, respectively, and δ is a set of system parameters. Then $\mathcal{M}$ is a transfer map of the system, connecting the initial state z_i at t_i (or s_i) to the final state z_f at t_f (or s_f). In the differential algebra framework one considers the equivalence classes $[\mathcal{M}]_n$ instead of $\mathcal{M}$. Each class $[\mathcal{M}]_n$ can be represented by the set of coefficient of the Taylor expansion of $\mathcal{M}$ about the point $z = 0$. Depending on the order of calculation (the highest order of the terms kept in the Taylor expansion), the number of the coefficients can be very large, and also it grows fast as the calculation order is increased. Table 3.1 shows the example of the human readable representation of the transfer map in the particle optical coordinates before the normal form transformation for a long dipole magnet.

Each row of the table describes one term of the Taylor expansion of the final coordinates x_f and a_f (divided by the horizontal line) in terms of the initial coordinates x_i and a_i. The column labeled "EXPONENTS" describes the exponents of each of the independent variables appearing in the respective term. The "ORDER" column contains the total order of the term, that is, the sum of the exponents, and the first column lists the double precision coefficient belonging to the respective term. For example, the sixth row in the upper part of the table shows the Taylor expansion coefficient of the $(x|xa^2)$ term, as the exponents are 1 for x and 2 for a. At the same time, the sixth row in the lower part of the the table shows the coefficient of the

```
 I   COEFFICIENT          ORDER EXPONENTS
 1   0.6234898018587336      1    1 0  0
 2   0.7818314824680298      1    0 1  0
 3  -.3056302334890786       2    2 0  0
 4   0.4874639560909119      2    1 1  0
 5   0.1173751344184454      2    0 2  0
 6  -.3056302334890786       3    1 2  0
 7   0.2437319780454559      3    0 3  0
 8  -.4670491981129435E-01   4    4 0  0
 9   0.1489837227175753      4    3 1  0
10  -.1782158313658518       4    2 2  0
11   0.9474825532788060E-01  4    1 3  0
12  -.1736113620668300E-01   4    0 4  0
13  -.9340983962258870E-01   5    3 2  0
14   0.2234755840763630      5    2 3  0
15  -.2546233897381215       5    1 4  0
16   0.1083071221753043      5    0 5  0
-----------------------------------------
 I   COEFFICIENT          ORDER EXPONENTS
 1  -.7818314824680298       1    1 0  0
 2   0.6234898018587336      1    0 1  0
 3  -.3909157412340149       2    0 2  0
 4   0.1110223024625157E-15  4    1 3  0
 5  -.9772893530850374E-01   4    0 4  0
 6  -.2220446049250313E-15   5    3 2  0
 7   0.1110223024625157E-15  5    2 3  0
-------------------------------------
```

Tab. 3.1. Transfer map in particle optical coordinates

```
I   COEFFICIENT             ORDER EXPONENTS
1   0.6234898018587336        1    1 0  0
2   0.7818314824680299        1    0 1  0
------------------------------------
I   COEFFICIENT             ORDER EXPONENTS
1  -.7818314824680299        1    1 0  0
2   0.6234898018587336        1    0 1  0
------------------------------------
```

Tab. 3.2. Transfer map in normal form coordinates

$(a|x^3a^2)$ term, as those elements of the transfer map which are zero are omitted in the representation.

It is clear from the representation of the transfer map, that the system under consideration is nonlinear. At the same time, after the normal form transformation is applied to this map, the resulting transfer map is linear (see Table 3.2). Thus, the motion of particles in the normal form coordinates can be described by the linear transfer matrix:

$$\begin{pmatrix} t_f^+ \\ t_f^- \end{pmatrix} = \begin{pmatrix} 0.6234898018587336 & 0.7818314824680299 \\ -.7818314824680299 & 0.6234898018587336 \end{pmatrix} \begin{pmatrix} t_i^+ \\ t_i^- \end{pmatrix}, \qquad (3.4.3)$$

where (t_i^+, t_i^-) and (t_i^+, t_i^-) are the initial and final normal form coordinates of the particle, respectively.

The beauty of the differential algebraic approach to the normal form transformation is in that the algorithm is constructive, and it allows to obtain not only the transfer map in the normal form coordinates, but also the transformation to that set of coordinates and its inverse. Therefore,

$$\begin{pmatrix} x_f \\ a_f \end{pmatrix} = \mathcal{A}^{-1} \circ \begin{pmatrix} 0.6234898018587336 & 0.7818314824680299 \\ -.7818314824680299 & 0.6234898018587336 \end{pmatrix} \circ \mathcal{A} \begin{pmatrix} x_i \\ a_i \end{pmatrix},$$
$$(3.4.4)$$

where $\mathcal{A}$ is map of the transformation to the normal form coordinates:

$$\begin{pmatrix} t^+ \\ t^- \end{pmatrix} = \mathcal{A} \begin{pmatrix} x \\ a \end{pmatrix}. \qquad (3.4.5)$$

4. DYNAMICS OPTIMIZATION IN THE TEVATRON

4.1   Skew Quadrupole Correction

Consider the problem of the optimization of the dynamics of particles in the proton–antiproton Tevatron collider. Increasing the luminosity reach of existing and future colliders demands considered and precise optical design and predictability in operation. Driven by nonlinear fields, high-order beam dynamics is generally difficult to control, calculate, and can severely limit a machine's region of stable operation. An approximately linear lattice is desirable for operational simplicity and understanding, and it also generally exhibits more robust, broader-range performance. Nonlinear sources arising from field and alignment errors and required correction elements are unavoidable. Successful management of the sources of nonlinearities, however, depends on the linear lattice. Attributes of the linear lattice and relative locations of sources generate interference, constructive or destructive, between the nonlinear terms depending on their periodicity. In a highly effective linear lattice design, the strongest nonlinear amplitudes can be mitigated passively by intelligently exploiting periodicity, phase advance and optimal placement of nonlinear correctors. Such a lattice enhances precision and predictability in the machine optics.

Passive cancellation, however, is generally not sufficient to address certain systematic or widespread field errors, and active correction in the form of added corrector elements is usually required. The overall lattice approach must be evaluated not only by its tolerance to errors, nonlinearities, and natural aberrations, but also by its potential for active correction. Such correction may be "global" in the sense that an error or aberration is corrected over one-turn optics. Global correction is not always adequate to maintain sensitive collider optics. Immediate — or "local" correction — of source terms, particularly if such terms propagate through the delicate optics of the interaction regions, may be an additional requirement for stability and linearity.

The case addressed in this work is the state of the Tevatron collider as of August 2004, where a strong, systematic, skew quadrupole error was present in the operational lattice as a result of a coil shift in the superconducting arc dipoles.

Technically the Tevatron is a superconducting synchrotron with six straight sections and six long arcs. Two of the straights are the well-known CDF and D0 detectors, and four other straights are used for minor experiments, acceleration, injection and extraction. The main part of each arc is occupied by the superconducting dipoles designed in the late 1970's to early 1980's. Due to the extensive use, over time some of the superconducting coils shifted, thus causing the skew quadrupole component to appear and grow to the values that could not be corrected using only the "passive" correctors available. Without introducing additional correctors or correcting the field errors in dipoles it was not possible to keep and improve the quality of the beam, and hence the luminosity.

The dynamics of the particles in the Tevatron can be described by a system of differential equations of the form

$$\dot{\vec{z}} = \vec{F}(\vec{z}), \qquad (4.1.1)$$

47

with

$$\vec{z} = \begin{pmatrix} x \\ y \\ l = k(t - t_0) \\ a = p_x/p_0 \\ b = p_y/p_0 \\ \delta = (E - E_0)/E_0 \end{pmatrix}, \qquad (4.1.2)$$

where x is the horizontal position of the particle relative to the reference particle that goes through the centers of the magnets, y is the vertical relative position, l characterizes the deviation in the time of flight with the coefficient k chosen in such a way that l has the dimension of distance, a and b are the reduced momenta in horizontal and vertical transversal directions respectively, δ is the reduced difference between the total energy of the particle under consideration (E) and that of the reference particle (E_0), and p_0 is the initial momentum of the reference particle.

By this definition of $\vec{z}$, the reference particle has coordinates $\vec{z} = 0$, and thus the vector $\vec{z}$ indeed describes relative motion.

The general form of the vector $\vec{F}$ on the right hand side can be found in Section 2.1.2 of Chapter 2. As the particles move in the electromagnetic field, the system (4.1.1) is Hamiltonian, as one can assume that the energy is constant at any given time, as we consider the state of the Tevatron at injection. The right hand side of the system possesses continuous partial derivatives with respect to the components of $\vec{z}$, and almost everywhere continuous (excluding a finite number of points) with respect to the independent variable s in some region U. Thus for any choice of the initial coordinates in U the system (4.1.1) possesses a uniques solution and the behavior of the system at $s = 0$ determines the dynamics of particles $\forall s > 0$. The right hand side of the system is a periodic function with a period $\tau > 0$, that is, $\vec{F}(s + \tau) = \vec{F}(s)$ and there is no such $0 < \tau_2 < \tau$ that $\vec{F}(s + \tau_2) = \vec{F}(s)$.

Assume that Eqs. (4.1.1) have been integrated to yield the function

$$\vec{z}(s_f) = \mathcal{M}_{s_i,s_f}(\vec{z}(s_i)), \tag{4.1.3}$$

where s_i and s_f are the initial and final values of the independent variable. The function $\mathcal{M}$ describes how individual state space points "flow" as time progresses, and in the theory of dynamical systems it is usually referred to as the flow of the differential equation. Hereafter this function is referred to as the transfer map (describing how state space points are transferred).

Let $\mathcal{M} = \mathcal{M}_{s_i,s_i+\tau}$ be the transfer map of one full revolution, the so-called first return map. Then one can trace the dynamics of particles after an arbitrary number of turns by applying the operator $\mathcal{M}$ over and over again to the set of the initial data.

The optimization problem is to uncouple the dynamics of particles in the planes (x,a) and (y,b). By definition the beam occupies a small subset of the phase space in the neighborhood of the reference particle with zero coordinates. Hence we can employ the differential algebra methods [12] and consider along with the transfer map $\mathcal{M}$ the equivalence class $[\mathcal{M}]_n \in {}_nD_v$, where n is the computation order, v is the number of phase space variables, and ${}_nD_v$ is the corresponding differential algebra. Differential algebra methods are so efficient that the orders up to 10 can easily be handled by any home PC. Also, as it was mentioned in Chapter 1, transfer map methods are more efficient than the methods requiring integration of individual orbits for some tasks, as one can calculate the transfer map (even with parameters) once and apply it over and over again.

4.1.1 Linear Problem

Let the system (4.1.1) be linear, or alternatively, consider the linearization of the full nonlinear system in the neighborhood of the origin: $\dot{\vec{z}} = \mathrm{Jac}(\vec{F})\big|_0 \cdot \vec{z}$. Then the conditions that the transfer map must satisfy in order to decouple the motion in the planes (x, a) and (y, b) can be written as

$$\frac{\partial x^{(f)}}{\partial y^{(i)}} = 0, \quad \frac{\partial x^{(f)}}{\partial b^{(i)}} = 0, \quad \frac{\partial a^{(f)}}{\partial y^{(i)}} = 0, \quad \frac{\partial a^{(f)}}{\partial b^{(i)}} = 0,$$
$$\frac{\partial y^{(f)}}{\partial x^{(i)}} = 0, \quad \frac{\partial y^{(f)}}{\partial a^{(i)}} = 0, \quad \frac{\partial b^{(f)}}{\partial x^{(i)}} = 0, \quad \frac{\partial b^{(f)}}{\partial a^{(i)}} = 0, \tag{4.1.4}$$

where $\vec{z} = (x, a, y, b, l, \delta)^\top$, and the indices (i) and (f) denote the initial and final conditions, respectively.

In the linear case the transfer map and its equivalence class $[\mathcal{M}]_n$ can be represented in the form of the matrix for the coefficients connecting the initial and final values:

$$z(\vec{s}_f) = \begin{pmatrix} (z_1|z_1) & \cdots & (z_1|z_v) \\ \vdots & \ddots & \vdots \\ (z_v|z_1) & \cdots & (z_v|z_v) \end{pmatrix} (z(\vec{s}_i)), \tag{4.1.5}$$

where $(z_i|z_j)$ is the coefficient of the dependence of the i-th component of the final state of the particle on the j-th component of the initial state. Consider only the transversal dynamics, that is, let $\vec{z} = (x, a, y, b)^\top$. In this case the condition for the decoupling of the horizontal and vertical planes has the form

$$z(\vec{s}_f) = \begin{pmatrix} (x|x) & (x|a) & 0 & 0 \\ (a|x) & (a|a) & 0 & 0 \\ 0 & 0 & (y|y) & (y|b) \\ 0 & 0 & (b|y) & (b|b) \end{pmatrix} (z(\vec{s}_i)). \tag{4.1.6}$$

So, to achieve minimal interdependence between the two planes, it is necessary to

minimize the following objective function:

$$J_1 = \left|\frac{\partial x^{(f)}}{\partial y^{(i)}}\right| + \left|\frac{\partial x^{(f)}}{\partial b^{(i)}}\right| + \left|\frac{\partial a^{(f)}}{\partial y^{(i)}}\right| + \left|\frac{\partial a^{(f)}}{\partial b^{(i)}}\right| +$$

$$+ \left|\frac{\partial y^{(f)}}{\partial x^{(i)}}\right| + \left|\frac{\partial y^{(f)}}{\partial a^{(i)}}\right| + \left|\frac{\partial b^{(f)}}{\partial x^{(i)}}\right| + \left|\frac{\partial b^{(f)}}{\partial a^{(i)}}\right| = \tag{4.1.7}$$

$$= |(x|y)| + |(x|b)| + |(a|y)| + |(a|b)| +$$

$$+ |(y|x)| + |(y|a)| + |(b|x)| + |(b|a)|,$$

which depends on up to 8 control parameters, representing the strengths of the skew quadrupole correctors in the Tevatron lattice, that is, $J_1 = J_1(\vec{u})$, where the components of $\vec{u}$ are the field strengths in the corresponding correctors. Both the components of $\vec{z}$, and J_1 depend continuously on $\vec{u}$ over some compact set for the parameters $\vec{u}$.

4.1.2 Nonlinear Problem

If the transfer map $\mathcal{M}$ is nonlinear, then the condition for the transversal motion to be decoupled assumes a more complicated form:

$$\frac{\partial^{i_1+i_2} x_k^{(f)}}{\partial\left(y_1^{(i)}\right)^{i_1}\partial\left(y_2^{(i)}\right)^{i_2}} = 0 \quad \frac{\partial^{i_1+i_2} y_k^{(f)}}{\partial\left(x_1^{(i)}\right)^{i_1}\partial\left(x_2^{(i)}\right)^{i_2}} = 0, \quad k = 1, 2, \tag{4.1.8}$$

where $\vec{z}$ is given in the indexed form for notational convenience: $\vec{z} = (x_1, x_2, y_1, y_2)^\top = (x, a, y, b)^\top$, $i_1, i_2 \in \mathbb{Z}_{\geq 0}$; $i_1 + i_2 \in \overline{1, n}$, n is the highest order of the nonlinearities taken into account, indices (i) and (f) denote the initial and final values, respectively.

In the nonlinear case the equivalence class cannot be represented in a matrix form. Instead, the following notation is introduced to denote the coefficients of the high order Taylor expansion

$$(z_j | z_1^{i_1} \ldots z_v^{i_v}), \tag{4.1.9}$$

where v is the number of phase space variables, j is an index of the component of $\vec{z}^{(f)}$; $\sum_{k=1}^{v} i_k \in \overline{1,n}$, $i_k \in \mathbb{Z}_{\geq 0}$, n is the order of computations (the highest order in the Taylor expansion). It is not hard to see that the linear matrix (4.1.5) follows this notation. For the linear case $n = 1$.

Using this notation for $\vec{z} = (x_1, x_2, y_1, y_2)^\top$ one obtains the following conditions:

$$(x_1|y_1^{i1} y_2^{i2}) = 0, \quad (x_2|y_1^{i1} y_2^{i2}) = 0, \quad (y_1|x_1^{i1} x_2^{i2}) = 0, \quad (y_2|x_1^{i1} x_2^{i2}) = 0, \quad (4.1.10)$$

for all possible combinations of $i_1, i_2 \in \mathbb{Z}_{\geq 0}$, such that $i_1 + i_2 \in \overline{1,n}$.

Thus, the nonlinear problem of uncoupling the dynamics in the horizontal and vertical planes can be reduced to the minimization problem for the following objective function:

$$
\begin{aligned}
J_2 &= \sum_{k=1}^{2} \left(\sum_{i_1+i_2=1}^{n} \left| \frac{\partial^{i_1+i_2} x_k^{(f)}}{\partial \left(y_1^{(i)}\right)^{i_1} \partial \left(y_2^{(i)}\right)^{i_2}} \right| + \sum_{j_1+j_2=1}^{n} \left| \frac{\partial^{j_1+j_2} y_k^{(f)}}{\partial \left(x_1^{(i)}\right)^{j_1} \partial \left(x_2^{(i)}\right)^{j_2}} \right| \right) = \\
&= \sum_{k=1}^{2} \left(\sum_{i_1+i_2=1}^{n} \left|(x_k|y_1^{i1} y_2^{i2})\right| + \sum_{j_1+j_2=1}^{n} \left|(y_k|x_1^{j1} x_2^{j2})\right| \right), \quad\quad (4.1.11)
\end{aligned}
$$

where, similar to the section 4.1.1, J_2 depends on up to 8 control parameters, that is, $J_2 = J_2(\vec{u})$, and the components of $\vec{u}$ are the strengths of the fields in the skew quadrupole correctors. $\vec{z}$ and J_1 depend continuously on $\vec{u}$ over some compact set for the parameters $\vec{u}$.

4.1.3 Tune Preservation

In Sections 4.1.1 and 4.1.2, the statements of the two problems — linear and nonlinear — for uncoupling of the transversal dynamics of the particles in the horizontal and vertical planes were discussed. Changes made to the skew quadrupole content of the lattice might result in the change of the tunes (eigenvalue phases of the transfer map).

Such a change is undesirable, and therefore along with one of the two problems of the skew quadrupole correction one should state the problem of the preservation of the tune. The constant part of the tune can be found using the following relations:

$$\mu_x = \arccos\left(\frac{1}{2}\left(\frac{\partial x^{(f)}}{\partial x^{(i)}} + \frac{\partial a^{(f)}}{\partial a^{(i)}}\right)\right),$$
$$\mu_y = \arccos\left(\frac{1}{2}\left(\frac{\partial y^{(f)}}{\partial y^{(i)}} + \frac{\partial b^{(f)}}{\partial b^{(i)}}\right)\right),$$

(4.1.12)

where $\vec{z} = (x, a, y, b)^\top$ is the vector of the phase space variables of the system (4.1.1) under consideration.

Hence, one should add one more objective function to the list of the functions to minimize:

$$J_3 = \left|\mu_x - \arccos\left(\frac{1}{2}\left(\frac{\partial x^{(f)}}{\partial x^{(i)}} + \frac{\partial a^{(f)}}{\partial a^{(i)}}\right)\right)\right| +$$
$$\left|\mu_y - \arccos\left(\frac{1}{2}\left(\frac{\partial y^{(f)}}{\partial y^{(i)}} + \frac{\partial b^{(f)}}{\partial b^{(i)}}\right)\right)\right|.$$

(4.1.13)

The strengths of the main quadrupoles are used as the control parameters for this particular problem. As all the focusing quadrupoles and all the defocusing quadrupoles are set to the same value of the strength throughout the ring, there are two independent parameters to control.

4.1.4 Introduction to the Solution Methods

Next sections address the methods to solve the problems from Sections 4.1.1–4.1.3 and corresponding algorithms, implemented during the work on the dissertation from 2003 to 2006. The computer implementation of the algorithms is done using Mathworks Matlab R13 and COSY INFINITY versions 8.0–9.0. An additional utility program to convert lattices [45] is written in PHP version 4.4.4 (PHP: Hypertext Preprocessor) [1].

FODO 1	D*2	FQ	SQC	D*2	D*2	DQ	D*2
FODO 2	D*2	FQ		D*2	D*2	DQ	D*2
FODO 3	D*2	FQ	SQC	D*2	D*2	DQ	D*2
FODO 4	D*2	FQ		D*2	D*2	DQ	D*2
FODO 5	D*2	FQ	SQC	D*2	D*2	DQ	D*2
FODO 6	D*2	FQ		D*2	D*2	DQ	D*2
FODO 7	D*2	FQ	SQC	D*2	D*2	DQ	D*2
FODO 8	D*2	FQ		D*2	D*2	DQ	D*2
FODO 9	D*2	FQ	SQC	D*2	D*2	DQ	D*2
FODO 10	D*2	FQ		D*2	D*2	DQ	D*2
FODO 11	D*2	FQ	SQC	D*2	D*2	DQ	D*2
FODO 12	D*2	FQ		D*2	D*2	DQ	D*2
FODO 13	D*2	FQ	SQC	D*2	D*2	DQ	D*2
FODO 14	D*2	FQ		D*2	D*2	DQ	D*2
FODO 15	D*2	FQ	SQC	D*2	D*2	DQ	D*2

Fig. 4.1. Lattice scheme before any correction

According to the formulation of the problems in Sections 4.1.1–4.1.3, it is necessary to minimize the function J_1 or J_2 depending on the kind of the problem under consideration, and the function J_3, the minimization of which guarantees that the tune deviation from the initial value is minimal. These two problems can be solved one after another, as the control parameters for J_1 and J_2 are the strengths of the skew quadrupole correctors, the number of which varies from 6 to 8 for each sector, while for J_3 the control parameters are the strengths of the main quadrupoles — focusing and defocusing.

It is desirable though to keep all the skew quadrupole correctors at the same strength due to the features of power supplies. So, the number of various control parameters goes down to 6 in all arcs. For an additional optimization step one can use different sets of parameters. Straight sections also have four pairs of correctors and if one wants to vary these pairwise, which gives 4 more control parameters.

Figure 4.1 shows a lattice scheme of the typical arc of the Tevtaron.

The scheme employs the following notation:

<FQ> — focusing quadrupole;

<DQ> — defocusing quadrupole;

<D*2> — two sections of the main bending magnet;

<D*2 FIX> — two sections of the main bending magnet to be fixed during the shutdown of August 2004;

<SQC> — skew quadrupole corrector, minimizing the influence of the skew quadrupole errors in bending magnets.

4.1.5   Skew Quadrupole Error Sources

During the Tevatron operation since early 1980's, due to the stress from the strong magnetic fields, the superconducting coils of the 774 main bending dipoles shifted, thus introducing a significant skew quadrupole component in the expansion of the magnetic field [57], which could not be effectively mitigated by the existing family of skew quadrupole correctors. The status of the collider as of the beginning of August 2004 was as follows: about 15% of all the dipoles were fixed, and the other 85% still had the skew quadrupole component in them. According to the plan of the shutdown works, up to 50% of the dipoles (total) could be fixed. So, there was a need of an effective pattern of the dipoles to fix to simplify the correction issue in such a way that the existing family of correctors could uncouple the motion in the horizontal and vertical planes. After the effective scheme was found the corrector strengths were set to the values minimizing the functions J_1, J_2, J_3 (one or more depending on the nature of the problem).

4.1.6 Initial Data

As all the calculations are performed in terms of the high-order Taylor expansions, it is necessary to first obtain the representation of the transfer map of one full revolution in terms of Taylor expansions. This is done using the code COSY INFINITY (COSY), which implements multidimensional differential algebra. Among the conveniences of such an approach is the fact that certain families of the optics elements can easily be turned on and off in order to study particular effects and phenomena, their correlation and the impact on the dynamics of particles in general.

The initial data — the description of the system lattice — were obtained from one of the Fermilab employees, Valeri Lebedev, in the format of the code list intended to run in the beam optics computation program OptiM [32]. To convert the existing lattice to COSY internal format, a converter program was written (the detailed description can be found in Appendix A). It is available on the web at `http://cosy.pa.msu.edu/converters/optiM2cosy/`. PHP 4.4.4 [1] was the language of choice for the converter. The main reasons for this choice were the simplicity of the code writing and debugging and the fact that PHP is a web-oriented programming language. As a result, the converter code can be used at virtually any web-server supporting PHP. Currently the following set of optics elements is supported: dipoles, quadrupoles, skew quadrupoles, sextupoles and skew sextupoles, thin lens approximation quadrupoles and sextupoles, solenoids, electrostatic separators, and octupoles. The file generated by the converter can be used in COSY with no further change to calculate the fifth order transfer map of one full revolution.

To ensure the conversion program works flawlessly, a number of tests were performed. First of all, the linear transfer matrices were compared among COSY, OptiM (Fig. 4.2), and also an independent implementation in COSY by Bela Erdelyi [22].
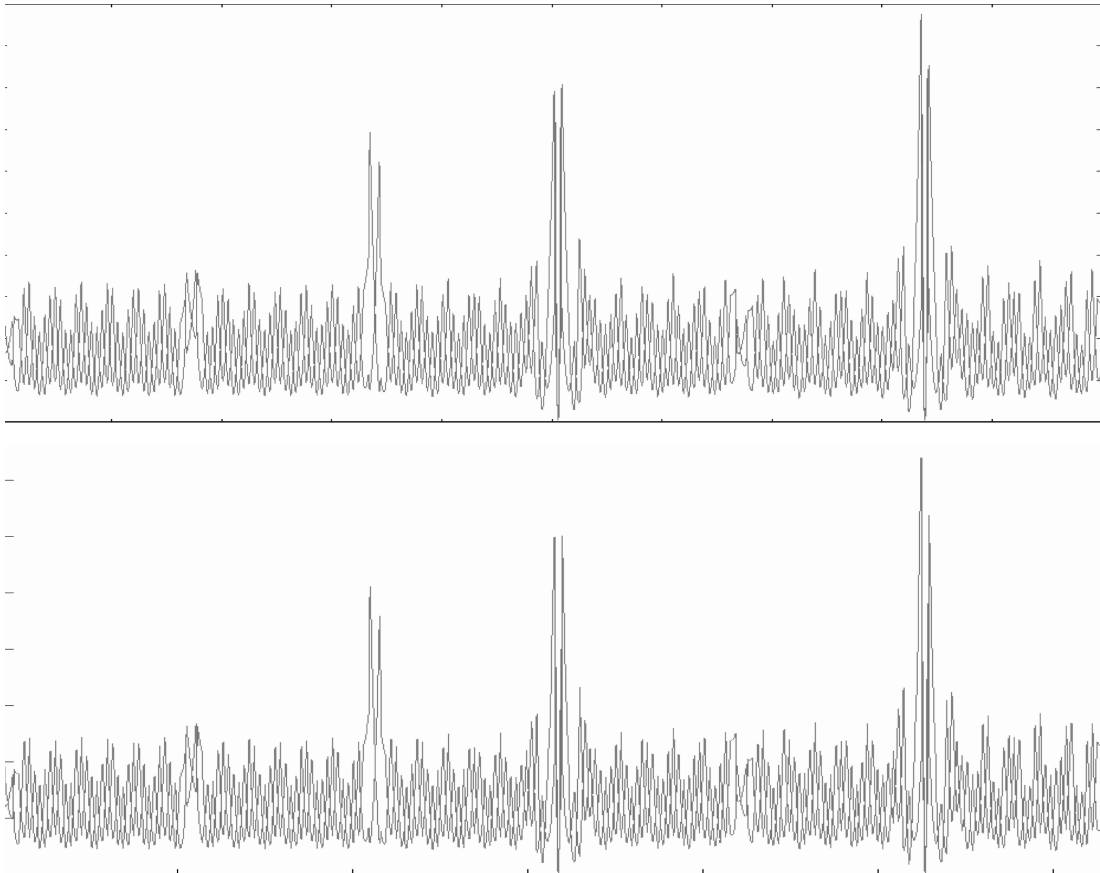
Fig. 4.2. Beta functions comparison, top - OptiM32, bottom - COSY INFINITY

Also the values of the beta functions [57] and the dispersion functions were compared. The quantitative result showed the discrepancy between the models within one percent, which was most likely caused by the differences in the solenoid element implementation in different codes [32, 35].

4.1.7   Model Details and Tracking Results

Typically 11th to 15th order maps were required for the complete convergence of the nonlinear effects (the phase portraits show no or little discrepancy when the order is increased further), but lower orders (7th, for example) provided a quicker check and served as the preliminary optimization results. The calculation order corresponds to the degree of the Taylor polynomial which is substituted for the function on the right hand side of the system (4.1.1).

Particles were launched at the CDF interaction point in steps of one sigma (for the normalized emittance of 10π at injection, $\sigma = 1.2 \cdot 10^{-4}$ m). Particles were tracked in COSY by applying the transfer map repetitively for typically 10,000 turns. Only the injection optics was being studied. It is important to note that the study is not, per se, a dynamic aperture one for which particles are launched along phase space vectors scaled to the linear injection ellipse and the transmitted transverse phase is mapped. In a predominately linear lattice, tracking along a single vector in one plane of phase space and then the other is sufficient to trace out the matched ellipse. Particles can be launched along the x or y axis, for example. The degradation of the linear motion as evidenced by dissolution or distortion of the linear invariant ellipses is then studied. Since the current study is directed toward optimizing the linear performance, this is the approach used for tracking and the criterion for improvement. In some cases other directions were also considered, for instance, the diagonals of the planes (x, a)
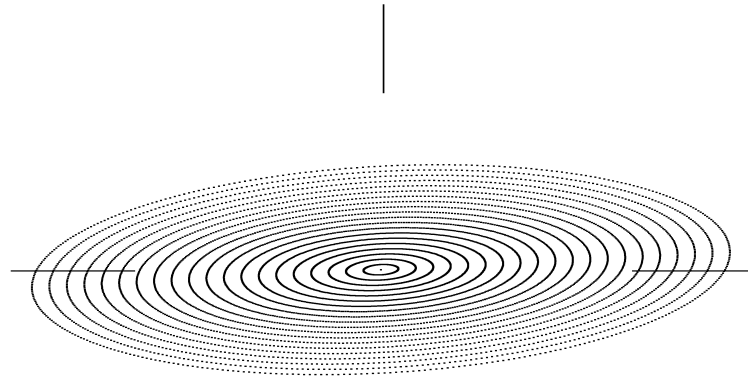
and (y, b).

The tracking results presented in this and subsequent sections are obtained for 10,000 turns with points plotted every 10th turn, and the scales are $2.7 \cdot 10^{-3}$ m for the x and y axes and $4.0 \cdot 10^{-3}$ for the a and b axes, if it is not mentioned otherwise. The tracking is performed with a symplectification algorithm written by Bela Erdélyi [23–25, 44] for the calculation order 7. All the particles are launched either along the x or y axis, which is explicitly mentioned in each figure caption. To start comparing the impacts of different sets of the nonlinear elements, in Fig. 4.3 the phase portraits for the linear motion are shown. This includes only pure dipoles, pure quadrupoles and no skew quadrupole errors in dipoles, and hence there is no coupling between the (x, a) and (y, b) planes.

According to the status of the Tevatron before August 2004, with 15% of the skew quadrupole errors removed in selected dipoles, the otherwise unchanged lattice shows significantly reduced stability (Fig. 4.4). Regular structures disappear and most of the outer particles can be considered lost in just 10,000 turns, while the realistic simulations require millions of turns. These phase portraits can be considered a starting point of the study of different schemes of the skew quadrupole correction.

4.1.8   Skew Quadrupole Circuits Optimization Proposals

As the scheme suggests (Fig. 4.1), each of the Tevatron arcs in the model framework has 15 FODO cells with the skew quadrupole correctors in every odd-numbered cell, which means one corrector every two FODO cells. The "O" section of the FODO cell contains four sections of the bending magnet, high order magnets, and various correctors. The skew quadrupole correctors are placed next to the horizontally-focusing quadrupoles only.

(a) (x, a) plane
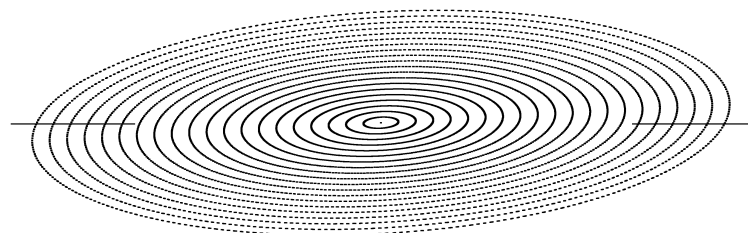
(b) (y, b) plane

Fig. 4.3. The (x, a) plane and (y, b) plane phase portraits, only dipoles and pure quadrupoles are active, and particles are launched along the x axis and the y axis, respectively. The scales are $2.7 \cdot 10^{-3}$ m for the x and y axes and $4.0 \cdot 10^{-3}$ for the a and b axes.
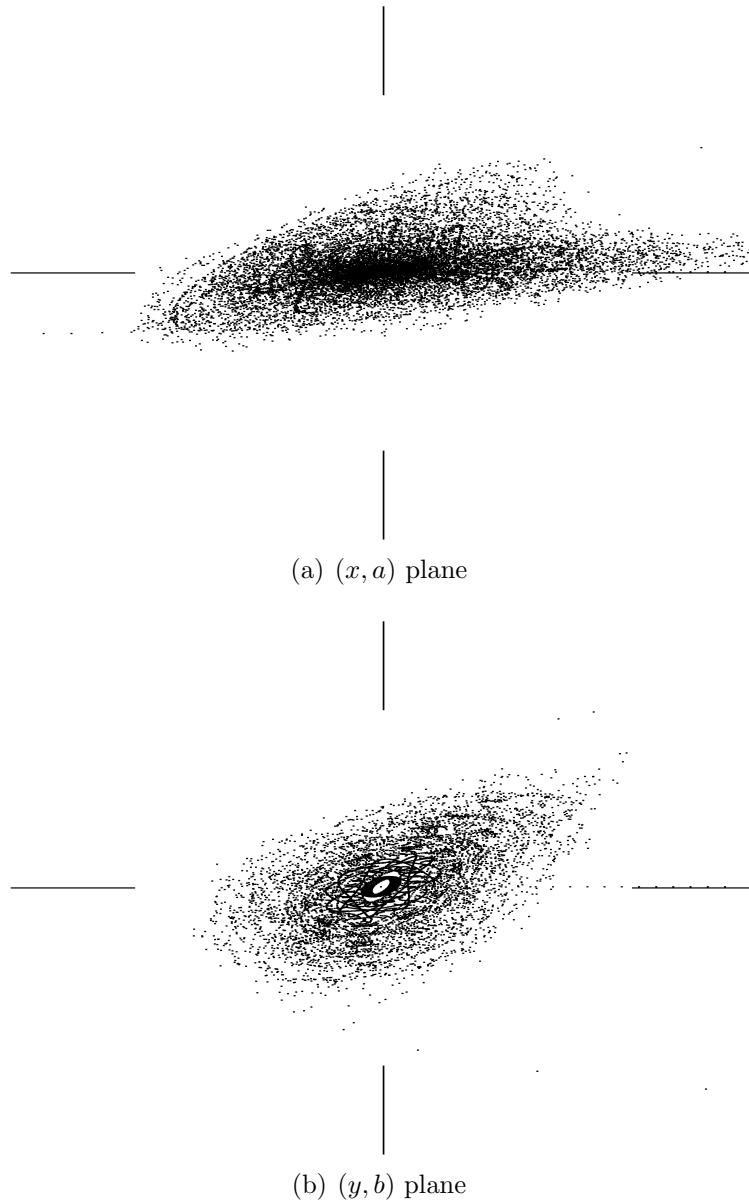
(a) (x, a) plane

(b) (y, b) plane

Fig. 4.4. The (x, a) plane and (y, b) plane phase portraits before the optimization, particles are launched along the x axis and the y axis, respectively. The phase portraits include all sextupole and skew quadrupole fields (correctors plus errors) in addition to quadrupoles and dipoles, where 15% of the skew quadrupole errors have been removed in specific dipoles. the scales are $2.7 \cdot 10^{-3}$ m for the x and y axes and $4.0 \cdot 10^{-3}$ for the a and b axes.

It is clear from Fig. 4.4 that one family of skew quadrupole correctors is not sufficient to correct all the skew quadrupole errors in dipoles along the ring. However, if 50% of the coil shift errors in dipoles are fixed, one circuit of the skew quadrupole correctors is capable of removing the coupling in the arcs. The problem here is to discover both the optimal dipole pattern for error correction and the new strengths for the skew quadrupole correctors.

An optimization with the corrector strengths set to different values is not practical. All the correctors in each arc have the same power supply, so it is more realistic to use one strength for all the correctors arc-wise or even ring-wise.

The optimization process itself consists of two steps. First, the optimization of each arc is performed using the skew quadrupole corrector strengths as control parameters. This optimization would be close to optimal if no skew quadrupole components existed in the straight sections of the Tevatron, but there are skew quadrupole error sources and correctors in the interaction regions. Because of these components and the residual skew terms from the arcs since the arcs are not perfectly regular, the one-turn transfer map has nonzero skew quadrupole terms which require correction also. To remove this smaller, final stage of coupling a second step of the optimization is required. In four of the six straight sections there exist eight skew quadrupole correctors and the strengths of these correctors are used to finish the skew-quadrupole term cancellation in the one-turn map.

As a result of the optimization, two optimization schemes were selected out of six, which differed in the dipole pattern used for correcting the skew quadrupole error. The first scheme, proposed by the author and Dr. Carol Johnstone (Fermilab) [48], attempts the elimination of skew quadrupole error source predominately in the vertical plane by fixing the two dipoles flanking each vertically-focusing arc quadrupole.

FODO 1	D*2	FQ	SQC	D*2	D*2 FIX	DQ		D*2 FIX
FODO 2	D*2	FQ		D*2	D*2 FIX	DQ		D*2 FIX
FODO 3	D*2	FQ	SQC	D*2	D*2 FIX	DQ		D*2 FIX
FODO 4	D*2	FQ		D*2	D*2 FIX	DQ		D*2 FIX
FODO 5	D*2	FQ	SQC	D*2	D*2 FIX	DQ		D*2 FIX
FODO 6	D*2	FQ		D*2	D*2 FIX	DQ		D*2 FIX
FODO 7	D*2	FQ	SQC	D*2	D*2 FIX	DQ		D*2 FIX
FODO 8	D*2	FQ		D*2	D*2 FIX	DQ		D*2 FIX
FODO 9	D*2	FQ	SQC	D*2	D*2 FIX	DQ		D*2 FIX
FODO 10	D*2	FQ		D*2	D*2 FIX	DQ		D*2 FIX
FODO 11	D*2	FQ	SQC	D*2	D*2 FIX	DQ		D*2 FIX
FODO 12	D*2	FQ		D*2	D*2 FIX	DQ		D*2 FIX
FODO 13	D*2	FQ	SQC	D*2	D*2 FIX	DQ		D*2 FIX
FODO 14	D*2	FQ		D*2	D*2 FIX	DQ		D*2 FIX
FODO 15	D*2	FQ	SQC	D*2	D*2 FIX	DQ		D*2 FIX

Fig. 4.5. Correction scheme I: the skew quadrupole error is removed in dipoles in each cell surrounding the defocusing quadrupole.

With one degree of freedom corrected, the remaining predominately horizontal sources can be corrected with the existing single family of the skew quadrupole correctors. The layout for Scheme I is shown in Fig. 4.5. One arc of the Tevatron is shown, and the others are similar. The dipoles with the skew quadrupole error are marked with the "D*2" symbol, and the fixed dipoles with the "D*2 FIX" symbol. The vertically-focusing main quadrupole is marked with "DQ" as it is defocusing in the horizontal plane.

The second approach proposed by Dr. Michael Syphers [51] is to correct the skew quadrupole errors in each FODO cell missing a skew quadrupole corrector. This scheme was further improved by removing specific correctors from the single family to provide for more consistent correction in each arc as a function of fractional phase advance. The Tevatron has a periodicity of five, that is, if we consider the linear dynamics, the phase advance of the particles after one cell is 72 degrees. Hence, after

five cells the particle has the same phase. Taking into account that all the skew quadrupole correctors in each arc have the same strength, it makes sense to have the same number of correctors for the following groups of cells to avoid over/under-correction: (1,6,11), (2,7,12), (3,8,13), (4,9,14) and (5,10,15). Looking at Fig. 4.1 (the situation before the correction), the triplets (1,6,11), (3,8,13) and (5,10,15) have two correctors, while the triplets (2,7,12) and (4,9,14) have one. For the Scheme II it is proposed to turn off the correctors in the cells 1, 3, 15, so that every triplet of the cells has one skew quadrupole corrector.

The underlying idea of the scheme is to correct the error locally at the source and remove it from cells without local correction. This scheme gives improved performance, particularly using one uniform corrector strength across all the arcs. The layout for the scheme is given in Fig. 4.6. The skew quadrupole error sources reside in odd cells with the skew quadrupole correctors marked with "SQC". Removing part of the correctors improved performance further, and these removed correctors are marked with "SQC RMV".

4.1.9 Optimization Results

The optimization itself is done in three stages. At first, the one-parameter minimization of J_1 or J_2 is performed for each particular sector out of six (the transfer map (4.1.3) of each individual arc is considered instead of the one-turn transfer map), as all the sectors are somewhat different. For example, in the straight sections between the sectors A and B, and C and D the two detectors CDF and DZero are located, which imposes some restrictions onto the last cells of A and C, and the first cells of B and D. This first optimization stage would be sufficient if there were no straight sections connecting the arcs. The straights too have optics elements alternating the

FODO 1	D*2	FQ	SQC RMV	D*2	D*2	DQ	D*2
FODO 2	D*2 FIX	FQ		D*2 FIX	D*2 FIX	DQ	D*2 FIX
FODO 3	D*2	FQ	SQC RMV	D*2	D*2	DQ	D*2
FODO 4	D*2 FIX	FQ		D*2 FIX	D*2 FIX	DQ	D*2 FIX
FODO 5	D*2	FQ	SQC	D*2	D*2	DQ	D*2
FODO 6	D*2 FIX	FQ		D*2 FIX	D*2 FIX	DQ	D*2 FIX
FODO 7	D*2	FQ	SQC	D*2	D*2	DQ	D*2
FODO 8	D*2 FIX	FQ		D*2 FIX	D*2 FIX	DQ	D*2 FIX
FODO 9	D*2	FQ	SQC	D*2	D*2	DQ	D*2
FODO 10	D*2 FIX	FQ		D*2 FIX	D*2 FIX	DQ	D*2 FIX
FODO 11	D*2	FQ	SQC	D*2	D*2	DQ	D*2
FODO 12	D*2 FIX	FQ		D*2 FIX	D*2 FIX	DQ	D*2 FIX
FODO 13	D*2	FQ	SQC	D*2	D*2	DQ	D*2
FODO 14	D*2 FIX	FQ		D*2 FIX	D*2 FIX	DQ	D*2 FIX
FODO 15	D*2	FQ	SQC RMV	D*2	D*2	DQ	D*2

Fig. 4.6. Correction scheme II: the skew quadrupole errors in dipoles are fixed in each even cell.

skew quadrupole component of the field as well as the skew quadrupole correctors. So a second, "global" stage of the optimization is required with the same functions, but with a different set of control parameters. Four pairs of correctors in the straight sections or all of the available correctors (including these in the arcs) could be used in the minimization procedure. Hence, the number of parameters varies from 4 to 10.

Various optimization methods and sequences of methods were used to solve the problem. Among them are the simplex method [41], the modified Newton method [33], and the simulated annealing method [31].

After the values for the skew quadrupole correctors minimizing J_1 or J_2 are found, it is important to ensure that the change of parameters did not change the tune. For the Tevatron $\mu_x = 0.585$, $\mu_y = 0.575$, and therefore all the values on the right hand side of (4.1.13) are known, and one can search for the minimum of J_3 using the strengths of the main focusing and defocusing quadrupoles. They have the same

strengths for all the sectors, so there are two control parameters.

The phase portraits of the system after the multi-stage optimization according to Scheme I are shown in Fig. 4.7. This scheme proved to be more stable under a perturbation of the system parameters, so it could be more reliable from the practical viewpoint, but it is less efficient in the sense of the horizontal and vertical plane decoupling.

Fig. 4.8 shows the phase portraits of the system, optimized using the Scheme II layout. From the qualitative point of view, this scheme application results in more closed uncoupled trajectories: up to 20σ in the horizontal plane and 12σ in the vertical plane, which is noticeably better than Scheme I. It also stays efficient even if all the correctors in the arcs are set to one strength throughout the ring. Nonetheless, it is worth noting that this scheme is sensitive to the small changes of the system parameters.

Scheme II with minor changes was implemented during the planned Tevatron shutdown in August 2004, and proved itself very efficient as a temporary solution before all the errors in dipoles could be corrected.

As the main aim of the optimization was the decoupling of the dynamics in the horizontal and vertical planes, to demonstrate the results, it is worth comparing the linear parts of the transfer maps before and after the optimization, represented in the matrix form for convenience.

The linear transfer map before the optimization is

$$
\begin{pmatrix}
-0.7553149 & 0.3637584 & 0.0663166 & -0.0971958 \\
-0.8640196 & -0.9507699 & -0.4305946 & 0.1421480 \\
-0.0251393 & -0.0621722 & -0.8060247 & 0.3353297 \\
-0.4966847 & 0.0614653 & -0.7083212 & -0.9862029
\end{pmatrix},
\tag{4.1.14}
$$

66

(a) (x, a) plane

(b) (y, b) plane
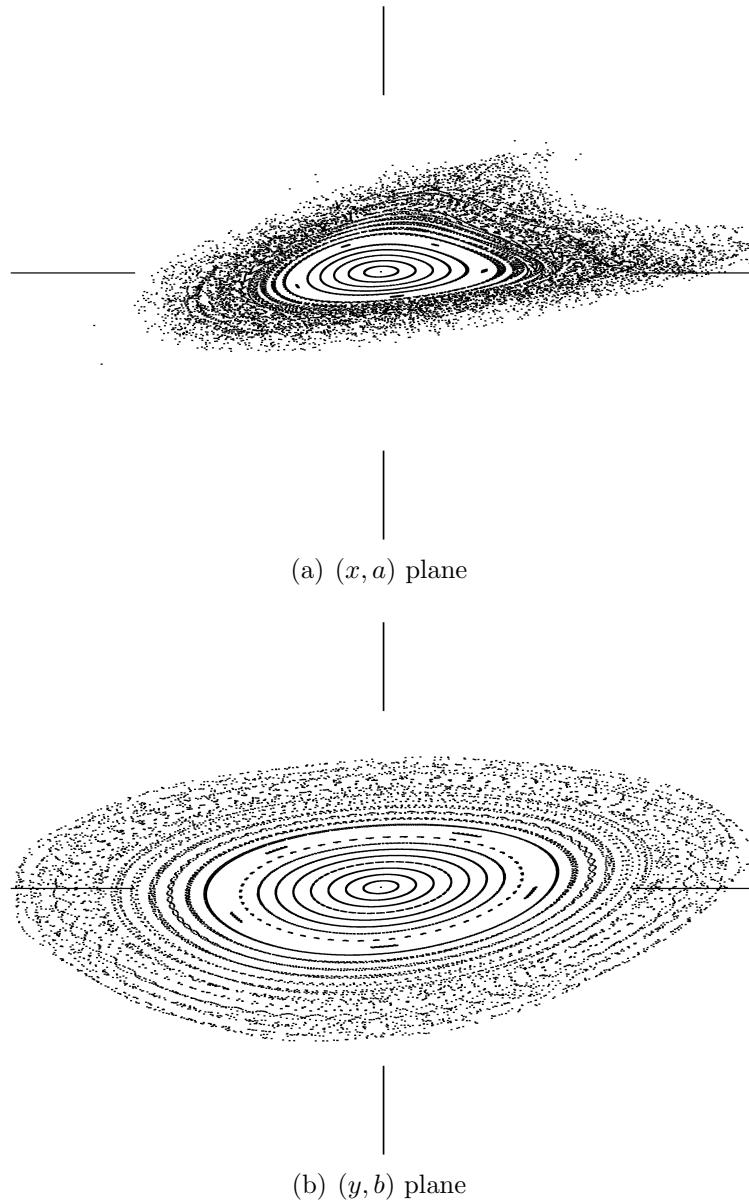
Fig. 4.7. The (x, a) plane and (y, b) plane phase portraits after the optimization with 50% skew quadrupole errors in dipoles, errors are fixed according to Scheme I: around each defocusing quadrupole; particles are launched along the x axis and the y axis, respectively. The scales are $2.7 \cdot 10^{-3}$ m for the x and y axes and $4.0 \cdot 10^{-3}$ for the a and b axes.

(a) (x, a) plane

(b) (y, b) plane

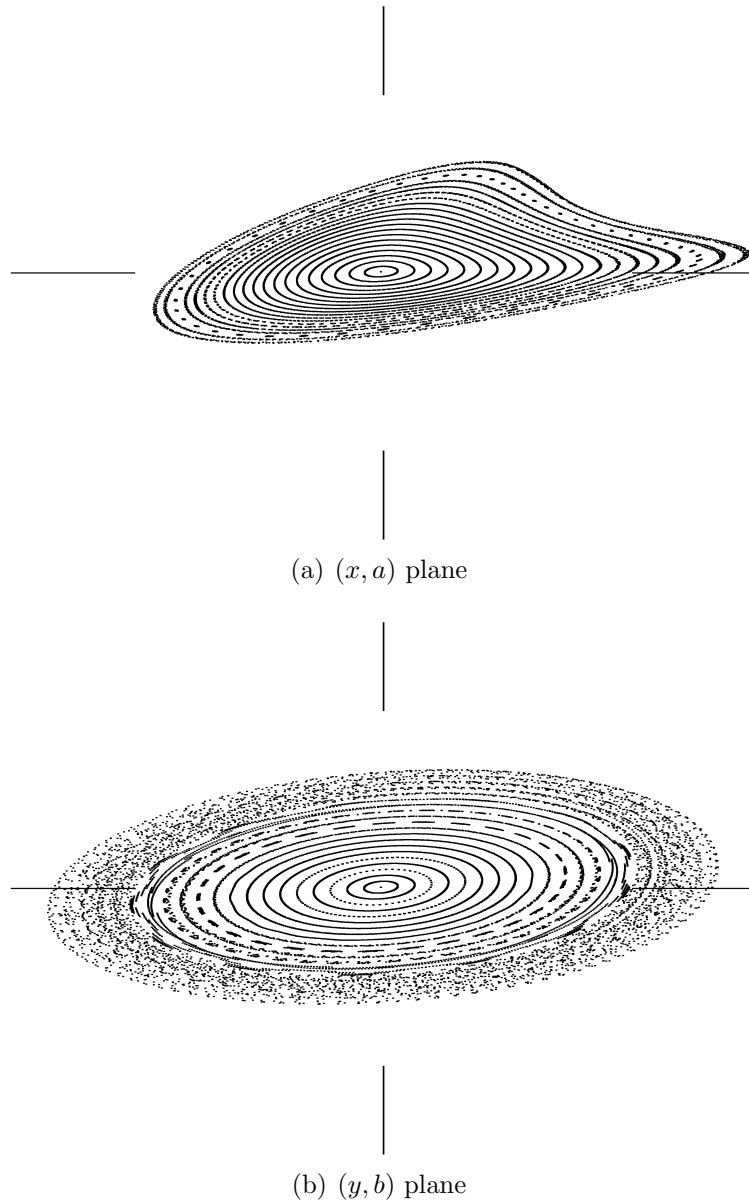Fig. 4.8. The (x, a) plane and (y, b) plane phase portraits after the optimization according to Scheme II: the skew quadrupole errors are removed in the two dipoles flanking each horizontally defocusing quadrupole, and particles are launched along the x axis and the y axis, respectively. The scales are $2.7 \cdot 10^{-3}$ m for the x and y axes and $4.0 \cdot 10^{-3}$ for the a and b axes.

and after the optimizaton —

$$
\begin{pmatrix}
-0.8023857 & 0.3107970 & \mathbf{0.0059011} & \mathbf{-0.00254055} \\
-0.7143330 & -0.9696470 & \mathbf{-0.0058075} & \mathbf{-0.00487758} \\
\mathbf{0.0043365} & \mathbf{-0.0022290} & -0.8445417 & 0.28890307 \\
\mathbf{-0.0077313} & \mathbf{-0.0060658} & -0.5409385 & -0.9990799
\end{pmatrix} . \qquad (4.1.15)
$$

Matrix elements responsible for the cross-coupling between the planes are marked with bold font (four elements in the upper right corner and four elements in the lower left corner). Eq. (4.1.15) shows that after the optimization these terms become up to 74 times smaller as compared to Eq. (4.1.14).

4.1.10   Summary

Studies conducted on the skew quadrupole correction case showed that if the skew quadrupole errors are left unchanged, one family of the skew quadrupole correctors is not enough to provide a sufficient correction, or the change of locations of the correctors is in order, which is not a feasible option. At the same time, if 50% errors are fixed, one corrector family can solve the dynamics decoupling problem successfully, even with all the correctors in the arcs set to one particular strength.

All the calculations were carried out in COSY using the following two sets of parameters:

- draft optimization cycle: 10^4 turns, 7th calculation order — takes about 5–10 minutes on an average laptop: Intel Celeron 1.5 MHz and 256 Mb RAM;

- final optimization cycle: 10^6 turns, 11th calculation order — takes 8 to 12 hours on the same machine.

It is worth noting that even the 7th order of calculation returns reliable results, allowing to estimate the efficiency of the optimization approach before turning to a more

lengthy cycle. Figure 4.9 demonstrates that the phase portraits for the parameter sets mentioned above are very similar, which justifies the use of the 7th order.

## 4.2   Calculation of Nonlinear Tune Shifts with Amplitude

The tune of the system is one of the most important characteristics of the dynamics of particles. For the linear system the tune stays constant, while in the nonlinear case it might change, mainly depending on the position of the particle in the beam (the so-called tune shift with amplitude), but also depending on other parameters of the system.

Consider the problem of evaluation of the tune shift with amplitude in the nonlinear case using some extra information obtained by the specific kind of measurements [46]. All the proposed methods have been tested on the Tevatron model [38] and measurements [6], but that does not mean that the algorithm for finding the tune shift with amplitude is not applicable to other machines. In fact, the algorithm should stay valid for any other synchrotron, as long as one can proceed with a linear normal form transformation (see Section 3.1 for conditions). The normal form transformation is the core of the method.

Suppose that one only has the information on the linear component of the dynamics of the particles in the accelerator. Assume that there is some extra information available: the size of the beam, the particle distribution type and also the results of the special type of measurements of the beam position. The corrector is introduced into the accelerator optics to kick the beam in the horizontal or vertical direction. Once the strength of the corrector is known, the displacement of the center of the
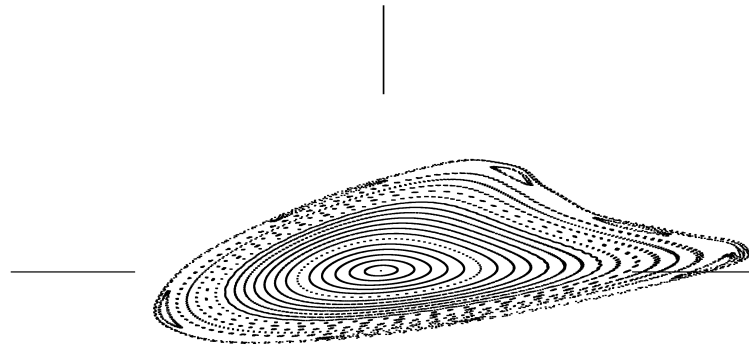
(a) 7th order, 10000 turns
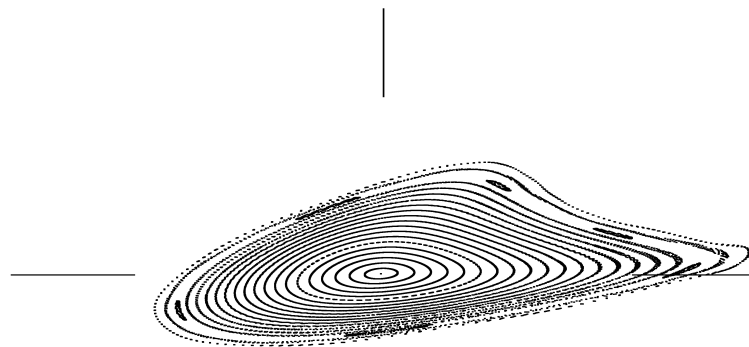
(b) 11th order, 1000000 turns

Fig. 4.9. Calculation order comparison and its influence on the phase portraits in the (x, a) plane. The scales are $2.7 \cdot 10^{-3}$ m for the x axis and $4.0 \cdot 10^{-3}$ for the a axis.
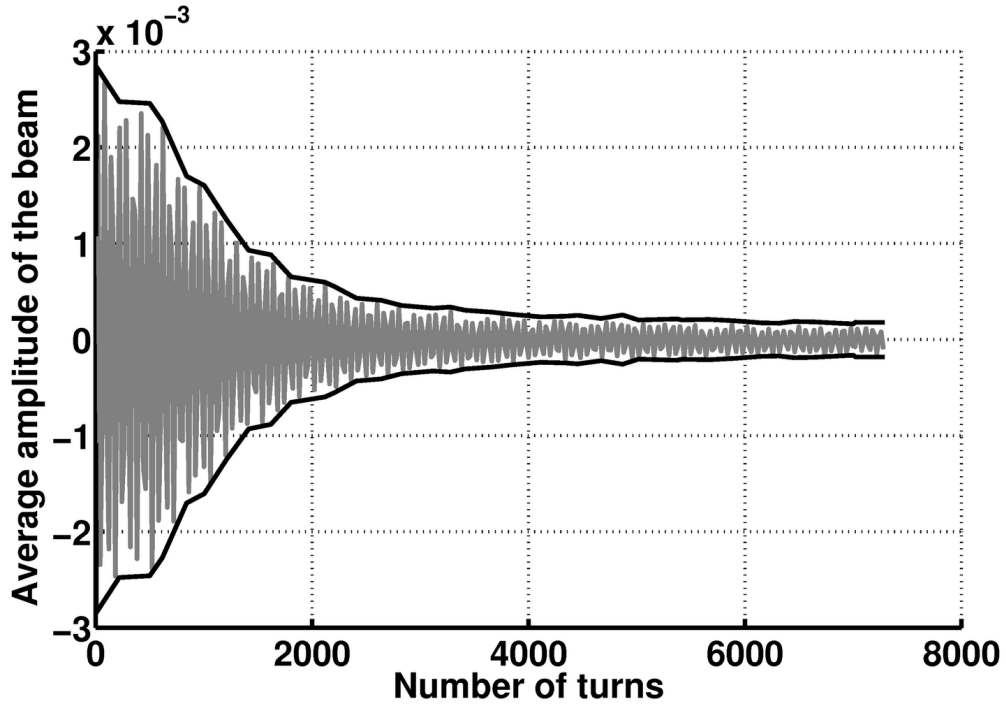
Fig. 4.10. Measurement results: horizontal position of the center of mass over a number of turns and its envelope

beam can be found. After the corrector is turned on and off instantaneously, the amplitude of the beam center of mass decreases due to the filamentation of the beam, not the damping, as the motion is symplectic. The position of the center of mass of the beam is then registered after each turn of the particles. One sample of the measurement data for the horizontal position is shown in Fig. 4.10.

The normal form transformation yields that in the nonlinear case the tune can be represented in the following form:

$$\mu = \mu_0 + c_1 r^2 + c_2 r^4 + \dots, \tag{4.2.1}$$

where μ_0 is a constant linear tune, c_1, c_2 are the coefficients of the higher order terms in the expansion of the dependence of the tune μ on the particle's amplitude in the

normal form coordinates, where the amplitude is defined to be $r = \sqrt{(t^+)^2 + (t^-)^2}$ for the particle with normal form coordinates (t^+, t^-).

As it is assumed that the linear component of the dynamics is known, the value of μ_0 is also known for each pair of the conjugate variables describing the transversal dynamics, while there is not enough information to find the coefficients in the expansion (4.2.1). The task is to find the connection between the number of turns N required for the amplitude of the central particle after the kick $r(N)$ to fall to the values comparable to the amplitude before the kick, which means that the absolute value of the derivative $r'(N)$ of the amplitude falls below the certain value.

4.2.1 Objective Functions for the Study

The purpose of the study is to restore at least the c_1 coefficient in the expansion (4.2.1) using the measurement results. If multiple measurements are available with various initial kicks, it might be possible to restore the second coefficient in the expansion, c_2.

Remark. N might be hard to find, so as an alternative one can use the following standard trick: take the number of turns $N_{1/2}$ required for the amplitude to fall to a half of its initial value. This would be a good reference point for the fall-off curve.

Hence, the objective function assumes the form

$$J_4(a, b) = |\eta(a, b) - N|, \tag{4.2.2}$$

where $\{\eta : r'|_\eta < \kappa, r'|_m > \kappa \ \forall m < \eta\}$, $r'|_m$ is the rate of change of the beam center of mass amplitude after k turns, and κ is the initial value of the amplitude before the kick;

$$J_5(a, b) = |\eta_{1/2}(a, b) - N_{1/2}|, \tag{4.2.3}$$

73

where $\{\eta_{1/2} : r|_{\eta_{1/2}} \leq \frac{1}{2}r|_0\}$, $r|_{\eta_{1/2}}$ is the beam center of mass amplitude after $\eta_{1/2}$ turns, and $r|_0$ is the beam center of mass amplitude immediately after the kick (the peak amplitude).

In both cases $\eta = \eta(r)$, and in turn, $r = r(x_c, y_c)$ where x_c, y_c are the coordinates of the center of mass after the kick in the normal form coordinates. Depending on the distribution of particles in the beam and the displacement of the beam due to the kick, the formulas for x_c, y_c will be different, and for certain cases they are derived in Sections 4.2.3–4.2.5. The control parameters are the coefficients c_1 and c_2 in the expansion of the tune (4.2.1).

All the numerical results of the subsequent subsections are based on the Tevatron model available on the Fermi National Accelerator Laboratory website [38]. The source code for the lattice is in the format of the MAD programming environment [3], for which a converter to COSY INFINITY is readily available. It is currently maintained by Dr. Kyoko Makino at Michigan State University [2], so there was no need to reimplement the converter.

4.2.2 Calculation Results versus Measurement Results

After the normal form transformation all the particles follow circles with angular velocity depending on the amplitude. This is the key fact allowing to establish a connection between the nonlinear tune shift with amplitude and the behavior of the beam.

Figure 4.11 schematically shows the positions of four particles with initial positions chosen along some fixed direction (ray), after several turns. Particles cannot leave their corresponding circles, but the rotation frequencies are different for different radii. Assume that the outer particles move faster than the inner particles. In this
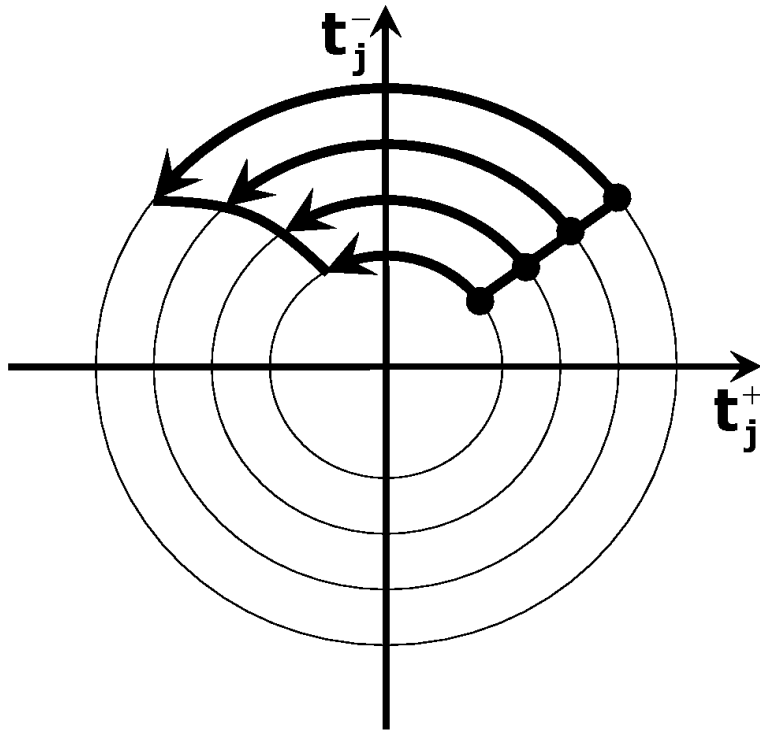
Fig. 4.11. Behavior of the particles in the normal form coordinates

particular case the outer particle will leave the inner particle behind in the phase. As a result of such a redistribution of particles the center of mass of the beam shifts toward the origin of the coordinate system and then oscillates around it.

Hence, if the center of the initial distribution of particles is displaced from the origin by means of an instantaneous transversal kick, as it is done to measure the trajectory with the beam position monitors (BPM), then the amplitude of the center of mass in the normal form coordinates decreases until it reaches a stable value.

As it is assumed that an accurate linear lattice description is available, one may use the linear normal form transformation, for which the information on the linear dynamics is sufficient, to get the information on the distribution of the beam in the linear normal form coordinates after the kick. The linear normal form transformation is discussed in great detail in [12], for a general transformation see also Chapter 3.

In such a coordinate system all the particles follow circles with the same angular frequency. Hence, the linear transformation does not give enough information on the nonlinear tune shift. At the same time the linear transformation is sufficient to get an approximate initial distribution of the beam in the normal form coordinates.

It is a fact that the nonlinear tune shift with amplitude depends on r^2, r^4, and so forth, where r is the amplitude of the particle in the normal form coordinates: $r = \sqrt{(t^+)^2 + (t^-)^2}$, that is,

$$\mu(r) = \mu_0 + c_1 r^2 + c_2 r^4 + \dots.$$

As a rule, $c_1 r^2$ is the dominating term in the expansion. Accelerator designers try to avoid high order nonlinearities, unless there is a specific need of them. Hence, finding the coefficient c_1 is the most important part. Later, if there are multiple measurements available, the coefficient c_2 could be attempted to be found as well.

In the nonlinear case all the particles of the beam follow concentric circles with frequencies depending on the amplitude, so the transfer map has the form:

$$\mathcal{M} = \begin{pmatrix} \cos 2\pi\mu(r) & -\sin 2\pi\mu(r) \\ \sin 2\pi\mu(r) & \cos 2\pi\mu(r) \end{pmatrix}. \tag{4.2.4}$$

If the transfer map $\mathcal{M}$ is known, one can track the behavior of particles for arbitrary many turns. That, in turn, allows to find the number of turns corresponding to the moment when the center of mass amplitude is back to its value before the kick, N, or it is at the half of its value after the kick, $N_{1/2}$. This establishes the connection between a and $N(N_{1/2})$. The number $N(N_{1/2})$ can be found from the measurements (Fig. 4.10). Hereafter, the common notation used is N, unless it is not obvious, whether N or $N_{1/2}$ is implied. Essentially these are the two different points on the graph characterizing the same curve.

The general scheme for establishing a connection between c_1 and N is as follows:

1. The outer particle of the beam having the amplitude R rotates with a frequency $\mu(R)$, and hence, after $1/(\mu(R) - \mu_0)$ turns this particle phase advance is 2π bigger (or smaller, depending on the sign of c_1) than that of the particle close to the origin; assume that the kick is weak enough and the beam is not displaced too far from the origin, and in fact, in most cases the kick is such that the origin is still inside the part of the phase space covered by the beam;

2. R depends on the strength of the kick and the initial particle distribution, the value of R can be found as the maximum of the deviations of particle positions from the origin after the linear normal form transformation, that is, all the components to find R are known;

3. The value of c_1 is not known, but one can always fix a certain c_1 and using the form of the transfer map (4.2.4) obtain the value of N as a function of c_1 and R;

4. Once the algorithm for finding $N(c_1)$ is established, it can be used multiple times to obtain the correct value of the coefficient c_1 for a known value of N inferred from the measurements as discussed above; it is a typical one-parameter optimization problem.

Hence, the problem under consideration has been reduced to establishing a dependence of N on various values of c_1 and R. Depending on the initial distribution of particles this can be a complicated task, which is not possible or not feasible to solve analytically to get an explicit expression for $c_1 = c_1(N)$. The next three subsections are dedicated to solving this problem numerically for various distributions.
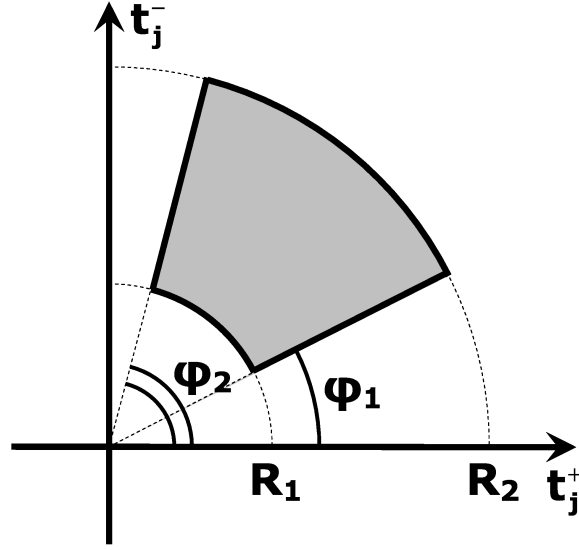
Fig. 4.12. Uniform particle distribution in the sector

4.2.3 Sector Approximation, Uniform Particle Distribution

Let our initial distribution be uniform in the sector bounded by the two radii R_1, R_2 and two angles φ_1, φ_2 (Fig. 4.12). After N turns each particle of this distribution will have the phase advance of

$$\theta_N(r) = 2\pi N \mu(r) = 2\pi N(\mu_0 + c_1 r^2 + c_2 r^4)$$

(orders up to 4 are taken into account). Hence, the particle with radius $R_1 < r < R_2$ located on the front (back) line of the distribution will have a phase difference of $\Delta\theta_N(r) = 2\pi N(\mu(r) - \mu(R_1))$ with respect to the inner particle.

To find the centroid of the resulting planar figure, bounded by two radii R_1, R_2

and two curves given by $\varphi_1 + \theta_N(r), \varphi_2 + \theta_N(r)$, three integral formulas are used:

$$
\begin{cases}
S = \displaystyle\iint r\,dr\,d\theta; \\[2mm]
x_c = \dfrac{1}{S} \displaystyle\iint r^2 \cos\theta\,dr\,d\theta; \\[2mm]
y_c = \dfrac{1}{S} \displaystyle\iint r^2 \sin\theta\,dr\,d\theta.
\end{cases}
$$

For the case under consideration:

$$
\begin{cases}
x_c^{(N)} = \dfrac{1}{S} \displaystyle\int_{R_1}^{R_2} \int_{\varphi_1+\theta_N(r)}^{\varphi_2+\theta_N(r)} r^2 \cos\theta\,d\theta\,dr; \\[4mm]
y_c^{(N)} = \dfrac{1}{S} \displaystyle\int_{R_1}^{R_2} \int_{\varphi_1+\theta_N(r)}^{\varphi_2+\theta_N(r)} r^2 \sin\theta\,d\theta\,dr.
\end{cases}
\tag{4.2.5}
$$

Hereafter, $x_c^{(N)}$ and $y_c^{(N)}$ are the coordinates of the beam center of mass in the normal form coordinate system (t^+, t^-).

Let us simplify the form of the last two integrals. Without loss of generality one can assume $-\varphi_1 = \varphi_2 = \varphi$ (the angle can be changed as only the radius is the quantity of interest). In addition to that, the coordinate θ is changed to $\psi + \theta_N(r)$. Then one has $d\theta = d\psi$, and the integrals transform to:

$$
\begin{aligned}
x_c^{(N)} &= \frac{1}{S} \int_{R_1}^{R_2} \int_{-\varphi+\theta_N(r)}^{\varphi+\theta_N(r)} r^2 \cos\theta\,d\theta\,dr = \\[2mm]
&= \frac{1}{S} \int_{R_1}^{R_2} \int_{-\varphi}^{\varphi} r^2 \cos(\psi + \theta_N(r))\,d\psi\,dr; \tag{4.2.6} \\[3mm]
y_c^{(N)} &= \frac{1}{S} \int_{R_1}^{R_2} \int_{-\varphi+\theta_N(r)}^{\varphi+\theta_N(r)} r^2 \sin\theta\,d\theta\,dr = \\[2mm]
&= \frac{1}{S} \int_{R_1}^{R_2} \int_{-\varphi}^{\varphi} r^2 \sin(\psi + \theta_N(r))\,d\psi\,dr. \tag{4.2.7}
\end{aligned}
$$

After integrating with respect to ψ under the remaining integral one can use the addition formulas:

$$
\begin{aligned}
\cos(a+b) &= \cos a \cos b - \sin a \sin b, \\[2mm]
\sin(a+b) &= \sin a \cos b + \cos a \sin b,
\end{aligned}
\tag{4.2.8}
$$

79

which ultimately results in

$$x_c^{(N)} = \frac{1}{S}\int_{R_1}^{R_2} r^2 \left\{\sin(\varphi + \theta_N(r)) - \sin(-\varphi + \theta_N(r))\right\} dr =$$

$$= \frac{1}{S}\int_{R_1}^{R_2} r^2 \left\{\sin\varphi\cos\theta_N + \cos\varphi\sin\theta_N + \sin\varphi\cos\theta_N - \cos\varphi\sin\theta_N\right\} dr =$$

$$= \frac{2}{S}\sin\varphi\int_{R_1}^{R_2} r^2 \cos\theta_N(r)dr.$$

$$y_c^{(N)} = \frac{1}{S}\int_{R_1}^{R_2} r^2 \left\{-\cos(\varphi + \theta_N(r)) + \cos(-\varphi + \theta_N(r))\right\} dr =$$

$$= \frac{1}{S}\int_{R_1}^{R_2} r^2 \left\{-\cos\varphi\cos\theta_N + \sin\varphi\sin\theta_N + \cos\varphi\cos\theta_N + \sin\varphi\sin\theta_N\right\} dr =$$

$$= \frac{2}{S}\sin\varphi\int_{R_1}^{R_2} r^2 \sin\theta_N(r)dr.$$

$$(4.2.9)$$

These last integrals cannot be found analytically due to the polynomial nature of the argument θ_N. Even if one assumes $\theta_N \propto r^2$, the result is a complicated expression given in terms of the Fresnel functions (Fig. 4.13, 4.14):

$$\int_{R_1}^{R_2} r^2 \cos\theta_N(r)dr = \frac{1}{4\pi Nc_1}\left(R_2\sin(2\pi Nc_1 R_2^2) - R_1\sin(2\pi Nc_1 R_1^2)\right) -$$

$$- \frac{1}{8\pi(Nc_1)^{3/2}}\left(\text{FresnelS}(2(Nc_1)^{1/2}R_2) - \text{FresnelS}(2(Nc_1)^{1/2}R_1)\right);$$

$$\int_{R_1}^{R_2} r^2 \sin\theta_N(r)dr = -\frac{1}{4\pi Nc_1}\left(R_2\cos(2\pi Nc_1 R_2^2) - R_1\cos(2\pi Nc_1 R_1^2)\right) -$$

$$- \frac{1}{8\pi(Nc_1)^{3/2}}\left(\text{FresnelC}(2(Nc_1)^{1/2}R_2) - \text{FresnelC}(2(Nc_1)^{1/2}R_1)\right),$$

$$(4.2.10)$$

where $\text{FresnelS}(x) = \int_0^x \cos(\frac{\pi}{2}t^2)dt$, and $\text{FresnelC}(x) = \int_0^x \sin(\frac{\pi}{2}t^2)dt$ [4].

The shape of the graph of the Fresnel functions explains the behavior of the beam center of mass shown in Fig. 4.10. To see even more resemblance, some individual BPM measurements are shown in Fig. 4.15.

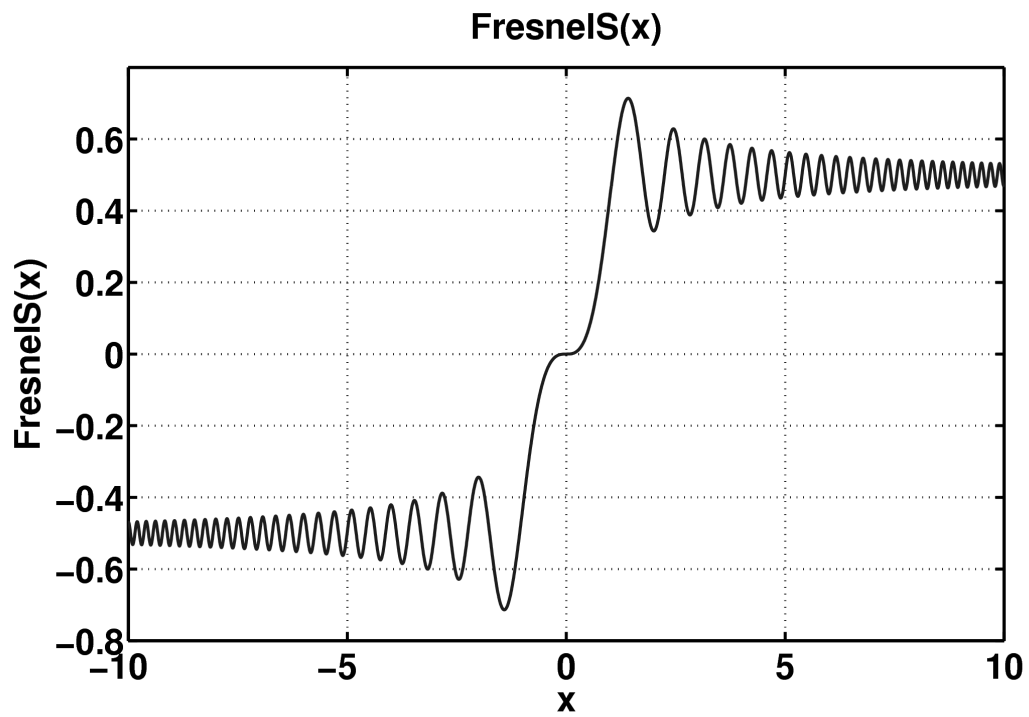This fact is easily explained by the properties of the Fresnel functions: both
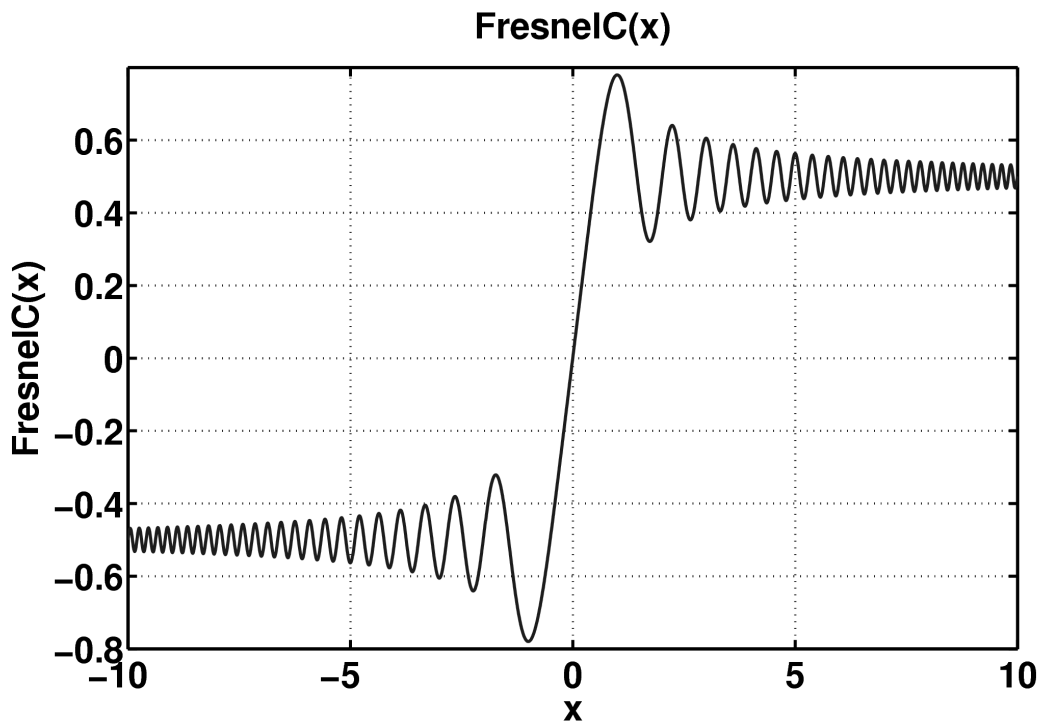
FresnelS(x)

Fig. 4.13. FresnelS function graph

FresnelC(x)
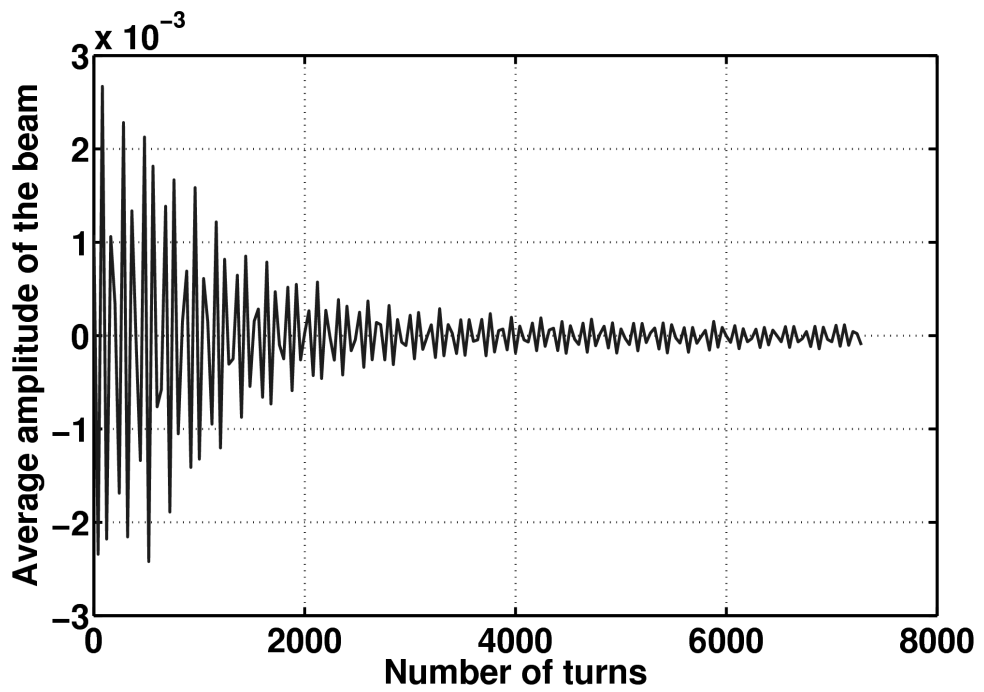

Fig. 4.14. FresnelC function graph
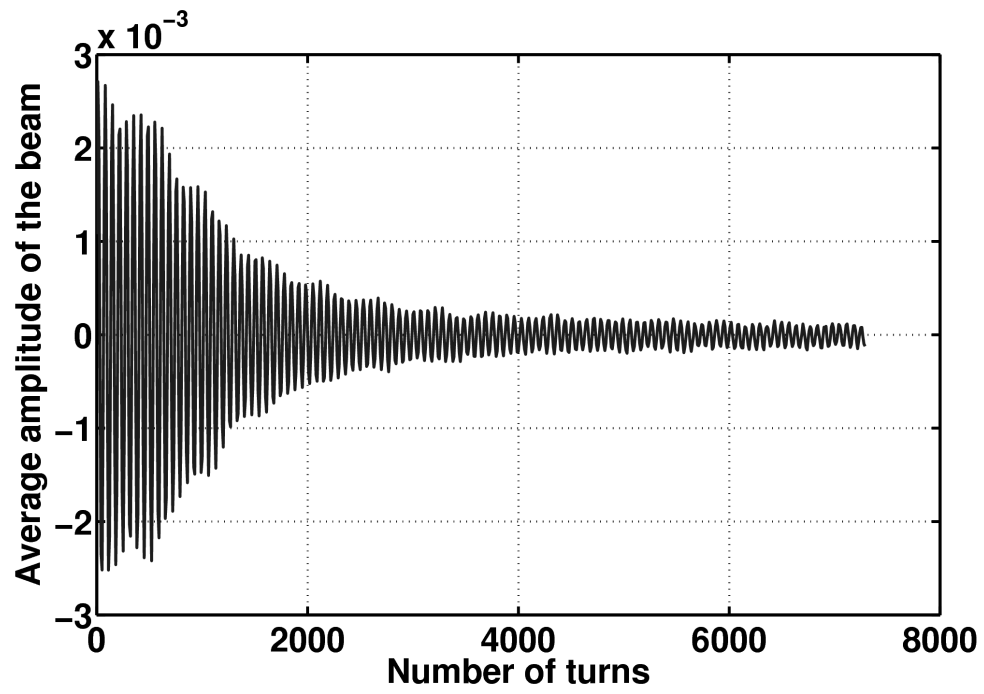
Fig. 4.15. Measurement samples

Properties of Fresnel Functions
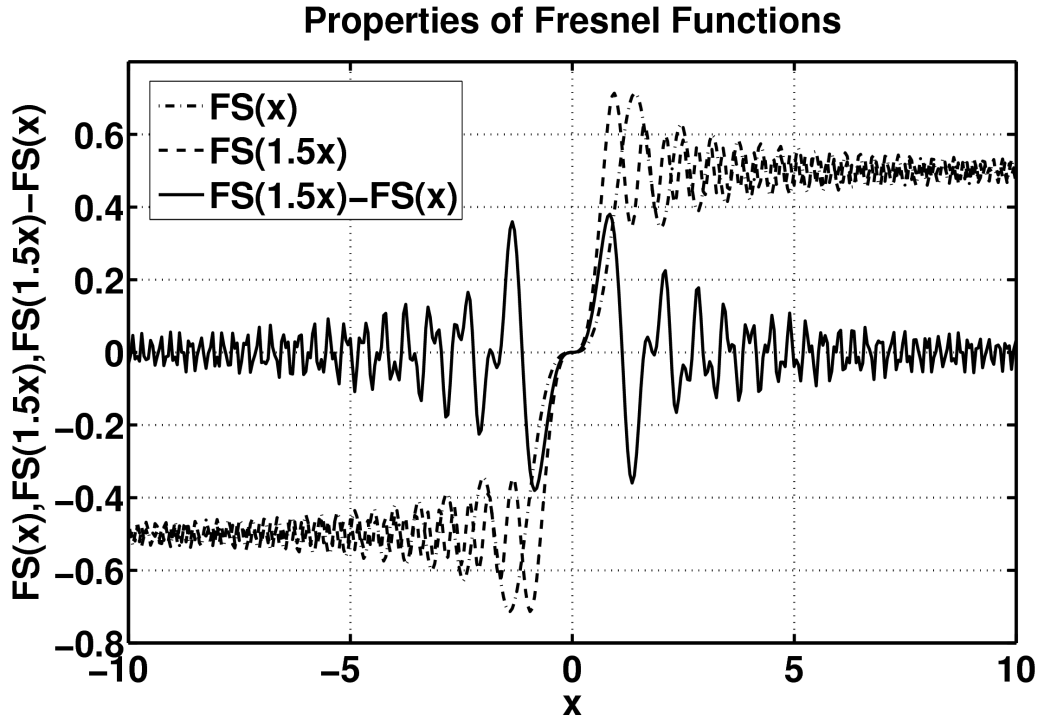
Fig. 4.16. FresnelS$(1.5x)$ − FresnelS(x) function graph

FresnelC(x) and FresnelS(x) oscillate around $\frac{1}{2}$ as $x \to \infty$ with slowly decreasing amplitude. Hence, the difference of the two FresnelC or FresnelS functions oscillates around zero, provided the arguments are proportional, which is the case in Eqs. (4.2.10). The graphs of the functions FresnelS$(1.5x)$ − FresnelS(x) and FresnelC$(1.5x)$ − FresnelC(x) are shown in Fig. 4.16 and Fig. 4.17, respectively.

To calculate the integrals (4.2.6–4.2.7) in the general case, numerical integration methods should be employed. For this study the adaptive Simpson quadrature method [39] is used. The main issue with the sector approximation is that it is not sharp enough, and only works for the beams which are displaced by the transversal kick in such a way that the whole beam is away from the origin. To handle the situation with the beam that crosses the origin, and to be more precise with the conclusions about the centroid, the attention should be paid to the exact shape and
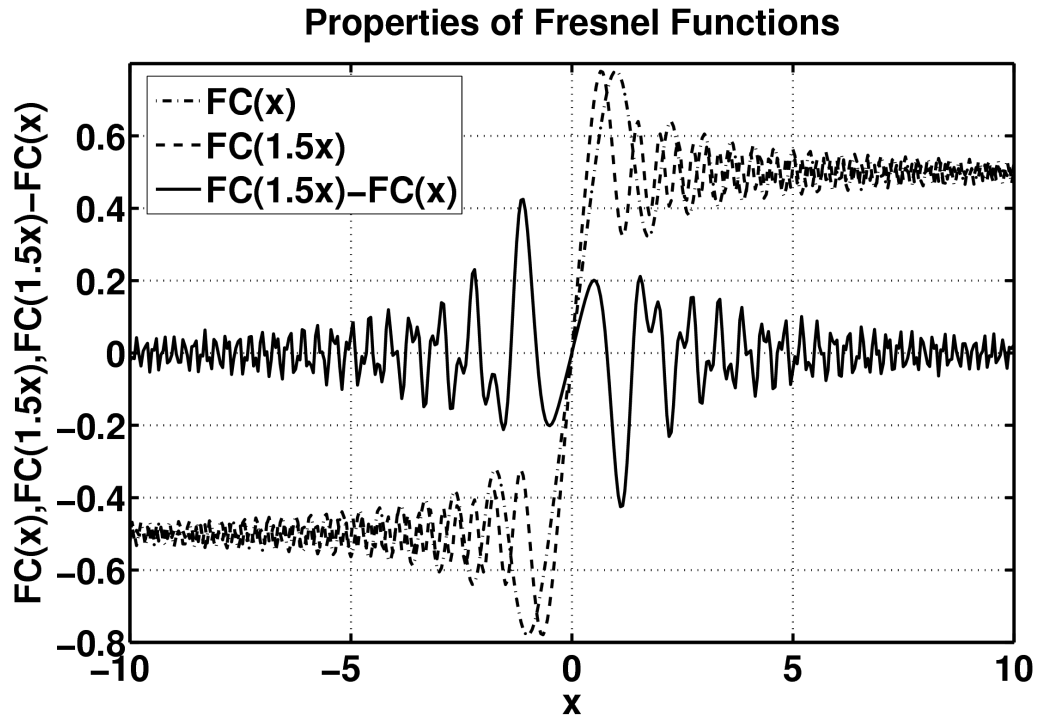
Fig. 4.17. FresnelC$(1.5x)$ $-$ FresnelC(x) function graph

position of the beam after the kick.

4.2.4 Elliptical Beam, Uniform Distribution

Let us assume that the particles in the beam are distributed uniformly (for simplicity, we consider the general case later), and the beam has an elliptical shape. Then after the transformation to the normal form coordinates the beam has the elliptical shape again, and the axes of the transversal section of the beam are equal. Then the boundary curve for the beam in the normal form coordinate pair is the circle, and the parametric representation for it can be found in the form of the equations for two half-circles: $(r, \varphi_1(r))$, $(r, \varphi_2(r))$. Without loss of generality it can be assumed that the resulting circle has its center on the horizontal axis, with the coordinates $(d, 0)$, where $d > 0$ is known. Let ρ be the radius of the beam, then the beam lies between

84
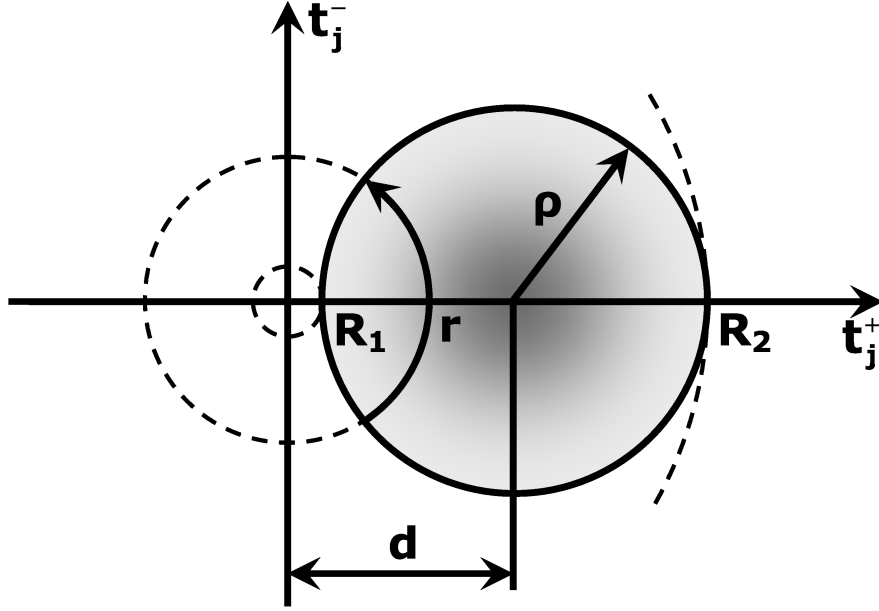
Fig. 4.18. $R_1 = d - \rho > 0$

$R_1 = d - \rho$ and $R_2 = d + \rho$, where it happens often that the radius R_1 is less than zero, which means that the origin $(0,0)$ gets inside the beam (Fig. 4.18–4.19). Both d and ρ parameters can be found by applying the linear normal form transformation to the displaced beam boundaries. Below it will be shown that the two cases $R_1 > 0$ and $R_1 < 0$ can be treated in a uniform way. For the moment let us assume that $R_1 > 0$.

Similar to the previous section, the centroid of the beam has the coordinates

$$\begin{cases} S = \displaystyle\int_{R_1}^{R_2}\int_{-\varphi(r)+\theta_N(r)}^{\varphi(r)+\theta_N(r)} r\,d\theta dr; \\[2ex] x_c^{(N)} = \dfrac{1}{S}\displaystyle\int_{R_1}^{R_2}\int_{-\varphi(r)+\theta_N(r)}^{\varphi(r)+\theta_N(r)} r^2\cos\theta d\theta dr; \\[2ex] y_c^{(N)} = \dfrac{1}{S}\displaystyle\int_{R_1}^{R_2}\int_{-\varphi(r)+\theta_N(r)}^{\varphi(r)+\theta_N(r)} r^2\sin\theta d\theta dr; \end{cases} \qquad (4.2.11)$$

the only difference being that φ is now a function of r. This double integral reduces
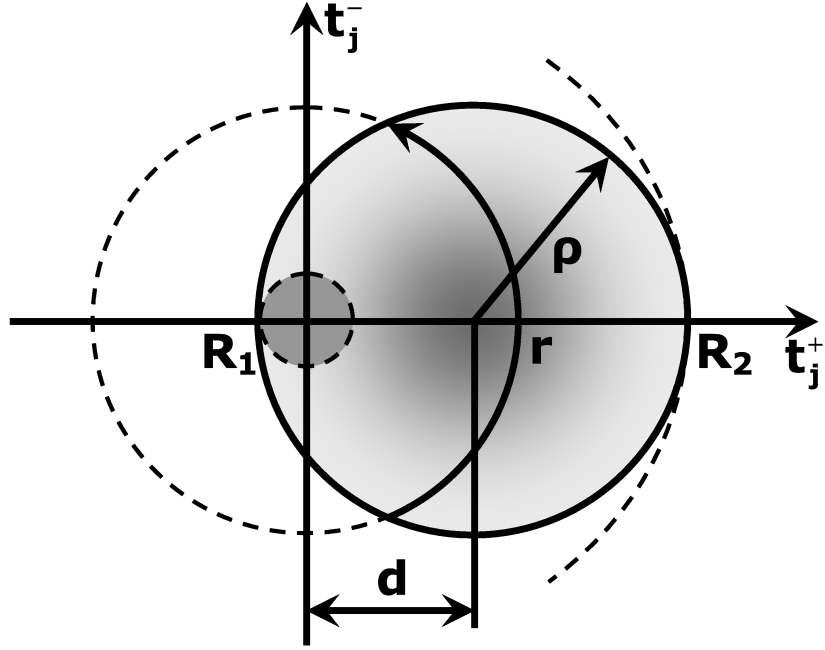
Fig. 4.19. $R_1 = d - \rho < 0$

to a simpler form, which is derived below, but the resulting single integral can only be found using numerical methods. The integrand is not simplified further here, as the non-uniform density beam case will be considered in the next subsection, which only makes the integrand more complicated, thus not allowing any simplification of the general form.

To simplify the integral expression, some additional information is needed on the intersection of the two circles, as we are integrating along the arcs of a circle and the boundary curve is also a circle. Let us consider the two circles: the first one centered at the origin $(0,0)$ and having a radius r, and the second one centered at $(d,0)$ and having a radius ρ (Fig. 4.20). This setup gives

$$\begin{cases} x^2 + y^2 = & r \\ (x-d)^2 + y^2 = & \rho \end{cases}. \tag{4.2.12}$$

Fig. 4.20. The intersection of two circles

Solving the system for x one obtains

$$x = \frac{r^2 - \rho^2 + d^2}{2d},$$

which yields

$$
\begin{aligned}
\cos\varphi(r) &= \frac{x}{r} = \frac{r^2 - \rho^2 + d^2}{2dr}, \\
\varphi(r) &= \arccos\left(\frac{r^2 - \rho^2 + d^2}{2dr}\right).
\end{aligned}
$$

Using the resulting expression for φ and Eq. (4.2.8), similar to what is done in

the previous subsection one gets

$$
\int_{R_1}^{R_2} \int_{-\varphi(r)+\theta_N(r)}^{\varphi(r)+\theta_N(r)} r^2 \cos\theta d\theta dr =
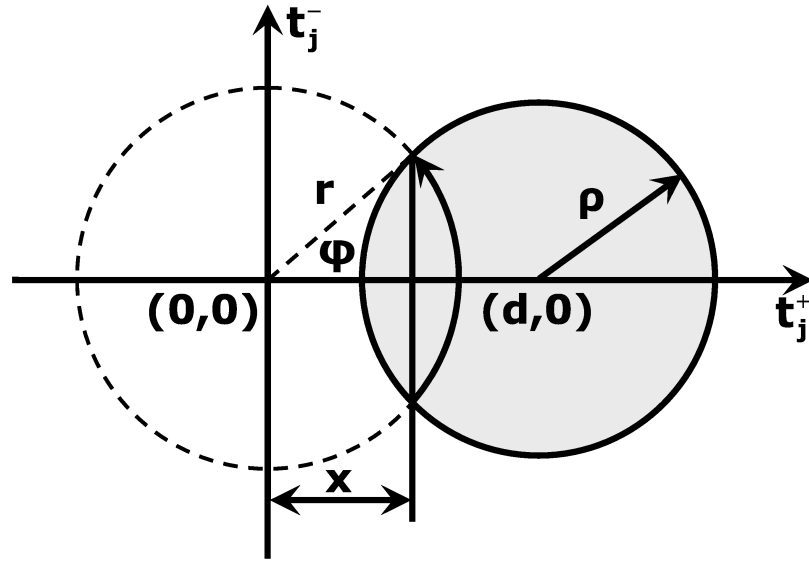$$

$$
= 2 \int_{R_1}^{R_2} r^2 \sin\varphi(r) \cos\theta_N(r) dr =
$$

$$
= 2 \int_{R_1}^{R_2} r^2 \sin \arccos\left(\frac{r^2 - \rho^2 + d^2}{2dr}\right) \cos\theta_N(r) dr =
$$

$$
= 2 \int_{R_1}^{R_2} r^2 \sqrt{1 - \left(\frac{r^2 - \rho^2 + d^2}{2dr}\right)^2} \cos\theta_N(r) dr,
$$

(4.2.13)

and hence

$$
\begin{cases}
S = \displaystyle\int_{R_1}^{R_2} r\sqrt{1 - \left(\frac{r^2 - \rho^2 + d^2}{2dr}\right)^2}\, dr; \\[4mm]
x_c^{(N)} = \dfrac{1}{S} \displaystyle\int_{R_1}^{R_2} r^2 \sqrt{1 - \left(\frac{r^2 - \rho^2 + d^2}{2dr}\right)^2} \cos\theta_N(r) dr; \\[4mm]
y_c^{(N)} = \dfrac{1}{S} \displaystyle\int_{R_1}^{R_2} r^2 \sqrt{1 - \left(\frac{r^2 - \rho^2 + d^2}{2dr}\right)^2} \sin\theta_N(r) dr.
\end{cases}
$$

(4.2.14)

In the special case of $R_1 = d - \rho < 0$ with the layout corresponding to Fig. 4.19, there are two choices:

- For $0 < r < |R_1|$, the intersection of the two circles in (4.2.12) is purely imaginary, and hence the whole contour $(r, \varphi \in [-\pi, \pi))$ belongs to the beam, and one can assume for such r that φ goes from $-\pi$ to π. This is the approach used later for the non-uniform distribution;

- As the set $\{(r, \varphi)|\ r \in (0, |R_1|), \varphi \in [-\pi, \pi)\}$ is symmetrical with respect to the origin, and the particles in the beam are distributed uniformly, the centroid of this part of the beam is $(0, 0)$, so it can be omitted, and all of the above formulas are applicable with no change if we put $R_1 = |d - \rho|$. Unfortunately, this approach does not work for the non-uniformly distributed beams.

88

4.2.5   Elliptical Beam, Normal or Arbitrary Distribution

Assume that the beam distribution is normal in both directions in every pair of coordinates, and each two directions are independent. As the beam is round in the normal form coordinates, the variances in both eigen-directions are the same $\sigma = \sigma_x = \sigma_y$, and hence the resulting density of the bivariate distribution is defined by the formula

$$f(x,y) = \frac{1}{2\pi\sigma^2} \exp\left(\frac{-((x-d)^2 + y^2)}{2\sigma^2}\right), \qquad (4.2.15)$$

as the mean values for the distribution are d and 0. Note that this formula is only valid for the initial distribution, when $\theta_N = 0$, and after N turns θ_N should be subtracted from the value of the angle.

A typical particle distribution after various numbers of turns is shown in Fig. 4.21.

In the case of the non-uniform distribution the expressions for S, x_c, and y_c are essentially the same as in Eqs. (4.2.14), except that now the integrand is complicated by the additional factor of $f(r\cos(\theta - \theta_N), r\sin(\theta - \theta_N))$. The component "$-\theta_N$" is introduced to always take the density of the initial normal distribution:

$$\begin{cases} S = \displaystyle\int_{R_1}^{R_2} \int_{-\varphi(r)+\theta_N(r)}^{\varphi(r)+\theta_N(r)} rf(r\cos(\theta - \theta_N), r\sin(\theta - \theta_N))d\theta dr; \\[2ex] x_c^{(N)} = \dfrac{1}{S} \displaystyle\int_{R_1}^{R_2} \int_{-\varphi(r)+\theta_N(r)}^{\varphi(r)+\theta_N(r)} r^2 \cos\theta f(r\cos(\theta - \theta_N), r\sin(\theta - \theta_N))d\theta dr; \quad (4.2.16) \\[2ex] y_c^{(N)} = \dfrac{1}{S} \displaystyle\int_{R_1}^{R_2} \int_{-\varphi(r)+\theta_N(r)}^{\varphi(r)+\theta_N(r)} r^2 \sin\theta f(r\cos(\theta - \theta_N), r\sin(\theta - \theta_N))d\theta dr. \end{cases}$$

In the case of negative R_1, the part of the beam inside the circle of radius $|R_1|$ cannot be omitted, and hence, the first of the two methods described at the end of the previous subsection is used and the integration goes from 0 to R_2 taking $\varphi \in [-\pi, \pi)$ for $0 < r < |R_1|$.
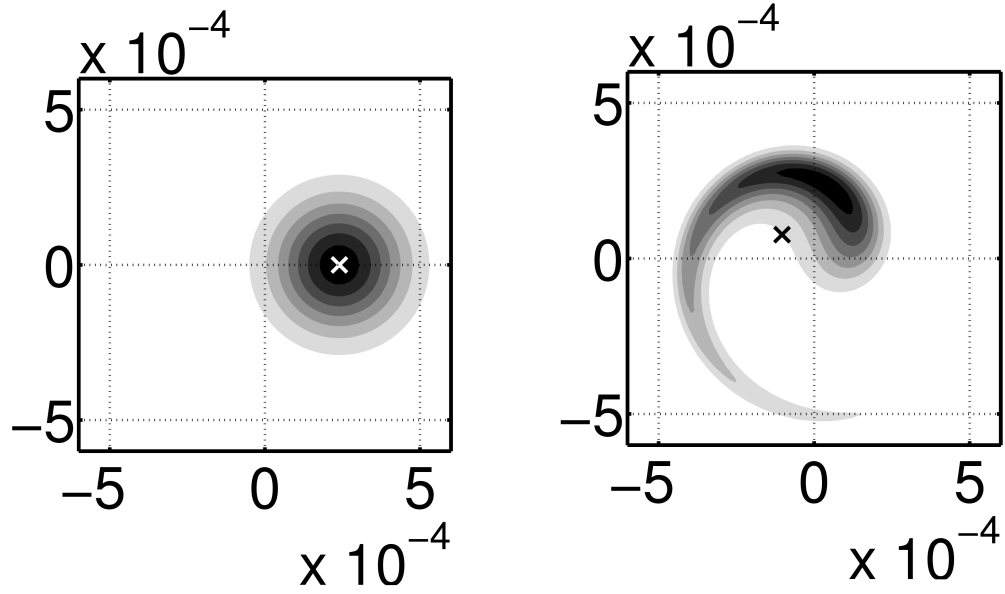
(a) initial distribution

(b) after 1000 turns
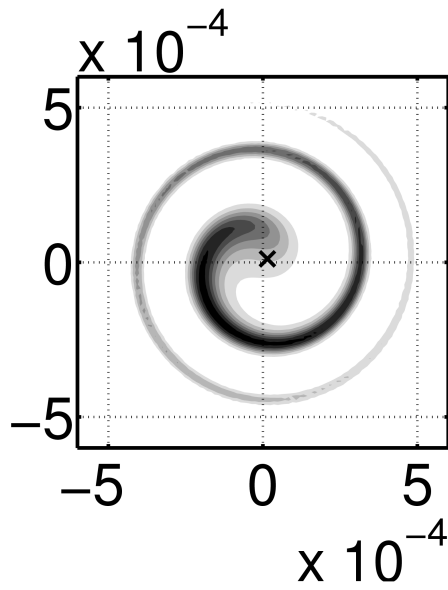
(c) after 3000 turns

Fig. 4.21. Particle distribution in the beam, the cross indicates the center of mass of the beam.

4.2.6 Numerical Experiment Results

The calculation method described above allows one to find the dependence $r = r(N, c_1, c_2)$ for the elliptical beams with an arbitrary particle distribution, the only requirement being that the initial distribution density function is known. Hence, for each pair of values c_1 and c_2, one can find $\eta(c_1, c_2)$ or $\eta_{1/2}(c_1, c_2)$ introduced in the beginning of the section as well as the corresponding values of the functions (4.2.2) and (4.2.3). Having these data available and employing various optimization methods, one can find the correct values of c_1 based on one particular measurement or both coefficients c_1 and c_2, provided that measurements for different kick strengths are available.

The numerical results for the Tevatron correspond to the values obtained by tracking the nonlinear model of the machine. Consider, for example, the function J_5, given by Eq. (4.2.3) and the results of the measurements shown in Fig. 4.10. The number of turns after which the amplitude of the center of mass falls down to a half of its value varies depending on the BPM, one of the total of 115 reliable measurements. Taking the average over all the BPMs one obtains that $N_{1/2} \approx 1000$, or more precisely, $N_{1/2} \in [900, 1100]$.

An optimization procedure results in the expected value of $c_1 = -2511$ for the initial beam amplitude after the kick of $r = 0.24 \cdot 10^{-3}$. Taking into account that $\mu_0 = 0.585$, one gets

$$\mu \approx \mu_0 + c_1 r^2 = 0.585 - 1.4463 \cdot 10^{-4}. \tag{4.2.17}$$

To conceive how close the obtained value of c_1 is to the realistic value of the tune shift with amplitude, a comparison was performed in COSY using the nonlinear model of the Tevatron available at the official lattice page at Fermilab [38]. The model
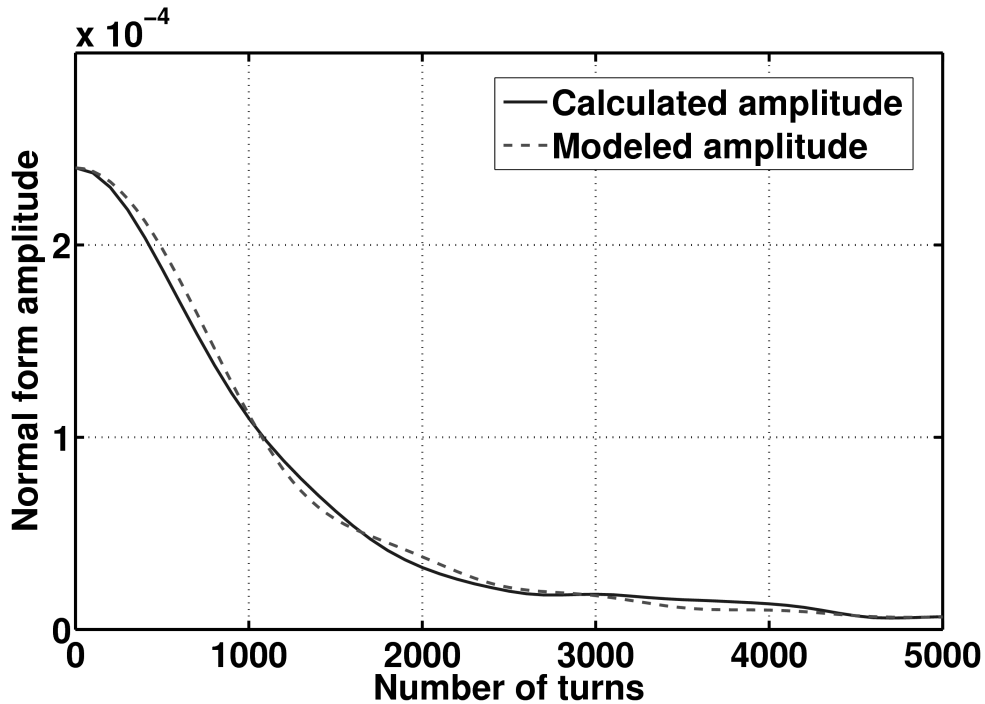
Fig. 4.22. Calculation results and the comparison with the nonlinear model

reflects changes made to the accelerator as of November 2005, while the measurement results are dated January 2006. Hence, there are strong reasons to assume that the model distribution tracking should yield results comparable to the calculated value of the tune shift, and therefore, the measurements. The COSY calculation shows that the expected value of c_1 for the nonlinear model should be -2541, which means the calculated value found by the optimization differs from the model value by not more than 2%. At the same time, only the information about the distribution of the particles in the beam, the size of the beam, and the linear dynamics was used to find the nonlinear tune shift. Necessary additional information was extracted from the measurements.

Figure 4.22 shows the graphs of the calculated amplitude with $c_1 = -2511$ and

the model amplitude with $c_1 = -2541$. The slight difference between the graphs can be explained not only by using different c_1's, but also by the fact that the fourth order term $c_2 r^4$ in the expansion of μ has not been taken into account. Also the model is just an approximation to the real machine's optics. At the same time, the similarity of the graphs allows to conclude that the model represents the real machine quite accurately, at least for the low order nonlinearities affecting the tune shift (mainly the sextupole content of the ring).

Also, the validity of the approach studied is perfectly supported by the independent calculations done years ago. There is an estimate of the nonlinear tune shift by R.Meller et al. [40], given by the following formula:

$$
\begin{aligned}
\mu &\approx \mu_0 - \kappa A^2, \\
\kappa &\approx \frac{1}{4\pi N_{1/2}},
\end{aligned}
\tag{4.2.18}
$$

where A is the amplitude of the center of mass of the beam, measured in σ units of the beam under consideration. This formula is derived for the beams with a normal distribution of the particles, and it represents a good approximation when the transversal kick is relatively weak (A is not too much greater then 1).

The value comparison of κA^2 from Meller's article to the value of $c_1 r^2$, obtained by the calculation using the algorithm described above, gives the following results: $\kappa = 7.96 \cdot 10^{-5}$, $A = 1.36$,

$$
\mu \approx \mu_0 + \kappa A^2 = 0.585 - 1.4723 \cdot 10^{-4},
\tag{4.2.19}
$$

that is, the difference between the values obtained using different approximations in Eqs. (4.2.17) and (4.2.19) is less than 2%.

4.2.7 Summary

Correspondence is found between the first and the most important term in the expansion of the nonlinear tune shift with amplitude and the BPM measurement results after the beam is kicked transversely. This correspondence can be found by minimizing the function (4.2.2) or (4.2.3). To be able to find the values of either one of the two functions it is necessary to have the information on the behavior of the amplitude r of the center of mass. This amplitude can be found in the most general case using the formulas (4.2.16) and $r = \sqrt{x_c^2 + y_c^2}$.

The COSY INFINITY's normal form transformation algorithm and built-in optimizers were employed to calculate the nonlinear tune shift with amplitude along with the numerical integration algorithm and visualization tools of Mathworks Matlab R13.

A method for the calculation of the nonlinear tune shift with amplitude was tested on the Tevatron BPM measurement results and compared to the nonlinear model calculations as well as the independent approximation formulas. In both cases the discrepancy was less than 2%, which can be considered a very good result taking into account that only the information on the one-turn linear transfer map and the geometry of the beam has been used, while the lack of information on the nonlinear behavior was compensated by a single BPM measurement with one particular perturbation (kick) strength.

After the coefficient c_1 has been found, one might try finding the coefficient c_2 if multiple measurement results are available. On the other hand, in the case of the Tevatron, $c_2 r^4$ is 1–2 orders smaller than $c_1 r^2$, so in this particular study there was no attempt made to find c_2.

5. MUON COLLIDER STORAGE RINGS: DYNAMICS AND OPTIMIZATION

5.1   50×50 GeV Collider IR High-Order Correction

The progress in the development of the Interaction Regions (IRs) for advanced future colliders, in particular various Muon Collider designs, requires a systematical high-order dynamics study. The effects from the high-order beam dynamics become more and more pronounced as the value of the β-function at the Interaction Point decreases to very small values, β^*=14 cm and β^*=4 cm for the 50×50 GeV Muon Collider and Higgs Factory, respectively, and β^*=1 cm for the proposed 750×750 GeV Muon Collider that matches the geometry of the Tevatron tunnel. This last lattice is described in detail in Section 5.2. Simultaneous control of geometric and chromatic aberrations is critical to the success of future machines and can only be achieved through the deliberate addition of the nonlinear fields in the Interaction Region itself. Therefore, there is a need of studying both the correction schemes and the unavoidable impact of the high-order correctors – sextupoles, octupoles and even duodecapoles – located

in the Interaction Region close to the low-beta quadrupoles.

Muon colliders have certain advantages over high-energy proton and electron colliders. The size of a muon collider is significantly smaller in the circumference than that of a proton collider since the rest energy of a muon is much less than that of a proton. When compared to electrons, however, the larger mass represents an advantage by reducing the synchrotron radiation and beamstrahlung, allowing for higher magnetic confinement, and reducing the size of the collider relative to an electron collider. On the other hand, muons are not stable and they decay relatively quickly ($\tau = 2.2\ \mu s$), so the acceleration must be rapid and the circumference of the ring must be as small as possible to minimize the luminosity degradation due to the decay. Also the muon decay is a source of secondary particles with relatively high energies — electrons and γ particles. These, in turn, result in a powerful energy flow, which could even destroy some important expensive components, especially the superconducting magnets, or spoil the measurement results.

The muon accelerating complex consists of a number of stages: Muon Production, Cooling, Acceleration, and finally the Collider Ring [5, 7]. The collider ring circulates beams of μ^+ and μ^- traveling in the opposite directions. Considerable design effort has been invested in a 50×50 GeV Muon Collider [28, 55] and a 2×2 TeV one [27, 56]. To reach the luminosity goal of 10^{35} cm^{-2} s^{-1}, the beta-function of the beam at the interaction point should be extremely small for the 2 TeV Collider: $\beta^* = 3$ mm. The collision spot is even smaller for the Linear Collider.

It is therefore useful to begin the study at the lower collision energy and less restrictive beam sizes. For the 50×50 GeV Higgs collider the value of the beta-function at the interaction should be $\beta^* = 4$ cm for a momentum spread of $dp/p \approx 0.12\%$, rms.

Many issues associated with the design of such a collider are summarized in [55].

Specifically, the tune shift with amplitude is a very important figure of merit to consider, especially the second order terms, which remain large in various proposed schemes [28, 55].

This study addresses the correction schemes and the effects of the high-order correctors located in the IR itself proximate to the low-beta quadrupoles, or focusing elements, to control the kinematic and geometric aberrations, the latter of which arise from the use of sextupoles for the chromatic correction. The dynamic aperture of the storage ring is the optimization criterion for the study. Finally, an increased dynamic aperture is indicative of the potential further reductions of the value of β^*.

5.1.1 Dynamic Aperture

Dynamic aperture studies to date of the Muon Collider storage rings can be found in [28]. In the following sections the dynamic aperture study and optimization are considered more systematically. As the collider storage ring is a circular accelerator where the muons stay for about 1000 turns, it is convenient to find the nonlinear transfer map of one full revolution and then apply it repetitively to study the stability of a particle distribution. According to [12], the study of the transfer map is sufficient for characterizing the stability of the design optics. The main tool for the study is COSY INFINITY [13] with its high order Taylor expansions of the flows of differential equations and differential algebraic tools to determine flows of differential equations. COSY allows such complicated objects as the nonlinear resonance strengths and the nonlinear amplitude dependent tune shifts to be computed and optimized, or the individual terms comprising these values to be addressed, all of which are important for a careful demonstration of the optimization.

The dynamics of particles is described by a system of differential equations of the
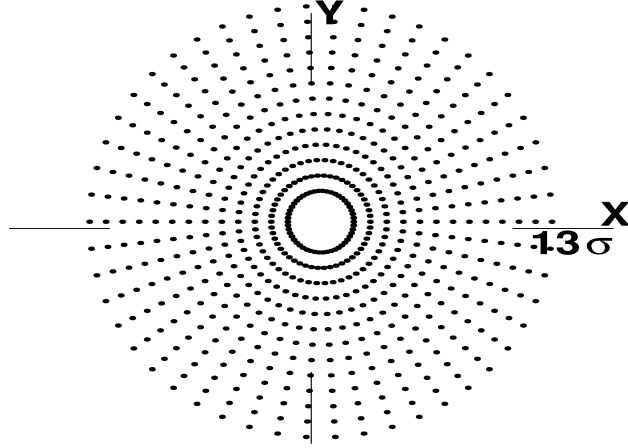
Fig. 5.1. The grid of points to determine the dynamic aperture

form (4.1.1) with the same restrictions as described in Section 4.1. The energy of the particles does not change as the muons are already at the desired energy. The main idea of the optimization is to minimize the particle losses for the maximal beam size. If at some point the coordinate of the particle is greater than the beam pipe size, this particle is considered lost. The number of the particles lost serves as a quantitative criterion of the practical stability.

Hereafter, the coordinate (in the (x, a) or (y, b) plane) of the particle farthest from the origin (from the trajectory of the reference particle), which remains stable for the 1000-turn storage cycle, is called the dynamic aperture. The dynamic aperture can be found using the method illustrated in Fig. 5.1. A grid of particles with the initial positions forming the concentric circles around the closed orbit (fixed point) is launched and tracked for a thousand turns. The radii of the circles increase in fixed steps until the trajectory is unstable, that is, until some of the outermost particles are lost, numerically. The largest radius for which all the particles remain in the beam pipe is considered to be the design dynamic aperture. The incremental step in the radius is taken to be in units of one sigma (σ) of the standard normal distribution of the particles with the normalized rms emittance of 90π mm mrad ($\sigma = 82 \cdot 10^{-6}$ m).

The beam is considered to be round. From an optics standpoint, elliptical beams are more manageable and less nonlinear than round beams in the design of Interaction Regions. Using a β^* ratio of 1:4 of the horizontal size to the vertical size (factor of 2 in the relative beam sizes), however, causes a decrease in the luminosity of a factor of 2, which is unacceptable. Therefore, the condition of round beams at the Interaction Point (IP) has been imposed in all current collider designs.

The optimization of the dynamic aperture by adding the high-order nonlinear correctors such as octupoles, decapoles, or duodecapoles to the superconducting IR quadrupoles and selecting the proper strengths for these correctors can be done in various ways targeting different objective functions and nonlinear terms. The initial dynamic aperture before any correction is introduced is 7σ (see Fig. 5.2(a)).

5.1.2 Minimization of the Nonlinearities

The discussion about the impact of the nonlinearities on the dynamics, and their correction in the Tevatron in the beginning of Section 4.1, stays valid for the Muon Collider. By interacting in a complicated way, the nonlinear components of the dynamics may significantly reduce the stability of the machine and can even lead to chaos. While in the linear case all the particles follow the closed orbits and stay stable forever, so the dynamic aperture is always bigger than the beam pipe size, in the nonlinear case this does not happen. Therefore, one of the ways to formulate a problem of maximization of the dynamic aperture is this: minimize all the important nonlinearities of at least lower orders (second and third) to make the dynamics as close to linear as possible. In terms of the Taylor expansions of the transfer maps and the corresponding equivalence classes $[\mathcal{M}]_n$, the objective function for the transversal

dynamics has the form:

$$J_6 = \sum_{k=1}^{4} \left(\sum_{i_1+i_2+i_3+i_4=2}^{3} \left| (z_k | z_1^{i_1} z_2^{i_2} z_3^{i_3} z_4^{i_4}) \right| \right), \qquad (5.1.1)$$

where $z(\vec{u}) = (z_1(\vec{u}), z_2(\vec{u}), z_3(\vec{u}), z_4(\vec{u}))^\top$ is the vector of the phase space coordinates of (4.1.1), $\vec{u}$ is the vector of the control parameters having the strengths of the high-order correctors in the lattice as its components, $(z_k | z_1^{i_1} z_2^{i_2} z_3^{i_3} z_4^{i_4})$ is the aberration of order $i_1 + i_2 + i_3 + i_4$, that is, the corresponding coefficient in the Taylor expansion of the phase space variable z_k. All the correctors are located in the neighborhood of the interaction point, and can be effectively thought of as additional superconducting coils in the superconducting quadrupoles of the final focus telescope. The number of parameters may vary, but the general idea is to keep it as small as possible.

5.1.3   Minimization of the Resonances

Another systematic approach to the problem is to find a corrector scheme which addresses the nonlinear resonances and/or minimized tune shifts with amplitude. Instead of minimizing specific nonlinear terms in the map, all the resonances or tune shifts up to a particular order are minimized. The strength of all the resonances can be found as a by-product of the application of the normal form transformation algorithm described in Chapter 3. In this case the objective function can be represented as

$$J_7 = \left\{ \sum_{m=2}^{4} \sum_{j=1}^{2} \left| \left(\mathcal{T}_{mj}^{\pm} | \vec{k}^+, \vec{k}^- \right) \right| : \left| \left(\prod_{l=1}^{v} r_l^{k_l^+ + k_l^-} \right) e^{i\vec{\mu}(\vec{k}^+ - \vec{k}^-)} - r_j e^{\pm i\mu_j} \right| < \kappa \right\},$$

$$(5.1.2)$$

where κ is some threshold characterizing the proximity to the resonance. J_7 depends on the control parameters $\vec{u}$ through the components $\mathcal{T}_{mj}^{\pm}$ connected to the elements of the transfer map $\mathcal{S}_{mj}^{\pm}$ after the corresponding stage of the normal form transformation. The form of J_7 is closely related to Eq. (3.1.10): the smaller the denominator is, the

harder it is to remove the unwanted $\mathcal{T}_{mj}^{\pm}$ term. As the strengths $\vec{u}$ of the correctors change, the form of the transfer map $\mathcal{M}$, and hence, $\mathcal{S}_m$ $\forall m = \overline{2, n}$ change as well. The dependence of J_7 on the control parameters is continuous, as it follows from the argument chain above.

5.1.4 Dynamic Aperture as the Objective Function

One more way to attack the problem of the storage ring performance optimization is to use the dynamic aperture itself as the objective function:

$$
\begin{aligned}
J_8 \;=\; & \Big\{ \max(r_1 + r_2) \Big| \mathcal{M}^k(x_i, a_i, y_i, b_i) = (x_f, a_f, y_f, b_f), |x_f| < \eta, |y_f| < \eta, \\
& i = \overline{1, N}, k = \overline{1, 1000}, \sqrt{x_i^2 + a_i^2} = r_1, \sqrt{y_i^2 + b_i^2} = r_2 \Big\},
\end{aligned}
\tag{5.1.3}
$$

where k is the number of turns to keep particles confined by η in both coordinates x_f and y_f, N is the number of particles in the grid which is used to determine the dynamic aperture, and $\vec{z}_i = (x_i, a_i, y_i, b_i)^\top$ is the phase space vector for the particle lying in the plane (x, a) on a circle of radius r_1, and in the plane (y, b) on a circle of radius r_2. For the uniform distribution of particles along the circle one obtains

$$
(x_j, a_j) = r_1 \cdot \mathrm{e}^{i\varphi_j(N)}, \quad \varphi_j(N) = 2\pi j/N;
\tag{5.1.4}
$$

$$
(y_l, b_l) = r_2 \cdot \mathrm{e}^{i\psi_l(N)}, \quad \psi_l(N) = 2\pi l/N,
\tag{5.1.5}
$$

which corresponds to the distribution of particles shown in Fig. 5.1.

Again, the transfer map $\mathcal{M}$ depends on the strengths of the correctors $\vec{u}$, added to the lattice for optimization purposes, and hence, $J_8 = J_8(\vec{u})$. The problem is to find a configuration of the corrector magnets which maximizes the value of J_8.

5.1.5 Advantages and Disadvantages of Different Optimization Approaches

The **first approach** to the optimization is to minimize some (or all, if possible) nonlinear coefficients in the transfer map of one full revolution up to possibly higher orders. The objective function J_6 from Section 5.1.2 corresponds to this case.

Calculations show that this approach is not very effective due to the fact that the number of the multipole correctors is very limited, while the number of the nonlinear coefficients in the transfer map is large. For example, for the third order the map of the storage ring lattice under consideration has 20 coefficients total, 10 in each plane. At the same time, the nonlinear coefficients are always connected to each other, so technically the number of parameters might be smaller than 20, but this very connection is the source of the problems. By minimizing specific nonlinearities, others are introduced of the same or higher order, and these often have an equally destructive impact on the behavior of the system.

This approach has been attempted and improved the dynamic aperture from 7σ to 10σ (Fig. 5.2), which is not a very significant result compared to the other two approaches.

The **second approach** (more systematic) is to find a correction scheme which addresses nonlinear resonances and/or minimizes tune shifts with amplitude. Instead of minimizing specific nonlinear terms in the map, all the resonances or tune shifts up to a particular order are minimized. The objective function J_7 from Section 5.1.3 corresponds to this approach. Unfortunately, the number of correctors available (three locations at most) does not allow for the removal of all the desired terms of order three or higher. Hence, the situation is similar to the previous approach: in minimizing

102

(a) before optimization
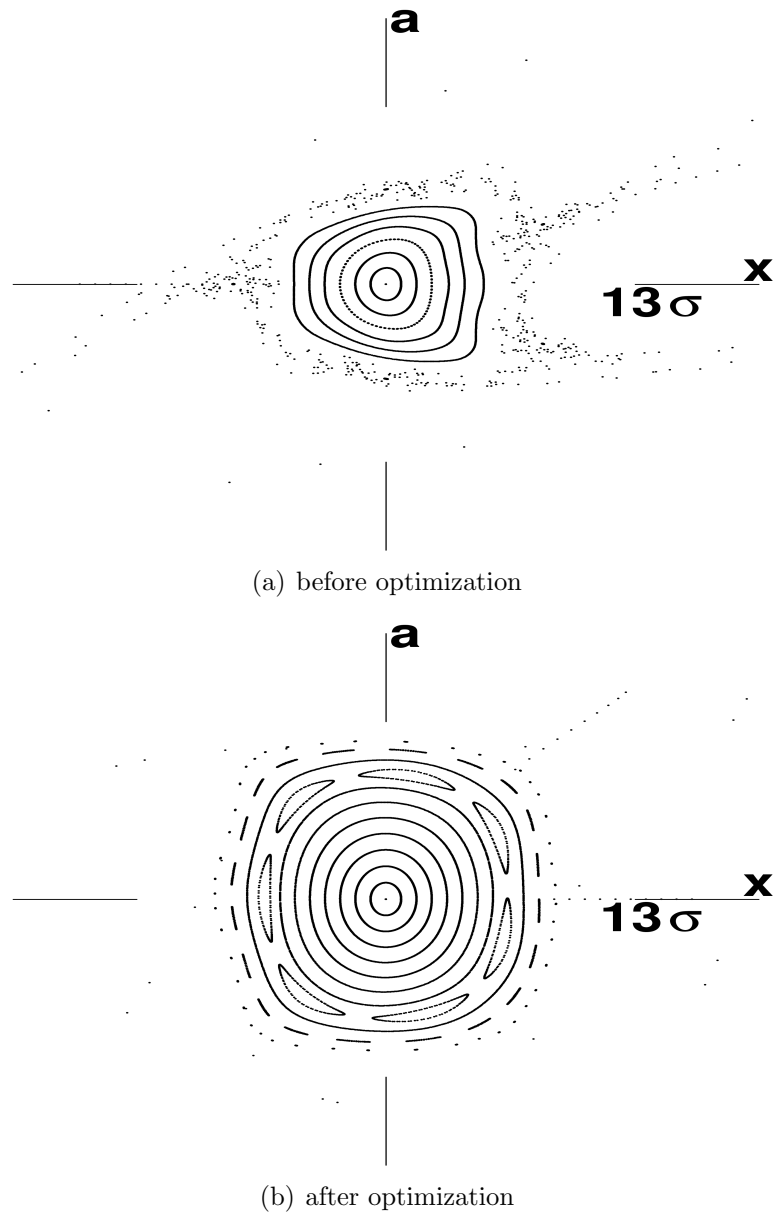

(b) after optimization

Fig. 5.2. The comparison of the phase space portraits before and after the optimization using the first approach (minimization of individual high order coefficients) in the (x, a) plane. Particles are launched along the x axis with an increment of one σ, $\sigma = 82 \cdot 10^{-6}$ m.

103

one term, others increase and cause comparable stability problems. Still, among different possible configurations there is one which requires three octupoles and one duodecapole and increases the dynamic aperture from 7σ to as high as 12σ. In this configuration the following high order coefficients in the amplitude-dependent tune shifts have been removed (2D simulation): $(x|x^2)$, $(y|x^2)$, $(x|y^2)$, $(y|y^2)$, $(x|x^4)$, $(y|y^4)$. There are no tune shifts of the third and fifth order, so the only terms up to the fifth order that remain in the tune shifts with amplitude are $(x|y^4)$, $(y|x^4)$, $(x|x^2y^2)$, $(y|x^2y^2)$. The phase portraits in Fig. 5.3 show that the second approach works significantly better than the first one.

The **third approach** — to take the dynamic aperture itself as the figure of merit — has been found to be the most effective way to maximize the dynamic aperture, and is at the same time the most straightforward. The objective function for this approach is J_8 from Section 5.1.4. Of course this approach leads to the increased volume of calculations inside the optimization loop as one needs to recalculate the dynamic aperture for each new value of the corrector strengths, which is more time consuming than the calculation of the resonances or tune shifts because particles are tracked for 1000 turns in each optimization step. This is not a serious limitation for a 7th order calculation though, and the 7th order is sufficient to determine the dynamic aperture. The situation here is to a large extent similar to that of the Tevatron, see Section 4.1.10. This approach is capable of finding a corrector configuration that achieves a dynamic aperture of 13σ using only two octupole correctors and no duodecapoles at all. It is possible that 13σ is the upper limit of the dynamic aperture for the particular storage ring under consideration.

The results of the third approach are shown in Fig. 5.4. The two other approaches have not been as successful and require further investigation. The problem with these

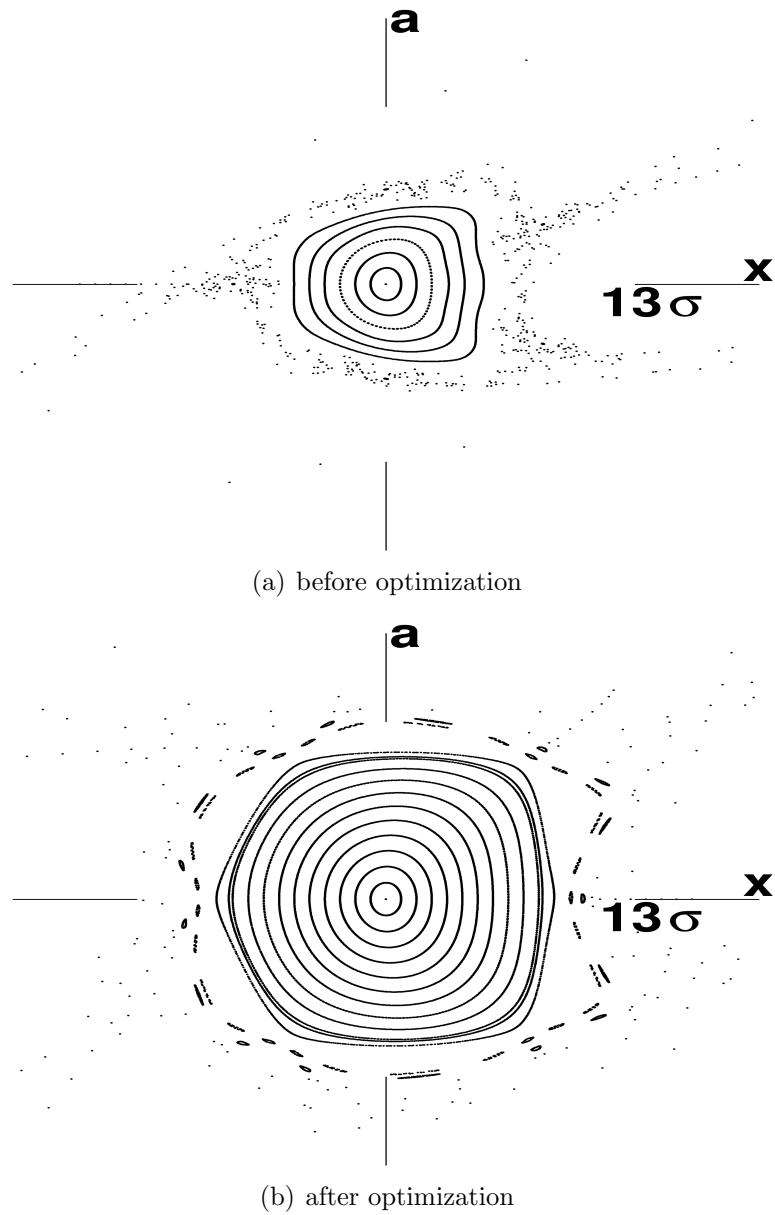(a) before optimization

(b) after optimization

Fig. 5.3. The comparison of the phase space portraits before and after the optimization using the second approach (minimization of the resonance strengths) in the (x, a) plane. Particles are launched along the x axis with an increment of one σ, $\sigma = 82{\cdot}10^{-6}$ m.

	nonlinear terms minimization	resonances minimization	dyn. aperture maximization
Dyn. aperture improvement	$7\sigma \Rightarrow 10\sigma$	$7\sigma \Rightarrow 12\sigma$	$7\sigma \Rightarrow 13\sigma$
Number of correctors	3 octupoles+ 2 duodecapoles	3 octupoles+ 1 duodecapole	2 octupoles

Tab. 5.1. Parameter comparison for various optimization approaches

approaches is the large number of values to minimize simultaneously and the absence of a well established algorithm for the search of the connection between different high order nonlinearities.

All the approaches attempted are summarized in Table 5.1.

5.1.6   Optimization Results

The tracking pictures showing the phase space portraits of the system after some number of turns are, in general, an effective tool to serve as a qualitative estimate for the dynamic aperture. To check that the third approach is efficient in general rather than for a particular choice of the initial coordinates of the particles being tracked, the Fig. 5.5–5.6 demonstrate the phase portrait comparison for the particles launched along the diagonal (x, y). From Fig. 5.5–5.6 it is clear that the dynamic aperture after the optimization is significantly larger than before the optimization, even though it is hard to estimate its exact value using phase portraits only. Therefore, for each approach the quantitative results are given explicitly.
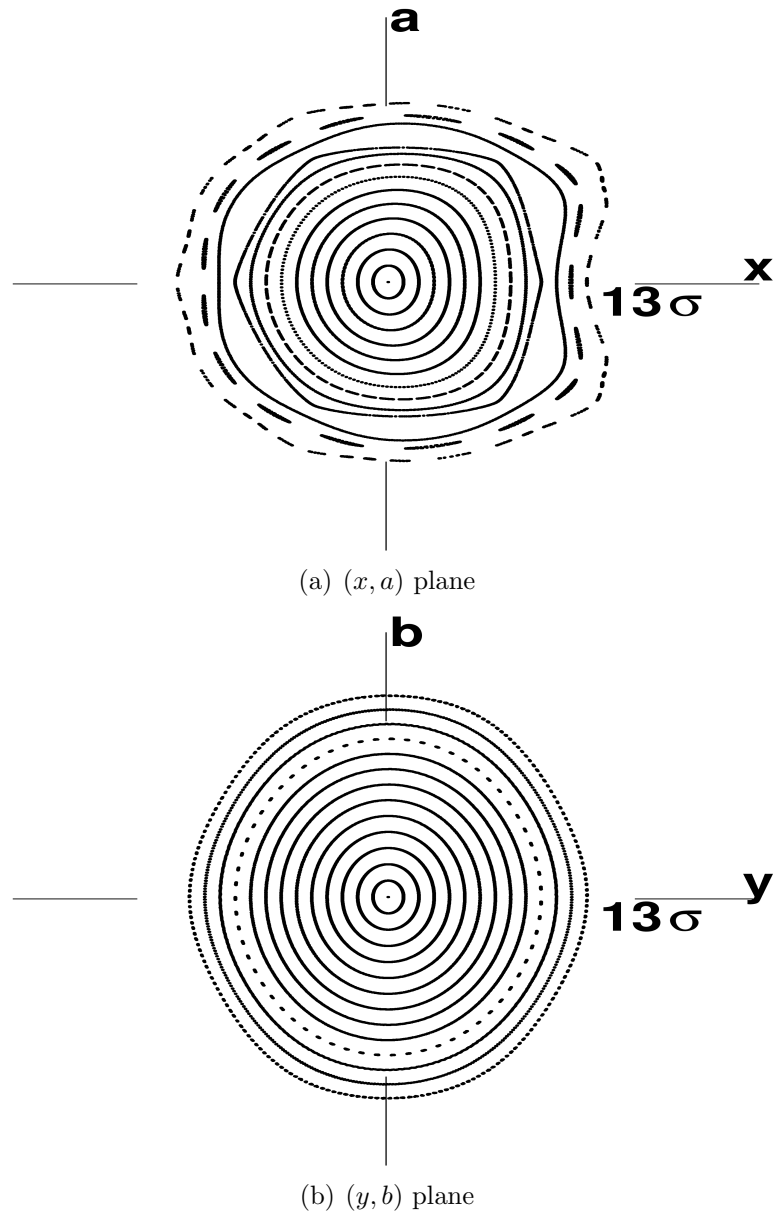
(a) (x, a) plane

(b) (y, b) plane

Fig. 5.4. Phase portraits after the optimization in the (x, a) and (y, b) planes. Particles are launched along the x and y axes, respectively, with an increment of one σ, $\sigma = 82 \cdot 10^{-6}$ m.

(a) before the optimization

(b) after the optimization

Fig. 5.5. The comparison of the phase portraits in the (x, a) plane before and after the optimization. Particles are launched along the (x, y) diagonal with a step of one σ.

108

(a) before the optimization

(b) after the optimization

Fig. 5.6. The comparison of the phase portraits in the (y, b) plane before and after the optimization. Particles are launched along the (x, y) diagonal with a step of one σ, $\sigma = 82 \cdot 10^{-6}$ m.
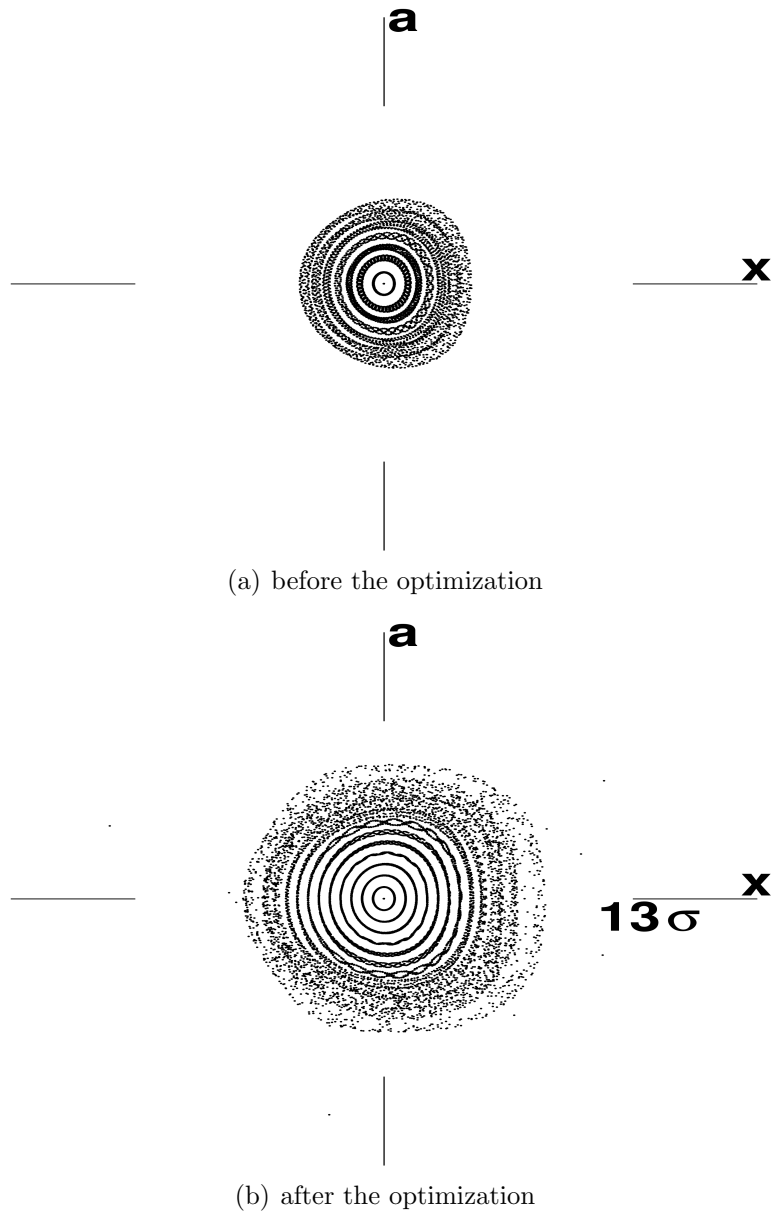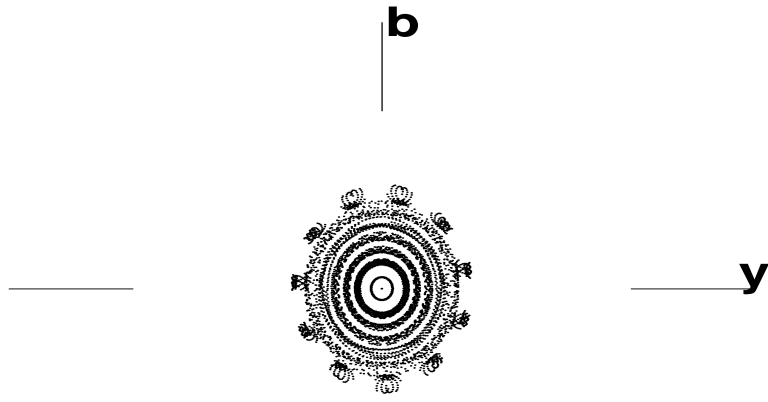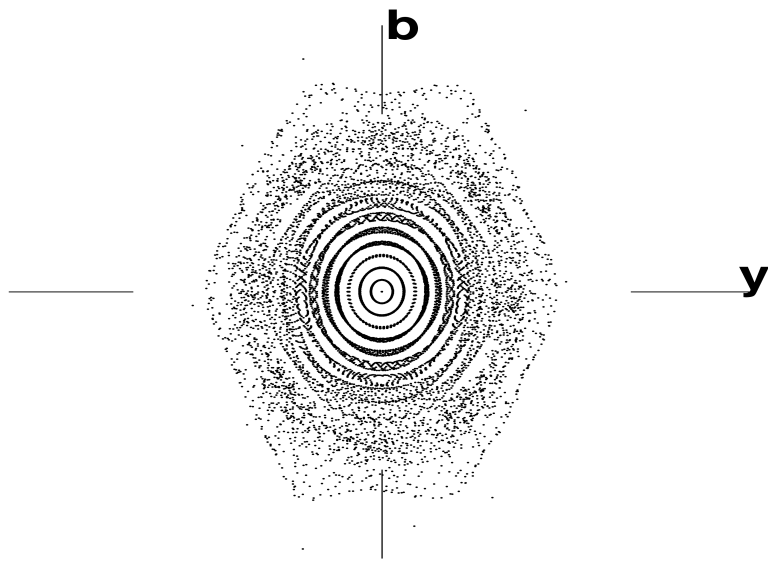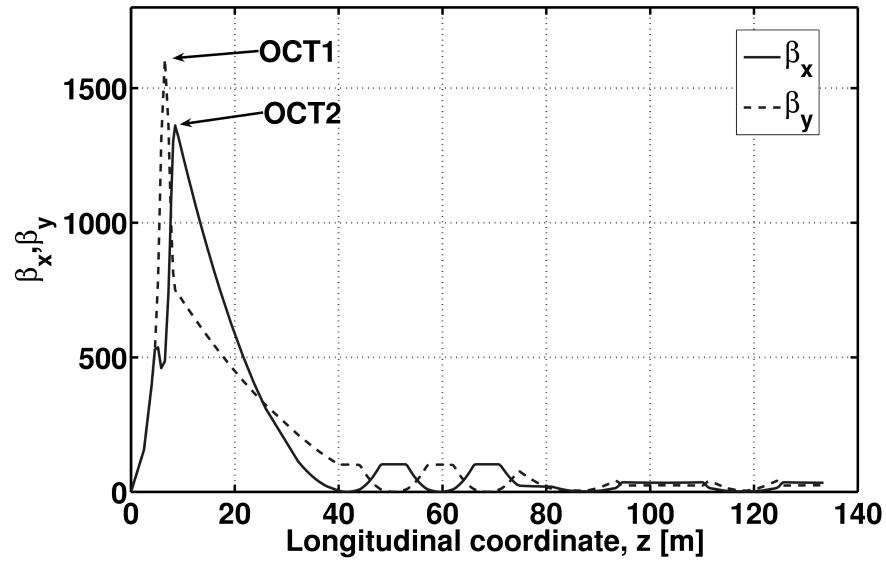
Fig. 5.7. The octupole correctors layout

5.1.7 Summary

A variety of approaches aimed at increasing the dynamic aperture was studied, and the one which produced the most effective way and produced the best results was determined. The results of the optimization using the chosen method developed for the study were presented and the dynamic aperture was found to increase almost by a factor of 2 compared to the situation before the optimization: 7σ to 13σ. Only two octupole correctors were required in the proximity of the interaction point (at the peaks of the beta functions in the x and y planes). Though the aim was to maximize the dynamic aperture, some of the higher order terms in the nonlinear resonance matrix decreased naturally by an order or two in magnitude. Their reduction serves as another strong, quantitative argument proving the efficiency of this optimization approach. The next logical step in the study might be to add higher order multipoles

(decapoles, duodecapoles), but a preliminary study showed them to be ineffective in the sense of improving the dynamic aperture further. For example, different configurations could be obtained with duodecapole and octupole fields which resulted in particles being stable at 14σ, while at the same time the particles at 13σ were lost. It appears that the correction of geometric aberrations and kinematic effects are almost completely represented by the third order terms.

5.2 750×750 GeV Collider Storage Ring Lattice for the Tevatron Main Ring

A new lattice for the Muon Collider storage ring with design collision energy of 750×750 GeV is discussed. The important building blocks of the lattice are the Final Focus Section, the Chromatic Correction Section, and the Arc Module, which are described below in detail. These components of the collider have been designed keeping in mind that the storage ring must approximately match the footprint of the Tevatron Ring in order to take advantage of existing services and tunnels. The model presented here relies heavily upon a previous, very efficient 50×50 GeV storage ring lattice design. The current design value for β^* (beta function at the collision point) is chosen to be 1 cm, which is less restrictive and has the advantage of lower chromaticities and longer bunch lengths (due to the hour-glass effect) than the previous standard lattice with a β^* of 3 mm.

5.2.1 Introduction

The idea is to design a lattice for the storage ring that fits or matches approximately the footprint of the Tevatron Main Ring tunnel with all its bends and straights.

111

The alternative idea might be to make another tunnel, which is slightly larger in the radius, around the currently available one to be able to use the current Tevatron tunnel infrastructure. Taking into account the current status of the Tevatron project, the Muon Collider might be a logical next step in utilizing the existing tunnel with its infrastructure, thus saving a large amount of expenses connected to building a new accelerator complex for muons.

5.2.2   750×750 GeV Lattice

Currently a 50% dipole packing fraction is used for the 750×750 GeV lattice, which results in an arclength of 5.85 km (6.283−0.432 km of straights) in the dipole field of 5.3 T. At 750 GeV this field strength is reasonable, and in fact, the ultimate energy might be increased to 1×1 TeV.

The 50×50 GeV lattice [29,55] is used as a baseline, and its components are scaled to handle the muons the the energy of 750 GeV. The layouts of both 50×50 GeV and 750×750 GeV lattices are shown in Fig. 5.8. The 50×50 GeV lattice is a highly optimized one which, in turn, is based on the 2×2 TeV lattice [27], and therefore there is a strong reason to assume the 750×750 GeV design shares most of the advantages with these other lattices.

The 50×50 GeV ring has a roughly racetrack design with two circular arcs separated by an experimental insertion on one side, and a utility insertion for injection, extraction, and beam scraping on the other. The experimental insertion includes the interaction region (IR) followed by a local chromatic correction section and a matching section. The chromatic correction section is optimized to correct the ring's linear chromaticity, which is almost completely generated by the low beta quadrupoles in the IR.

50x50 GeV

750x750 GeV

IR

ARC

ARC repeated
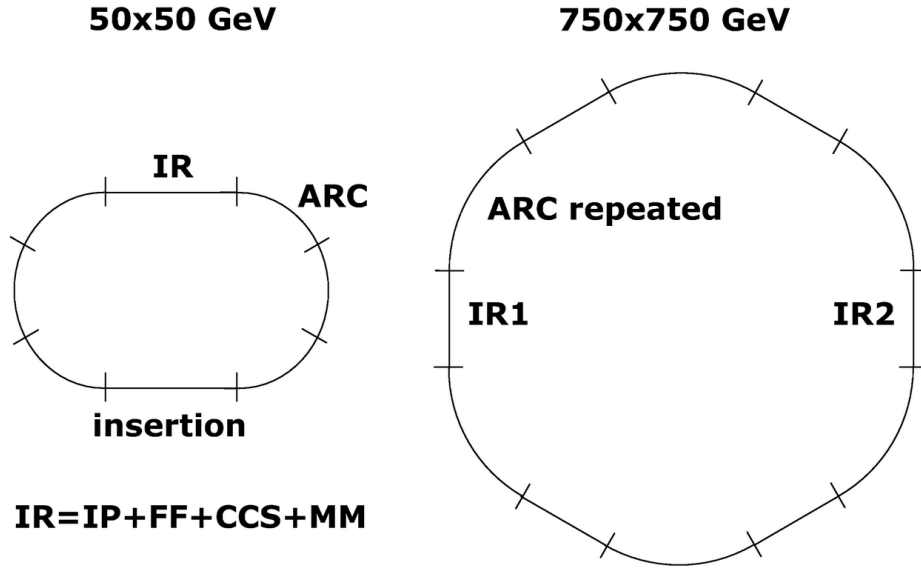
insertion

IR1

IR2

IR=IP+FF+CCS+MM

Fig. 5.8. The baseline 50×50 GeV lattice scheme compared to the 750×750 GeV lattice scheme.

The 750×750 GeV lattice design uses the same building blocks as the 50×50 GeV version, as it can be seen from Fig. 5.8: the final focusing section (FF), the chromaticity correction section (CCS), the matching module (MM), and the arc (ARC). The difference in the layouts is dictated by the fact that the 750×750 GeV lattice must match the Tevatron footprint. So the final focus section is placed in one of the straight sections of the Tevatron ring, while the chromaticity correction section and the matching section occupy parts of the Tevatron arc. The arcs of the original design are repeated in the arcs of the Tevatron as many times as necessary.

There are two IRs in the proposed lattice design to compensate for the luminosity loss due to the increased β^* as described in Section 5.2.6.

The main parameters of the 750×750 GeV lattice are summarized in Table 5.2 (second column). Similar parameters for the other lattices — 2×2 TeV (first column) and 50×50 GeV (third column) — are shown for comparison.

	4/1.5 TeV	1.5 TeV (this design)	100 GeV
β^* [mm]	3	10	40
l^* (IP to quad) [m]	4	5.5	4.5
peak β [km]	145	35	1.4
IR quad aperture [cm]	10	10	10
Poletip field [T]	12	9	8
$\epsilon_N(95\%)$ [mm mrad]	$841\pi/315\pi$	1306π	2176π
$\Delta p/p(95\%)[\%]$	.01-.08	$\geq$ .018-.144	$\geq$ .036-.288
$\xi_x(IR + CCS)$	-1500	-456	-53
$\xi_y(IR + CCS)$	-2000	-645	-73
α_{IR}	3.6×10^{-4}	1.0×10^{-3}	3.0×10^{-2}
IR length [m]	1300	506	137
α_{arc}	-2.1×10^{-3}	-9.3×10^{-3}	-9.5×10^{-2}
Arc length [m]	187	70	31

Tab. 5.2. Parameter comparison for various storage rings lattices

5.2.3 Final Focus Section

The low beta function values at the IP are mainly produced by three strong superconducting quadrupoles in the Final Focus Telescope with pole-tip fields of 9 T. Because of significant, large-angle backgrounds from the muon decay, a background-sweep dipole is included in the final focus telescope and placed near the IP to protect the detector and the low-β quadrupoles [30]. The bend starts at 35 meters, so the FF section fits the Tevatron straight section footprint. The layout of the preliminary Final Focus section design is shown in Fig. 5.9.

5.2.4 Chromatic Correction Section

A local chromatic correction of the Muon Collider interaction region is required to achieve broad momentum acceptance. The Chromaticity Correction Section (CCS) contains two pairs of sextupoles, one pair for each transverse plane, all placed at the locations with high dispersion. The sextupoles of each pair are located at positions of
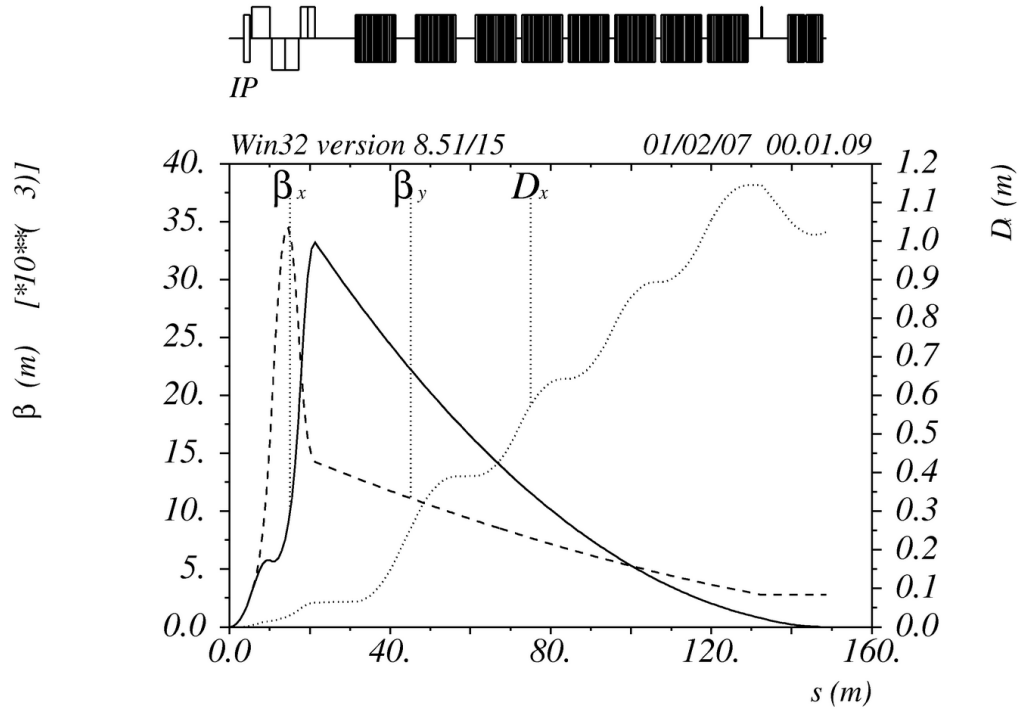
Fig. 5.9. The final focus section beta functions and dispersion plots

equal, high beta values in the plane (horizontal or vertical) whose chromaticity is to be corrected, and very low beta waist in the other plane. Moreover, the two sextupoles of each pair are separated by a betatron phase advance of near π, and each sextupole has a phase separation of $(2n + 1)\frac{\pi}{2}$ from the IP, where n is an integer. The result of this arrangement is that the geometric aberrations of each sextupole is cancelled by its companion while the chromaticity corrections add. The sextupoles of each pair are centered about a minimum in the opposite plane $(\beta_{min} < 1)$, which provides a chromatic correction with a minimal cross correlation between the planes. A further advantage to locating the opposite planes minimum at the center of the sextupole, is that this point is $\frac{\pi}{2}$ away from, or "out of phase" with, the source of chromatic effects in the final focus quadrupoles; that is, the plane not being chromatically corrected is treated like the IP in terms of the phase to eliminate a second order chromatic aberration generated by an "opposite-plane" sextupole. The repetitive symmetry
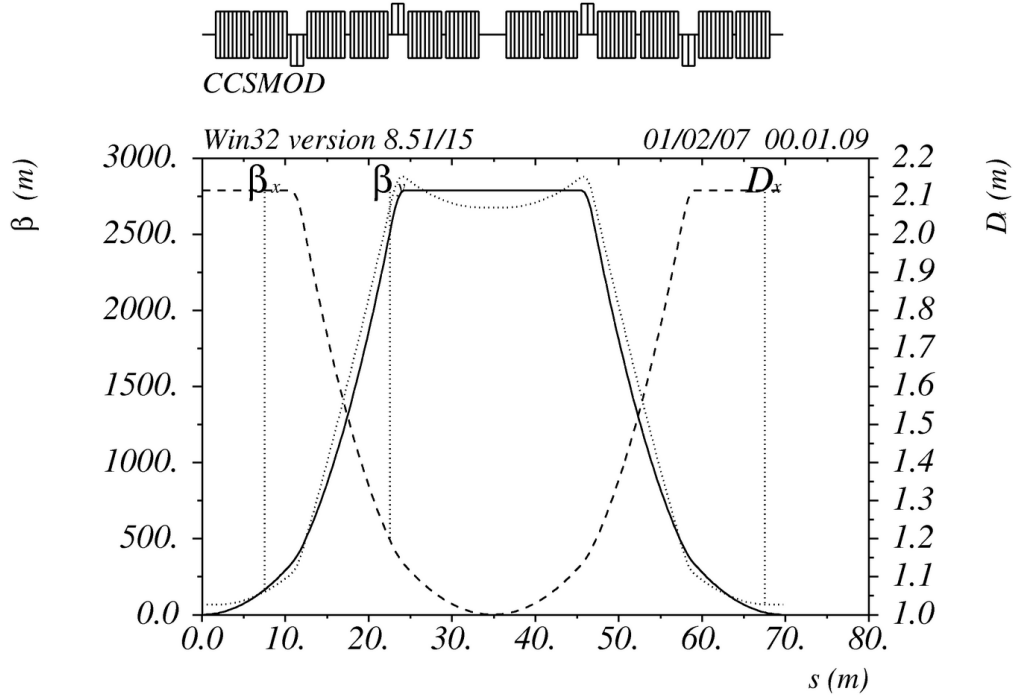
Fig. 5.10. The chromaticity correction section beta functions and dispersion plots

and the fact that the transfer map of the section is unity implies that the important aberration $(x|\delta\delta)$ vanishes as well. The layout of the CCS is shown in Fig. 5.10.

5.2.5 Arc Module

The Flexible Momentum Compaction module (Fig. 5.11) provides negative momentum compaction values compensating for the positive momentum compaction generated by the Chromaticity Correction Section. Small beta functions are achieved through the use of a doublet focusing structure which produces a low beta simultaneously in both planes. At the dual minimum, a strong focusing quadrupole is placed to control the derivative of the dispersion with little impact on the beta functions. (The center defocusing quadrupole is used only to clip the point of the highest dispersion.) Ultimately a dispersion derivative can be generated which is negative enough to drive the dispersion negative through the doublet and the intervening waist.

116
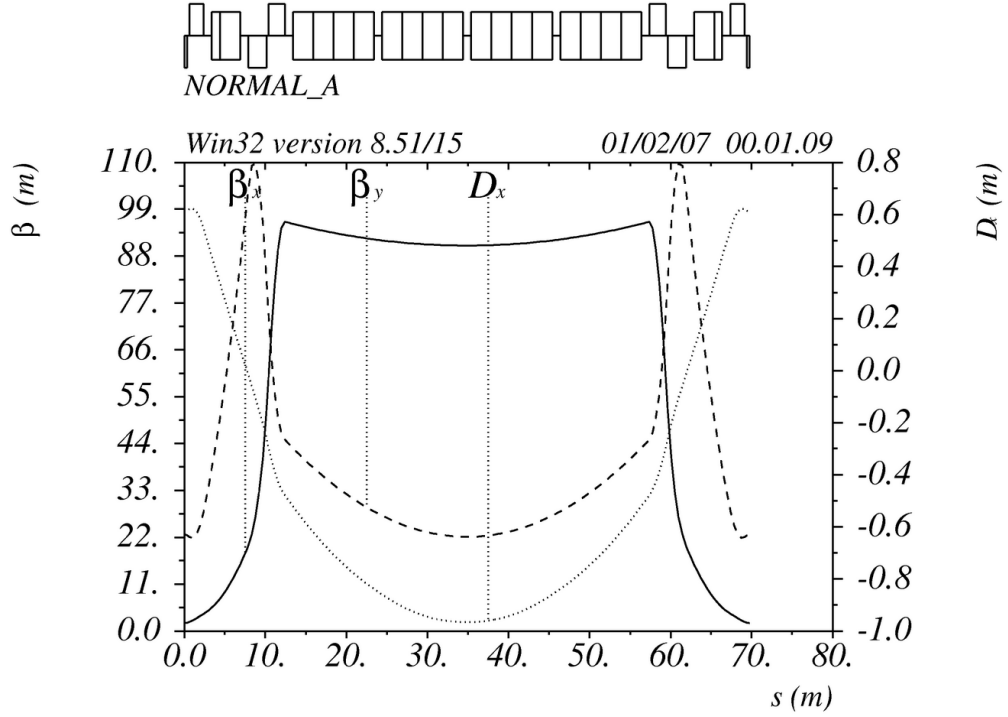
Fig. 5.11. The arc module beta functions and dispersion plots

5.2.6 Advantages and Disadvantages of the New Design

The proposed design has a lot of advantages. As the lattice is isochronous, a bunch length change is prevented, which is very important for controlling the hour-glass effect. β^* is chosen to be 1 cm, which has the advantage of lower chromaticities and longer bunch lengths (due to the hour-glass effect), and also the apertures can be chosen smaller than the 3 mm lattice ones. Smaller chromaticities lead to weaker chromatic aberrations and larger momentum acceptance. All these facts contribute to a larger dynamic aperture.

As for the disadvantages, the choice of larger β^* leads to an undesirable decrease in luminosity. According to the formulas from [19, 20]:

$$L \propto \frac{1}{\beta^*},$$

where L is the luminosity. For $\beta^* = 3$ mm the hour-glass reduction factor is $\eta_A =$

117

0.76, while the disruption enhancement is $f_D = 1.5$. Overall, $H_D = \eta_A f_D = 1.14$. For $\beta^*_{new} = 1$ cm one has $\eta_A \rightarrow 1$, $f_D \rightarrow 1$, and hence

$$\left(\frac{L_{old}}{L_{new}}\right)_{eff} = 1.14\frac{\beta^*_{new}}{\beta^*_{old}} = 3.8.$$

Therefore, the luminosity for $\beta^* = 1$ cm is 3.8 times smaller than for $\beta^* = 3$ mm. However, the loss of luminosity can be compensated by the increased momentum aperture and by using the 2 IRs in the ring (see the scheme in Fig. 5.8).

One other problem arises due to the fact that one is trying to match the lattice to the existing geometry, which puts more constraints on the building blocks of the lattice.

The last and the most important for now is the one of shielding the IP and securing the temperature of the superconducting magnets from the undesired effect of electrons and γ rays produced by the muon decay. However, this problem is beyond the scope of this dissertation work and will be considered separately.

APPENDICES

APPENDIX A

TEVATRON LATTICE CONVERTER FROM OPTIM TO COSY INFINITY

In this Appendix the detailed description of the program [45] converting the Tevatron machine lattice source file from OptiM [32] code to COSY INFITITY [13,36] is given. Only the transverse dynamics changing elements are considered.

A.2 Introduction

The Tevatron lattice description in the form of the code list for OptiM — the program written at Fermi National Accelerator Laboratory — is based on the current magnets layout with several corrections added for a model to correspond the experimental measurements. To analyze the transversal dynamics of the particles in the Tevatron using the program COSY INFINITY, the code list of the lattice description needs to be converted to COSY lattice elements description format. The situation is being complicated by the fact that OptiM and COSY use different units of measure: in OptiM all the units are SGS, while in COSY most of the units are SI, so great care about it should be taken during the conversion of the lattice.

A.3   Tools for Conversion

The converter program is written in PHP language version 4.4.4 [1]. This programming environment has been chosen to provide the availability of fast online conversion of the source code. As PHP is a web-oriented language, the resulting program can be run on any web server having PHP support.

Moreover PHP has a variety of standard functions to work with strings, which is very convenient as the converter program is mainly a text file parser.

A.4   Source Code Details

The source code in OptiM format has several sections to parse:

1. A section with different variables declaration and value assignment, the so-called "math header";

2. A section containing values for initial energy and mass of the particles under consideration, emittances, betatron functions and other parameters;

3. A lattice description section, consisting of a set of references to the lattice element names, as well as the number of periods, telling the system to repeat the same elements set several times;

4. A section describing elements, including all the lattice element names and parameters; the number of mandatory and optional parameters varies with the type of the element.

Each line of the source file can contain a comment, starting with the "#" sign. Such a line is ignored at runtime.

A.5 COSY Code Details in Connection to OptiM Code

To convert the source code to COSY, all the sections should be treated and parsed separately. As the OptiM program requires no explicit variable declaration (all the variables are available at the moment they are first referenced), while COSY requires one, the first section of the OptiM program splits into two sections:

1. Section with variable declaration;

2. Section with value assignment.

These two sections go to different places of the destination COSY code, namely, one before the main procedure call and the other one inside it.

Additional problem arises as COSY is case-insensitive. So the two variables "e1" and "E1", treated as different by OptiM, will be treated as the same variable by COSY. To solve this problem the idea of a cache has been utilized. If the case-insensitive name of the variable coincides with the name existing in the cache, this variable gets another unique name.

The section, describing various parameters characterizing the beam, is partially converted to the set of calls to standard COSY initialization procedures, such as OV, RP, etc. Currently, only two parameters are taken into account: the initial beam energy and the particles mass.

Element names and their order in the lattice from the subsequent section of the source file go into a separate array. The names themselves are not used in the final COSY code, but they are preserved as comments to each lattice element function call along with the number of the element:

```
QUADRUPOLE 81.4578 gqH_3 0;{qH_3F #1948}

DRIFT 0.17178;{oDQOUT #1949}

DRIFT 0.168275;{oDPIN5LOC #1950}

DRIFT 0.381;{oDHQUADC #1951}

M_ELEMENT 2 0 0;{mTSX #1952}

M_ELEMENT 1 0 0;{mTQX #1953}
```

Each element name contains the information about the element type. The first letter of the name is this type (e.g. "q" stands for "quadrupole", "o" – for "drift", "s" – for "sextupole" and so on). This information is used by the converter to determine the function corresponding to the element.

The set of parameters of each element is being taken from the last section of the source OptiM file. For the moment only the limited set of elements is implemented (according to the needs of the study), namely, those influencing the transverse motion of the particles (no RF cavities). At the same time, the support for these elements can easily be added, as COSY has a very wide range of standard elements. The only problem one might experience is the problem of units of measure conversion, which is unavoidable.

In OptiM optional parameter values can be assigned explicitly or not assigned at all. For COSY output, the values not explicitly assigned are substituted with some default values and treated correctly in each individual case.

Each section of the source code can contain lines with comments, these lines are treated individually for each section and included into the destination file to maintain the completeness of the information contained in the source file.

A.6   Summary of Functionality of the Resulting

COSY Output

Currently, the converter program is intended for use with a Tevatron model only and convert only the transversal dynamics. Some of the elements absent in the description of the Tevatron lattice are not implemented, e.g. such element types as 'transfer matrix' element. This element type allows to substitute an element or a set of elements with a predefined linear transfer map in OptiM.

The initial aim of the program was to just convert OptiM source code to COSY code, which can be run right away and return the transfer map of the Tevatron for one turn (the only thing to specify is the calculation order for COSY). But with minor changes this program can do much more. As it advances all the elements of the given lattice one by one, it is easy to add some more special function calls for a predefined set of types of elements. Another opportunity is to edit a code wrapper for some element type, and have this change in all subsequent conversions of the source OptiM code.

As the converter program is written in PHP, it is easy to perform updates to the COSY code if the OptiM description is changed.

OptiM is aimed to assist with the linear optics design of particle accelerators, while COSY INFINITY is commonly used for high-order analysis of the lattice, fast high-order transfer map retrieval and paritcle tracking.

A.7   Code List of Element Wrappers

Each of the implemented structure element types has its own designated procedure — a wrapper preparing standard COSY procedure call. Code lists of all available wrappers with parameters and unit conversions are summarized in this section.

1. Drift — free space, element type 'o' or 'i'

```
PROCEDURE DRIFT L;

VARIABLE L0 1;

L0:=L;

DL L0;

endprocedure;
```

The procedure DRIFT has only one input parameter: the length of the drift. The conversion of the units from $[cm]$ to $[m]$ is done by the converter program, so technically the procedure DRIFT does nothing, but the wrapper DRIFT might still be needed in case of extending functionality of the procedure. E.g. in one of the variations the summation of the lengths of individual elements has been added to each wrapper, so the procedure DRIFT changed:

```
PROCEDURE DRIFT L;

VARIABLE L0 1;

L0:=L;

DL L0;

current_length:=current_length+L0;

endprocedure;
```

2. Dipole — element of type 'b' or ''d':

```
PROCEDURE DIPOLE L B G ANGLE1 ANGLE2 TILT;

VARIABLE B0 1;

VARIABLE L0 1;

VARIABLE G0 1;
```

125

```
VARIABLE TILT0 1;

VARIABLE NT 1;

VARIABLE KN 1 1;

VARIABLE S1 1 1;

VARIABLE S2 1 1;

VARIABLE R 1;

VARIABLE PHI 1;


NT:=1;

L0:=L/100;{in meters}

IF (B=0);

  DL L0;

ELSEIF TRUE;

  B0:=ABS(B)/10;{in Tesla}

  G0:=G*10;{in T/m}

  R:=CONS(P0)/(CLIGHT*1e-6)/B0;

  KN(1):=G0/R/B0;

  S1(1):=ANGLE1*DEGRAD;{rad}

  S2(1):=ANGLE2*DEGRAD;{rad}

  PHI:=L0/R/DEGRAD;

  TILT0:=TILT;

  ROTATE TILT0;{rotate coordinate frame}

  MCLK  L0 PHI 0.05 KN S1 S2 NT;{standard COSY call}

  ROTATE -TILT0;{rotate back}

ENDIF;
```

```
ENDPROCEDURE;
```

This procedure takes six parameters: the length of the element in $[cm]$, the bending magnetic field in $[kG]$, the field gradient $[kG/cm]$, the entrance and exit angles in $[deg]$ and the roll angle in $[deg]$. All the necessary unit conversions are done inside the wrapper that ultimately calls a standard COSY function MCLK. The procedure ROTATE allows to work with "skew" elements. It rotates the coordinate frame through the given angle:

```
procedure rotate phi;

variable M 3000 4;

variable i 1;

M(1):=COS(PHI*DEGRAD)*MAP(1)+SIN(PHI*DEGRAD)*MAP(3);

M(3):=-SIN(PHI*DEGRAD)*MAP(1)+COS(PHI*DEGRAD)*MAP(3);

M(2):=COS(PHI*DEGRAD)*MAP(2)+SIN(PHI*DEGRAD)*MAP(4);

M(4):=-SIN(PHI*DEGRAD)*MAP(2)+COS(PHI*DEGRAD)*MAP(4);

LOOP i 1 4;

   MAP(i):=M(i);

ENDLOOP;

endprocedure;
```

3. Long quadrupole — element of type 'q':

```
PROCEDURE QUADRUPOLE L G TILT;

VARIABLE L0 1;

VARIABLE G0 1;

VARIABLE TILT0 1;
```

```
LO:=L/100;{in meters}

IF (G=0);

  DL LO;{if there is no field - just put drift}

ELSEIF (1=1);

  GO:=G*10;{in Tesla/m}

  TILTO:=TILT;

  ROTATE TILTO;

  MQ LO GO*0.05 0.05;

  ROTATE -TILTO;

ENDIF;

ENDPROCEDURE;
```

This procedure takes three parameters: the length in $[cm]$, the field gradient in $[kG/cm]$ and the roll angle in $[deg]$.

4. Multipole kick — element of type 'm':

```
PROCEDURE M_ELEMENT m B TILT;

VARIABLE BO 1;

VARIABLE TILTO 1;


IF (B#0);{if the field is non-zero}

  IF (m=1);{quadrupole}

    TILTO:=TILT;

    ROTATE TILTO;

    BO:=B/10;{in Tesla}
```

128

```
    MQ 1e-6 (B0/1E-6)*0.05 0.05;

    DL -1e-6;

    ROTATE -TILT0;

  ENDIF;

  IF (m=2);{sextupole}

    TILT0:=TILT;

    ROTATE TILT0;

    B0:=B*10;{in Tesla/m}

    MH 1e-6 (B0/1E-6)*0.05*0.05 0.05;

    DL -1e-6;

    ROTATE -TILT0;

  ENDIF;

  IF (m=3);{octupole}

    TILT0:=TILT;

    ROTATE TILT0;

    B0:=B*1000;{in Tesla/m}

    MO 1e-6 (B0/1E-6)*0.05*0.05*0.05 0.05;

    DL -1e-6;

    ROTATE -TILT0;

  ENDIF;

ENDIF;

ENDPROCEDURE;
```

This is a rather complicated procedure compared to all others. It is designed
to facilitate various kinds of multipole kicks — short multipoles that can be
treated as 'zero-length' elements. The procedure takes three parameters: the

number of multipole harmonic (1 – quadrupole, 2 – sextupole, etc.), the integral of the multipole gradient in $[kG/cm^{m-1}]$ and the roll angle in $[deg]$.

5. Solenoid — element type 'c':

```
PROCEDURE SOLENOID L B A;
VARIABLE L0 1;
VARIABLE B0 1;
VARIABLE A0 1;


L0:=L/100;{in meters}
B0:=B/10;{in T}
IF (B0=0);
   DL L0;{if no strength is given}
ELSEIF TRUE;
   A0:=A/100;{in meters}
   CMS B0 A0 L0;
ENDIF;
ENDPROCEDURE;
```

This procedure takes three parameters: the length of the solenoid in $[cm]$, the strength of the field in $[kG]$ and the aperture in $[cm]$.

APPENDIX B

GRAPHICAL USER INTERFACE FOR THE TEVATRON SIMULATIONS IN COSY INFINITY

COSY INFINITY does not have the tools to give the user graphical interface. Therefore, to make the user interaction with the program for the Tevatron simulations more efficient, a graphical user interface (GUI) was developed and implemented in Matlab (see the screenshot of the main working window Fig. B.1). This GUI can be obtained from the author of the dissertation upon request.

This GUI allows the user to run the Tevatron simulations without knowing the COSY's internal language. There are four groups of parameters the user can control:

- **Lattice options** allow to select which families of elements are turned on/off while calculating the transfer map:

    - Skew quadrupoles in dipoles on — turns on/off the skew quadrupole errors in dipoles;

    - Skew quadrupole correctors on — turns on/off the skew quadrupole correctors according to the currently implemented correction scheme;
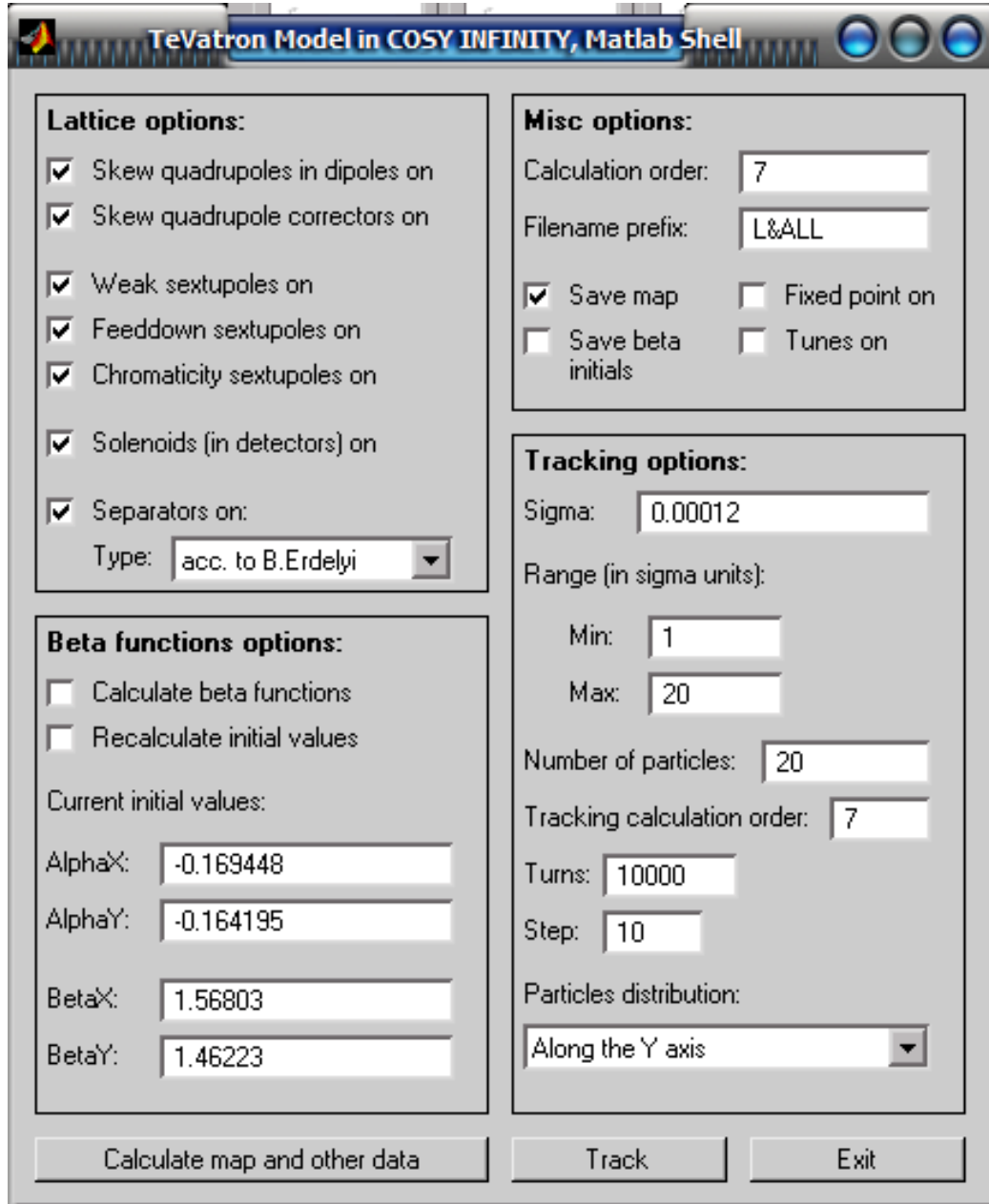
Fig. B.1. Tevatron simulation GUI

- Weak sextupoles on — turns on/off the weak sextupole errors, mainly in dipoles;

- Feeddown sextupoles on — turns on/off the feeddown sextupole families;

- Chromaticity sextupoles on — turns on/off the sextupole family responsible for the chromaticity correction;

- Solenoids (in detectors) on — turns on/off the solenoidal fields in the CDF and D0 detector areas;

- Separators on — turns on/off the sets of the separators which bring the protons/antiprotons to their respective helices.

- **Beta function options** allow to choose whether the beta functions will be calculated along with the transfer map:

- Calculate beta functions — turns on/off the beta function calculation;

- Recalculate initial values — turns on/off the recalculation of the initial values of the Twiss parameters using the periodicity conditions;

- Current initial values — current values of the Twiss parameters, γ_x and γ_y are calculated using the formulas $\gamma_{x,y} = (1 + \alpha_{x,y}^2)/\beta_{x,y}$, can be changed to the desired values.

- **Miscellaneous options** allow to choose the order of calculations and various logging options:

- Calculation order — usually set to 7 for intermediate tracking results and 11 or 13 for the final results;

- Filename prefix — tells the program, which filename prefix is used for .map and .log files, containing the transfer map and the current run log, respectively;

- Save map — turns on/off the transfer map saving to file;

- Save beta initials — the initial values of the the Twiss parameters will be saved as defaults for the next run;

- Fixed point on — turns on/off the fixed point calculation;

- Tunes on — turns on/off the tunes calculation.

- **Tracking options** allow to change the particle tracking settings:

  - Sigma — the value of the normal distribution parameter σ, the beam is assumed round, so $\sigma_x = \sigma_y = \sigma$;

  - Range — characterizes the minimal and maximal radii of the particles being tracked in σ units;

  - Number of particles — how many particles are being tracked;

  - Tracking calculation order — might only be lower than the transfer map calculation order;

  - Turns — the number of turns the particles are being tracked;

  - Step — the number of turns after which the particle trace is saved, in other words, the number of turns after which the dot on the phase space plot is set;

  - Particles distribution — the particles can be launched along the x axis, the y axis or along the (x, y) diagonal, other patterns can easily be arranged;

The main working buttons are the "Calculate map and other data", in which case only the transfer map and related information such as the beta function values are calculated; and the "Track" button which triggers the transfer map recalculation if the transfer map has not been calculated previously, followed by the particle tracking procedure according to the parameters set. If any of these buttons is pressed Matlab initiates the COSY code list assembly procedure, substituting all the updated parameters as necessary, after that COSY is called as an external command to run the assembled code. As one can see the Matlab GUI gives the user a lot of freedom to choose the transfer map calculation and tracking parameters.

This Matlab utility was used to obtain all the phase portraits in section 4.1.

BIBLIOGRAPHY

[1] PHP: Hypertext Preprocessor. Available at `http://www.php.net`.

[2] The MAD to COSY Converter. Available at `http://cosy.pa.msu.edu/converters/mad2cosy`.

[3] Methodical accelerator design. `http://mad.home.cern.ch/mad/`.

[4] M. Abramowitz and I. A. Stegun (Eds.). *Handbook of Mathematical Functions with Formulas, Graphs, and Mathematical Tables*, pages 300–302. New York: Dover, 1972.

[5] S. Ahn and et al. Muon colliders: A scenario for the evolution of the Fermilab accelerator complex. Technical Report Fermilab-FN-677, Fermilab, 1999.

[6] Y. Alexahin. Private communication.

[7] M. M. Alsharoá and et al. Recent progress in Neutrino Factory and Muon Collider research within the Muon Collaboration. *Phys. Rev. ST Accel. Beams*, 6:081001, 2003.

[8] M. Berz. Introduction to beam physics. Lecture Notes. Virtual University Beam Physics Course, available at `http://bt.pa.msu.edu/pub/papers/bphy861/bphy861.pdf`.

[9] M. Berz. Differential algebraic formulation of normal form theory. In M. Berz, S. Martin, and K. Ziegler, editors, *Proc. Nonlinear Effects in Accelerators*, pages 77–86. IOP Publishing, 1992.

[10] M. Berz. *From Taylor Series to Taylor Models*, pages 1–27. American Institute of Physics CP405, 1997. Chapter in: Nonlinear Problems in Accelerator Physics.

[11] M. Berz. *Differential Algebraic Techniques*. World Scientific, 1999. Chapter in: Handbook of Accelerator Physics and Engineering.

[12] M. Berz. *Modern Map Methods in Particle Beam Physics*. Academic Press, San Diego, 1999. Also available at `http://bt.pa.msu.edu/pub`.

[13] M. Berz. COSY INFINITY version 8.1 user's guide and reference manual. Department of Physics and Astronomy MSUHEP-20704, Michigan State University, 2002. `http://cosy.pa.msu.edu/cosymanu/index.html`.

[14] M. Berz and et al. The COSY INFINITY web page. `http://cosy.pa.msu.edu`.

[15] M. Berz, K. Makino, Y.-K. Kim, and P. Snopok. Long-term stability of large particle accelerators. *ECMI Newsletter*, 39, 2006.

[16] M. Berz, K. Makino, and W. Wan. An introduction to the physics of beams. IOP Publishing, forthcoming.

[17] G. I. Budker. Accelerators and colliding beams (in russian). In *Proceedings of the 7th International Conference on High Energy Accelerators*, volume 1, page 33, Yerevan, 1969.

[18] D. C. Carey, K. L. Brown, and F. Rothacker. Third-order TRANSPORT with MAD input. A computer program for designing charged particle beam transport systems. Technical Report FERMILAB-Pub-98/310, Fermi National Accelerator Laboratory, 1998. Also available at `http://rampex.ihep.su/manuals/transport.pdf`.

[19] P. Chen. Disruption, beamstrahlung, and beamstrahlung pair creation. Technical Report SLAC-PUB-4822, SLAC, 1988. Contributed to the DPF Summer Study High Energy Physics in the 1990's, Snowmass, Colorado, June 27-July 15, 1988.

[20] P. Chen and K. Yokoya. Disruption effects from the interaction of round e+e- beams. *Phys Rev. D 38*, 38(3):987–1000, 1988.

[21] E. D. Courant and H. S. Snyder. Theory of the alternating-gradient synchrotron. *Annals of Physics*, 3:1–48, 1958.

[22] B. Erdélyi. Private communication.

[23] B. Erdélyi. *Symplectic Approximation of Hamiltonian Flows and Accurate Simulation of Fringe Field Effects*. PhD thesis, Michigan State University, East Lansing, Michigan, USA, 2001.

[24] B. Erdélyi and M. Berz. Optimal symplectic approximation of Hamiltonian flows. *Physical Review Letters*, 87,11:114302, 2001.

[25] B. Erdélyi and M. Berz. Local theory and applications of extended generating functions. *International Journal of Pure and Applied Mathematics*, 11,3:241–282, 2004. Available at `http://bt.pa.msu.edu/pub`.

[26] N. Gelfand. Reshimming the Tevatron dipoles. Technical Report Beams-doc-1290-v1, FNAL, August 2004.

[27] C. Johnstone and A. Garren. An IR and chromatic correction design for a 2 TeV Muon Collider. In *Proceedings of the Workshop on New Directions for High-Energy Physics*, page 222, 1996.

[28] C. Johnstone and A. Garren. 50-on-50 GeV Muon Collider storage ring. In *Higgs Factory 2001 Snowmass Report*, 2001.

[29] C. Johnstone, W. Wan, and A. Garren. Lattice design for a 50-on-50 GeV Muon Collider. In *Proceedings of the 1999 Particle Accelerator Conference*, pages 3065–3067, New York, 1999.

[30] C. J. Johnstone and N. V. Mokhov. Optimization of a Muon Collider interaction region with respect to detector backgrounds and the heat load to the cryogenic systems. Technical Report Fermilab-Conf-96/366, Fermilab, 1996.

[31] S. Kirkpatrick, C. D. Gelatt, and M. P. Vecchi. Optimization by simulated annealing. *Science, Number 4598, 13 May 1983*, 220, 4598:671–680, 1983. `http://citeseer.ist.psu.edu/kirkpatrick83optimization.html`.

[32] V. Lebedev. OptiM – computer code for linear and non-linear optics calculations, 2004. `http://www-bdnew.fnal.gov/pbar/organizationalchart/lebedev/OptiM/optim.htm`.

[33] K. Levenberg. A method for the solution of certain problems in least squares. *Quart. Appl. Math.*, 2:164–168, 1944.

[34] K. Makino and M. Berz. Remainder differential algebras and their applications. In M. Berz, C. Bischof, G. Corliss, and A. Griewank, editors, *Computational Differentiation: Techniques, Applications, and Tools*, pages 63–75. SIAM, 1996.

[35] K. Makino and M. Berz. Solenoid elements in COSY Infinity. *Institute of Physics CS*, 175:219–228, 2004.

[36] K. Makino and M. Berz. COSY INFINITY version 9. *Nuclear Instruments and Methods*, A558:346–350, 2005.

[37] D. Marquardt. An algorithm for least-squares estimation of nonlinear parameters. *SIAM J. Appl. Math.*, 11:431–441, 1963.

[38] M. A. Martens. Tevatron lattice page. `http://www-ap.fnal.gov/~martens/tev_lattice/tev_lattice.html`.

[39] W. M. McKeeman. Algorithm 145: Adaptive numerical integration by Simpson's rule. *Communications of the ACM*, 5(12):604, 1962.

[40] R. E. Meller, A. W. Chao, J. M. Peterson, S. G. Peggs, and M. Furman. Decoherence of kicked beams. Technical Report SSC-N-360, SSCL, 1987.

[41] J. A. Nelder and R. Mead. A simplex method for function minimization. *The Computer Journal*, 7:308–313, 1964.

[42] D. Neuffer. Colliding muon beams at 90 GeV. Technical Report FN-319, Fermi National Accelerator Laboratory, 1979.

[43] R. B. Palmer, A. Sessler, A. Skrinsky, and et al. Muon colliders. In *Proceedings of 9th Advanced ICFA Beam Dynamics Workshop*, 1995.

[44] M. L. Shashikant, M. Berz, and B. Erdélyi. COSY INFINITY's EXPO symplectic tracking for LHC. *IOP CP*, 175:299–306, 2004.

[45] P. Snopok. A converter program for Tevatron lattices from OptiM to COSY INFINITY. Technical Report MSUHEP-40909, Department of Physics and Astronomy, Michigan State University, East Lansing, MI 48824, 2004.

[46] P. Snopok, M. Berz, and C. Johnstone. Calculation of nonlinear tune shift using beam position measurement results. Technical Report MSUHEP-070421, Department of Physics and Astronomy, Michigan State University, East Lansing, MI 48824, 2007.

[47] P. Snopok, C. Johnstone, and M. Berz. Simulation and optimization of the Tevatron accelerator. In H. M. Bücker, G. Corliss, P. Hovland, U. Naumann, and B. Norris, editors, *Automatic Differentiation: Applications, Theory, and Tools*, Lecture Notes in Computational Science and Engineering. Springer, 2005.

[48] P. Snopok, C. Johnstone, M. Berz, D. A. Ovsyannikov, and A. D. Ovsyannikov. Study and optimal correction of a systematic skew quadrupole field in the Tevatron. In *Nuclear Instruments and Methods in Physics Research A*, volume 558, pages 142–146, 2006.

[49] P. Snopok, C. Johnstone, and A. Garren. Recent progress in Muon Collider lattice design. Technical Report MSUHEP-070420, Department of Physics and Astronomy, Michigan State University, East Lansing, MI 48824, 2007.

[50] D. J. Summers. Muon acceleration to 750 GeV in the Tevatron, 2007. Neutrino Factory and Muon Collider Collaboration, UCLA, available at `http://www.cap.bnl.gov/mumu/conf/MC-070129/DSummers1-070129.pdf`.

[51] M. Syphers. Private communication.

[52] M. Syphers. Strong transverse coupling in the Tevatron. Technical Report Beams-doc-1159-v1, FNAL, May 2004.

[53] M. Syphers. Tevatron accelerator physics. Technical Report Beams-doc-1046-v1, FNAL, February 2004.

[54] F. F. Tikhonin. On the effects with muon colliding beams. Technical Report P2-4120, JINR, Dubna, 1968.

[55] D. Trbojevic, K. Y. Ng, and W. Weishi. A lattice for the 50 GeV Muon Collider ring. In S. Myers and et al., editors, *EPAC'98 Proceedings*, pages 362–364, 1998.

[56] D. Trbojevic, R.B. Palmer, E.D. Courant, J. Gallardo, S. Peggs, S. Tepikian, and K. Y. Ng. A lattice for the Muon Collider demonstration ring in the RHIC tunnel. In *Proceedings of the 1997 Particle Accelerator Conference*, 1997.

[57] S. Turner, editor. *CERN Accelerator school, Fifth General Accelerator Physics Course*, volume I. CERN, Geneva, January 1994.

[58] W. Wan. Private communication.